Nuclear functions of Myosin VI

Dissertation

zur Erlangung des Grades
"Doktor der Naturwissenschaften"
(Dr. rer. nat.)

am Fachbereich Biologie
der Johannes Gutenberg-Universität Mainz

Jie Shi

geboren am 12.01.1996 in Beijing

September 2023

Declaration

I, Jie Shi, confirm that the work presented in this thesis is my own. Where information has been derived from other sources, I confirm that it has been indicated in the thesis.

Abstract

Maintenance of genome stability is of high importance for the accurate transmission of genetic material. Genome instability can result from a plethora of endogenous and exogenous sources that create DNA damage or replication stress. To counteract the various types of damage and stress, as well as to keep the genome intact, numerous repair and stress resolution pathways have evolved as cellular defence mechanisms.

While cytoplasmic functions of the actin cytoskeleton have long been well characterised, including cell migration and intracellular transport, its functions in the nucleus have only in recent years gradually emerged. Filamentous actin (F-actin) was found to play a role in the repair of DNA double strand breaks (DSBs) as well as in the replication stress response. Myosins are actin-based molecular motor proteins that support the various functions of F-actin, out of which myosin VI (myo6) stands out with its unique directionality of walking towards the minus end of actin filaments. Similar to F-actin, its cytoplasmic functions such as endocytosis, autophagy, and cell migration have been well described, while its nuclear functions, except for its role in transcription, remained enigmatic up until now. Therefore, my PhD thesis focussed on the investigation of myo6's nuclear functions.

In my thesis, I have shown the contribution of myo6 to the repair of DSBs by the homologous recombination (HR) pathway, correlating well with published data on F-actin's function in HR. I have additionally demonstrated another function of myo6 in the protection of stressed replication forks. Results of DNA fibre assays that I performed have indicated the cooperation of myo6 with the well-established fork protector WRNIP1 in fork protection, downstream of fork reversal. Furthermore, by using a dominant negative approach, I showed the essentiality of the actin-associated motor domain of myo6, as well as its ubiquitin-binding MyUb domain in its fork protection function. Finally, using a combination of the dominant negative approach and the DARPin technology, I could provide evidence that it is the nuclear pool of myo6 rather than the cytoplasmic pool, which is responsible for its fork protection function. Taken together, I have demonstrated two novel functions of myo6, and additionally optimised and characterised a powerful DARPin-tool for differentiating the contributions of nuclear and cytoplasmic myo6 that could be highly beneficial for characterisation of its other unknown functions that remain to be discovered.

Zusammenfassung

Die Aufrechterhaltung der Genomstabilität ist von großer Bedeutung für die korrekte Weitergabe von genetischem Material. Genom-Instabilität kann aus einer Vielzahl endogener und exogener Quellen resultieren, welche DNA-Schäden oder Replikationsstress verursachen. Um den verschiedenen Arten von Schäden und Stress entgegenzuwirken und um das Genom intakt zu halten, gibt es zahlreiche Reparatur- und Stressbewältigungswege als zelluläre Abwehrmechanismen.

Während die zytoplasmatischen Funktionen des Aktin-Zytoskeletts, wie z.B. die Zellmigration und der intrazellulären Transport, seit langem gut charakterisiert sind, wurden seine Funktionen im Zellkern erst in den letzten Jahren allmählich bekannt. Es wurde festgestellt, dass filamentöses Aktin (F-Aktin) bei der Reparatur von DNA-Doppelstrangbrüchen (DSBs) sowie bei der Reaktion auf Replikationsstress eine Rolle spielt. Myosine sind Aktin-basierte molekulare Motorproteine, welche die verschiedenen Funktionen von F-Aktin unterstützen, wobei Myosin VI (myo6) durch seine einzigartige Orientierung in Richtung des Minus-Endes von Aktin-Filamenten hervorsticht. Ähnlich wie bei F-Aktin sind seine zytoplasmatischen Funktionen, wie z.B. die Endozytose, die Autophagie und die Zellmigration, gut beschrieben, während seine Funktionen im Zellkern, abgesehen von seiner Rolle bei der Transkription, bisher unerforscht sind. Daher konzentrierte sich meine Doktorarbeit auf die Untersuchung der Funktionen von myo6 im Zellkern.

In meiner Dissertation habe ich einen Beitrag von myo6 zur Reparatur von DSBs mittels homologer Rekombination (HR) gezeigt, was gut mit den veröffentlichten Daten über die Funktion von F-Aktin bei der HR korreliert. Darüber hinaus habe ich eine weitere Funktion von myo6 beim Schutz von gestressten Replikationsgabeln nachgewiesen. Die Ergebnisse der von mir durchgeführten „DNA-Fiber“ Experimente deuten darauf hin, dass myo6 mit dem bekannten Protektor-Protein WRNIP1 beim Schutz von Replikationsgabeln zusammenarbeitet, ein Event welches der Umkehr von Replikationsgabeln nachgeschaltet ist. Darüber hinaus habe ich mit Hilfe eines dominant-negativen Ansatzes gezeigt, dass die Aktin-assoziierte Motordomäne von myo6, sowie seine Ubiquitin-bindende MyUb-Domäne, für die Funktion des Schutzes von Replikationsgabeln unerlässlich sind. Schließlich konnte ich durch eine Kombination aus dominant-negativen Ansätzen und der DARPin-Technologie nachweisen, dass der nukleäre und nicht der zytoplasmatische Pool von myo6 für

seine Schutzfunktion der Replikationsgabeln verantwortlich ist. Insgesamt habe ich zwei neue Funktionen von myo6 nachgewiesen und darüber hinaus ein leistungsfähiges DARPin-Werkzeug zur Unterscheidung der Beiträge von nukleärem und zytoplasmatischem myo6 optimiert und charakterisiert, das für die Charakterisierung weiterer unbekannter Funktionen von großem Nutzen sein könnte.

Acknowledgments

Contents

List of figures

List of tables

Chapter 1

Introduction

1.1 Genome stability

As DNA holds the source of genetic material and is essential for all known life, maintaining genome stability is of high importance[1]. However, the genome is susceptible to many kinds of exogenous as well as endogenous damages and stresses. If left unresolved or resolved incorrectly, mutagenesis or even cell death would occur, thus emphasizing the significance of maintaining genome stability[2]. To counteract this, cells have evolved numerous repair pathways or protection mechanisms; each specialised to tackle a specific type of damage or stress[3]. It should however also be noted that while mutations can be deleterious on one hand, they also promote genetic diversity and contribute towards evolution on the other hand[4,5].

1.1.1 DNA damage

The various types of damage that are inflicted on our DNA include base damage/modifications, bulky lesions, DNA crosslinks, single strand breaks (SSBs) and double strand breaks (DSBs)[6]. Each type of damage occurs at a different frequency and varies in its severity. For example, SSBs are a common source of damage, with tens of thousands occurring per cell per day, while DSBs are rare, only occurring at a frequency of 10-50 per cell per day, but a severe threat[7,8]. To counteract DNA damage, major repair pathways have evolved, which include base excision repair (BER), nucleotide excision repair (NER), mismatch repair, single strand break repair and double strand break repair[9].

1.1.1.1 Base excision repair

BER is responsible for the repair of damaged bases that typically result from oxidation, deamination and methylation. Loss of bases that result in apurinic/apyrimidinic (AP or abasic) sites are also repaired by BER. This type of base damage/loss present a small lesion that does not majorly distort the DNA backbone[10,11]. The initial step of the repair pathway begins with recognition of the damaged site by enzymes, named glycosylases. 11 glycosylases have been discovered in humans, each responsible for damage-specific recognition. After recognition, excision of the damaged base and hydrolysis of

the DNA backbone are carried out by the glycosylases and the AP endonucleases respectively, leaving a single stranded break. This is subsequently filled in with a correct base and ligated by either DNA polymerase β (Pol β) and XRCC1-DNA ligase IIIα (Lig3α) or DNA polymerases δ/ε (Pol δ/ε) and DNA ligase I (Lig1)[12].

1.1.1.2 Nucleotide excision repair

While BER resolves small DNA lesions, nucleotide excision repair (NER) resolves lesions that causes potential distortion of the DNA helix. It is divided into two sub pathways: global genomic repair (GGR) and transcription-coupled repair (TCR). The former recognizes and repairs helix-distorting lesions anywhere in the genome, while the latter repairs lesions that block transcription[13,14]. The first damage recognition step is sensed by DDB1/DDB2 in GGR or the elongating RNAPII in TCR. This is followed by recruitment of TFIIH, which unwinds the DNA and verifies the lesion. Subsequent incision of the DNA around the lesion is carried out by the ERCC1–XPF and XPG endonucleases. After excision, Pol δ, DNA polymerase κ (Pol κ) or Pol ε fill in the DNA, which is ligated by Lig1 or Lig3 in the final step of the pathway to complete repair[15,16].

1.1.1.3 Mismatch repair

The mismatch repair pathway, as the name suggests, is responsible for the correction of DNA mismatches generated during replication. Same as the above mentioned repair pathways, recognition is first carried out by MutSα (heterodimer of MSH2/MSH6) or MutSβ (heterodimer of MSH2/MSH3). Excision of the DNA by MutLα and Exo1 ensues, after which DNA re-synthesis and ligation is carried out respectively by Pol δ and Lig1[17–19].

1.1.1.4 Single strand break repair

Being one of the most common sources of DNA damage, tens of thousands of SSBs arise per cell per day, due to disintegration of the DNA backbone or the generation of intermediates from other repair pathways such as BER[20]. Breaks that occur independently of other repair pathways are sensed by PARP1, which leads to recruitment of XRCC1 protein complexes to process the DNA. Most SSBs, which are the consequence of a single missing nucleotide, are filled by Pol β. A minority of SSBs, which require more than one missing nucleotide to be filled, involve Pol β and/or Pol δ/ε. These two different scenarios lead to different, albeit interchangeable, ways of ligation of the DNA by the XRCC1/Lig3α and PCNA/Lig1 complexes respectively[21].

1.1.1.5 Double strand break repair

Although arising very rarely compared to some other types of DNA damage, at only 10-50 occurrences per cell per day[22], DSBs are considered potentially the most dangerous. DSBs occur when both the two complementary DNA strands are inflicted with breaks in close proximity of each other, leading to two broken ends of the DNA that lose their physical association[23]. If left unrepaired or repaired incorrectly, DSBs could not only trigger carcinogenesis and senescence but also lead to cell death even in the case of only one single unrepaired DSB in the cell[8,24,25]. The severity of DSBs thus highlight the essentiality of DSB repair pathways, in order to avoid the disastrous consequences.

Cells have evolved a number of DSB repair pathways, of which two are the dominant ones: non-homologous end joining (NHEJ) and homologous recombination (HR). In addition to these two primary pathways, there are alternative pathways to repair DSBs. They are single-stranded annealing (SSA) and alternative end joining (AltEJ)[26,27]. AltEJ is sometimes also referred to as microhomology-mediated end joining (MMEJ).

The SSA repair pathway relies on homologous sequences that flank the DSB on both sides of the break. An initial resection step is carried out, after which replication protein A (RPA) coats the single-stranded DNA (ssDNA) (Figure 1.1A)[27]. After displacement of RPA, the homologous sequences are annealed, to form a bridging intermediate. Further processing of the protruding ssDNA ends is performed, to complete repair that results in deletion of DNA between the homologous sequences. As a result, SSA is a relatively mutagenic repair pathway[28,29].

Similar to SSA, AltEJ also requires the presence of homology sequences in close proximity of the DSBs[27]. However, one difference lies in the length of the homologous sequences, which are comparably shorter for AltEJ. AltEJ only requires approximately 2-20 base pairs, while SSA generally requires more than 20 base pairs[30]. AltEJ also begins with resection of the DNA, followed by coating of the ssDNA by RPA. Limited displacement of RPA is followed by alignment of the homologous sequences flanking the DSB. Subsequent gap-filling by DNA polymerase θ (Pol θ) ensues[31]. As AltEJ results in deletions around the break, it is also considered a mutagenic repair pathway, that could potentially lead to genomic instability[32,33].

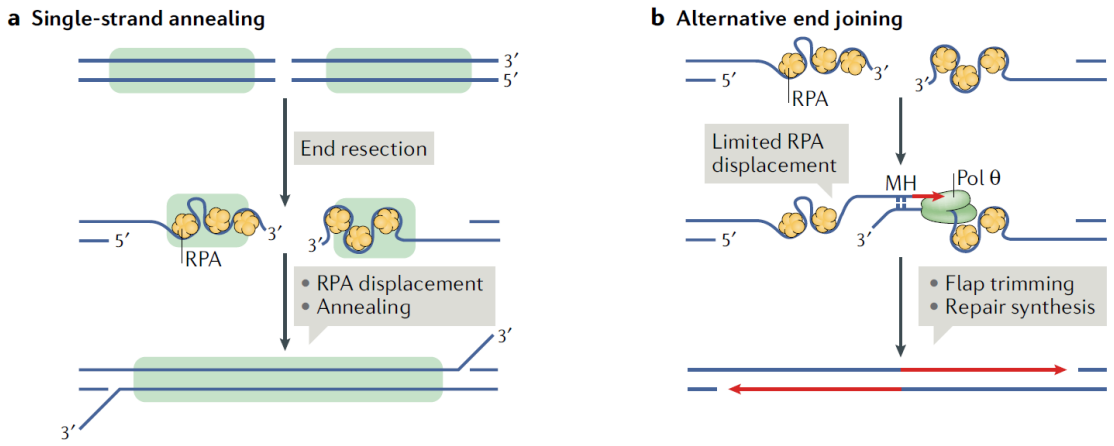

Figure 1.1 Alternative pathways for repairing DSBs (adapted from Scully et al, 2019)[27]**.** **(A)** Schematic of SSA. Resection is first carried out around the DSB, followed by annealing of the homologous sequences in the close proximity of the break and subsequent processing of the protruding ssDNA. While it results in repair of the break, the SSA is potentially mutagenic, due to the deletion of the DNA between the homologous regions. **(B)** Schematic of AltEJ. Resection is first carried out, followed by annealing of the micro-homologous sequences of approximately 2-20 bases pairs in the close proximity of the break. Pol θ subsequently performs gap-filling. Similar to SSA, AltEJ also results in deletions and is considered a mutagenic repair pathway.

NHEJ, as the predominant DSB repair pathway, functions throughout the entire cell cycle, and is responsible for repairing up to approximately 80% of DSBs[30,34]. Initiation begins with binding of the Ku70-Ku80 heterodimer, followed by recruitment of a number of downstream factors (Figure 1.2). One of these factors is DNA-PKcs, which binds to the Ku heterodimer to form a holoenzyme and subsequently phosphorylate repair factors[34]. Although NHEJ does not rely on the presence of homologous sequences and functions to ligate the broken ends in an efficient manner, the broken ends are often incompatible for direct ligation[30]. This therefore calls for another end-processing step that involves factors such as Artemis, DNA polymerase μ (Pol μ) and DNA polymerase λ (Polλ), tyrosyl-DNA phosphodiesterase 1 (TDP1) and polynucleotide kinase 3′-phosphatase (PNKP). After end-processing is completed, a ligation step is carried out by DNA ligase IV and XRCC4, to restore DNA integrity[35]. Despite the high usage of NHEJ, processing of the breaks in the pathway, which could include excision, modification or addition of nucleotides, results in the potential of the pathway to be mutagenic[35–38].

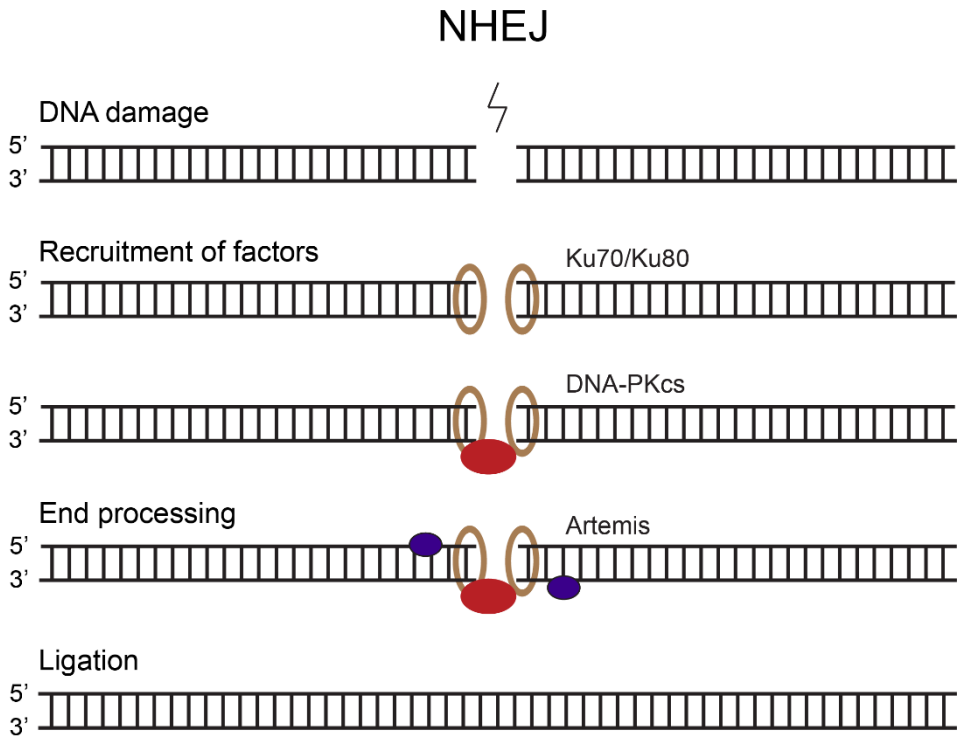

Figure 1.2 NHEJ is the predominant pathway for the repair of DSBs.
Once DNA damage occurs in the form of DSBs, cells frequently make use of NHEJ, to repair the damage. As the initial step, the Ku70-Ku80 heterodimer binds to the broken DNA ends. This is followed by the recruitment of downstream factors, including DNA-PKcs that phosphorylate repair factors. Subsequent end-processing of the breaks is carried out by factors such as Artemis to ensure compatibility of the broken ends for the final ligation step by DNA ligase IV and XRCC4.

The second main DSB repair pathway is HR. In comparison to NHEJ, it is significantly more complex and time-consuming but is advantageous in the sense that it is considered generally error-free[39]. Also unlike NHEJ, which functions in all cell cycle phases, HR only functions in S and G2 phase, when a sister chromatid is present[40]. The multistep pathway begins with short-range resection of the DNA, carried out by the MRE11-RAD50-NBS1 (MRN) complex and CtIP, to generate a 3' ssDNA overhang (Figure 1.3). Further resection of the DNA, named long-range resection, is subsequently performed by nucleases EXO1 and DNA2[41,42]. Once the DNA is resected, RPA coats the ssDNA rapidly. After RPA-ssDNA filaments are formed, RPA undergoes phosphorylation by phosphoinositide 3-kinase (PI3K)-like protein kinase (PIKK) family kinases: ataxia telangiectasia and Rad3-related protein (ATR) and ataxia telangiectasia mutated (ATM), as well as cyclin-dependent kinase (CDK) and DNAPKcs[43,44]. Subsequently, with assistance from BRCA1 and BRCA2, RPA is

displaced by Rad51. This leads to the search of a homologous sister chromatid, strand invasion and finally, accurate repair[45,46].

As discussed above, multiple pathways exist to repair DSBs. This raises the question of how cells make the choice among them to carry out repair. One crucial factor that affects the decision is resection of DNA. Two well established factors, 53BP1 and BRCA1, play opposing roles in driving the decision of pathway choice. 53BP1 forms complexes with additional NHEJ factors to protect the broken ends from resection. BRCA1, on the contrary, promotes resection to carry out HR[47,48]. Resection is also influenced by the cell cycle phase. The activity of CDKs increase as cells enter S-phase, leading to phosphorylation of HR factors such as CtIP, which is an essential factor that contributes to DNA resection and subsequent repair by HR. In addition, the G1 to S phase transition is simultaneously accompanied by the upregulation by other HR factors, promoting HR as the repair pathway of choice in this cell cycle phase[27,49]

Another factor that is taken into account in the pathway choice is the chromatin environment. Recent data imply that the open and active euchromatin regions typically engage HR upon DSB formation, while closed and repressed heterochromatin regions are generally more likely to be repaired by NHEJ[50,51].

Being the hub for the recruitment of downstream NHEJ factors, the Ku70/80 heterodimer has also been suggested to drive pathway choice[52]. It has been well established that the rapid binding of Ku70/80 to DSBs with high affinity is required for triggering DSB repair by NHEJ[53,54]. Moreover, recent findings have revealed that its removal by Valosin-containing protein (VCP)/p97 is also a prerequisite for HR to be carried out[52].

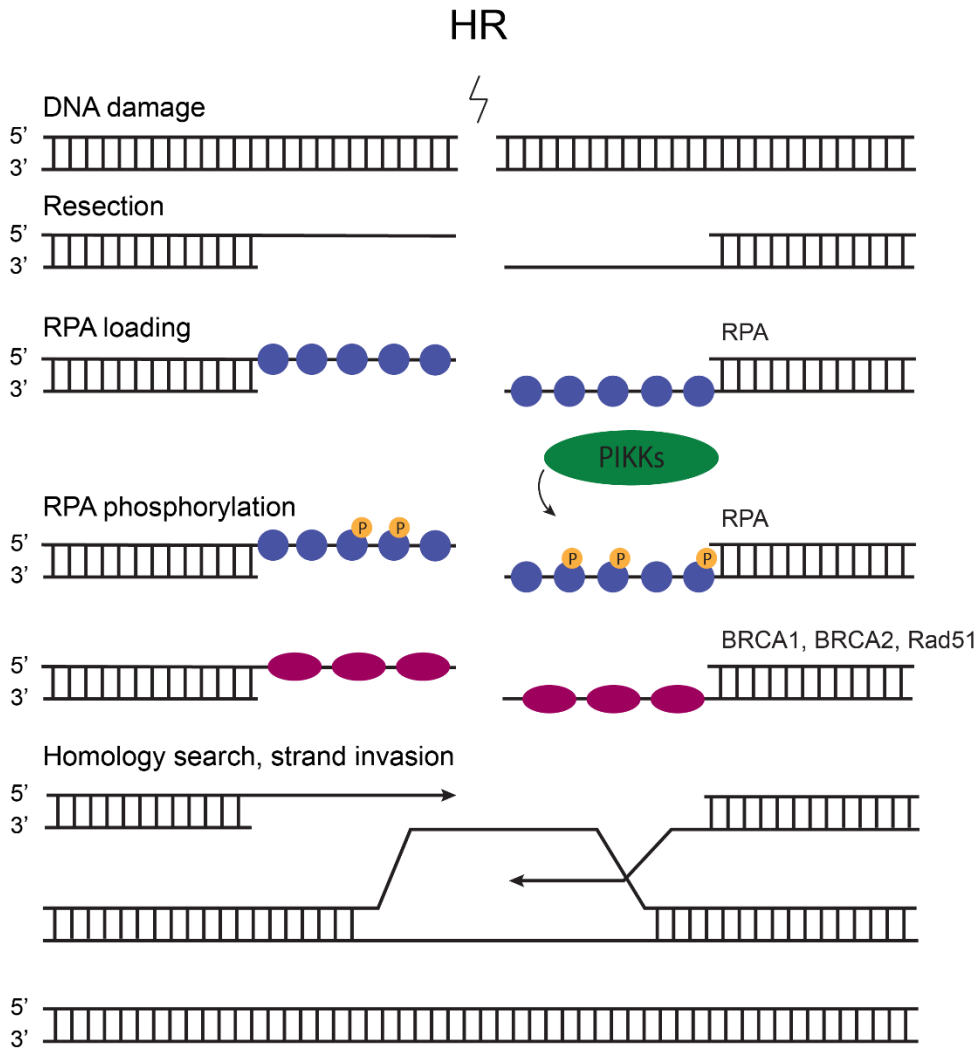

Figure 1.3: HR is considered an error-free pathway to repair DSBs.
After the occurrence of DSBs, initial resection of the DNA is required for HR to be carried out. This is followed by RPA binding to ssDNA, after which it is phosphorylated by PIKKs. With the assistance of factors such as BRCA1 and BRCA2, Rad51 replaces the RPA, to form Rad51-ssDNA filaments. Subsequently, homology search and strand invasion are carried out, leading to accurate repair of the DSB.

1.1.2 Replication stress

The complex process of DNA replication that involves the interplay of numerous factors, is carried out to perform the essential duplication of the genome[55,56]. A serious threat to the process is replication stress. This is defined as endogenous or exogenous stress that affects replication dynamics and creates replication errors[57–59]. A plethora of sources including DNA breaks, lesions, crosslinks, or depletion of dNTPs [60,61] result in replication stress (Figure 1.4). Consequences of replications stress are severe and include initiation of malignancy, senescence and even apoptosis[58,62]. To counteract

this, cells have a few mechanisms to resolve the stress and ensure faithful duplication of DNA.

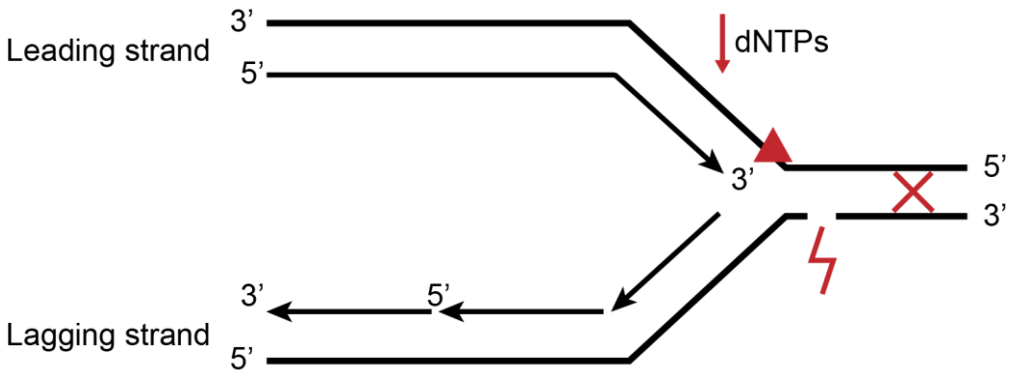

Figure 1.4: Replication stress is a major source of genome instability.
Sources of replication stress (red) include but are not limited to depletion of dNTPs (arrow), lesions (triangle), DNA breaks (gap in the DNA) and crosslinks (cross).

1.1.2.1 Translesion synthesis

Translesion synthesis (TLS) functions as a defence mechanism that is capable of synthesizing DNA past lesions[63]. Proliferating cell nuclear antigen (PCNA) is firstly mono-ubiquitylated[64], after which translesion polymerases DNA polymerase ζ (Pol ζ), DNA polymerase ι (Pol ι), DNA polymerase η (Pol η), DNA polymerase κ (Pol κ), and REV1 are recruited to take over synthesis from the replicative polymerases Pol ε or Pol δ. The accuracy of TLS is low however, due to the polymerases' tolerance of potentially incorrectly incorporated bases and the absence of proofreading[65–67].

1.1.2.2 Re-priming

Another mechanism for overcoming replication stress is re-priming. This occurs downstream of a lesion, mediated by the DnaG primase in *E.coli*, the Pol α/primase complex and Ctf4 in budding yeast, and PrimPol in vertebrates, which possesses both primase and polymerase activities[68]. The damaged DNA is left behind, as ssDNA gaps, to be repaired after replication is completed[69–71].

1.1.2.3 Fork reversal

While fork reversal is now widely acknowledged as a protection mechanism against replication stress, for a long period of time, it was regarded more as a result of replication failure. With the emergence of electron microscopic approaches to visualize reversed forks as well as mounting evidence of numerous factors to play a role in the

pathway, fork reversal is now considered an important response to different types of stress[72,73].

The process begins with unwinding of the newly-synthesized strands from the parental strands, which is followed by the re-annealing of the parental strands (Figure 1.5). In the final step, the newly-synthesized strands are also annealed together, to form a 4-way junction (Figure 1.5 bottom), also referred to as a “chicken foot” structure. The annealed newly-synthesized strands form the regressed arm of the reversed fork[73].

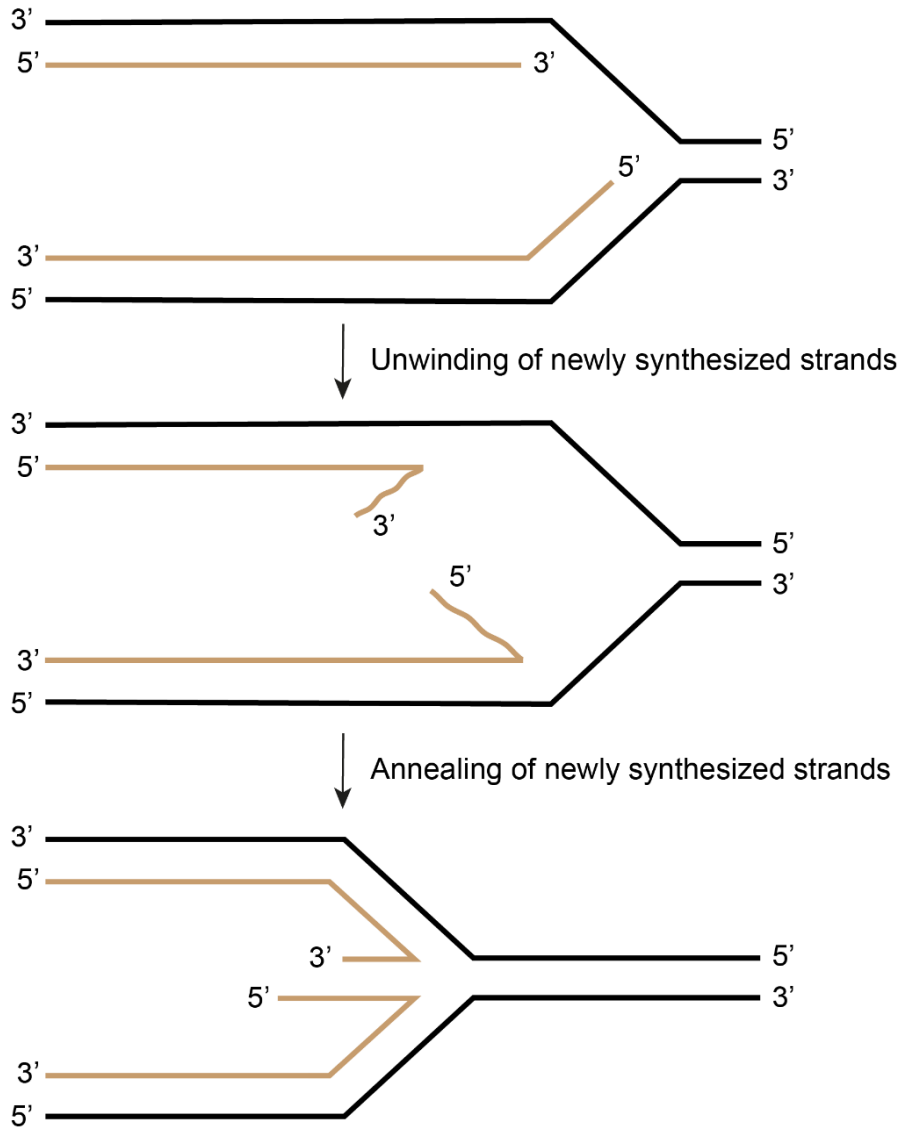

Figure 1.5: The process of fork reversal results in a 4-way junction (adapted from Neelsen and Lopes, 2015)[73]**.**

Fork reversal includes unwinding of the newly synthesised strands, re-annealing of the parental strands and a final annealing of the newly synthesised strands to form the 4-way junction with a regressed arm. Parental strands are shown in black and newly-synthesised strands are shown in brown.

By using electron microscopy, researchers observed clear reversed fork structures (Figure 1.6) and determined the percentage of forks that undergo reversal upon replication stress[74]. Results obtained with electron microscopy showed that approximately 15-30% of forks reverse, with the frequency of fork reversal varying depending on different types of genotoxic stress[74]. Further research in the field has shown that it is not only forks that are directly challenged by lesions to undergo reversal, but other unchallenged forks experience a global slow-down, due to the activation of ATR. This is proposed to afford more time for the repair of the lesions in the template strand and avoid encountering the lesions by ongoing forks[75].

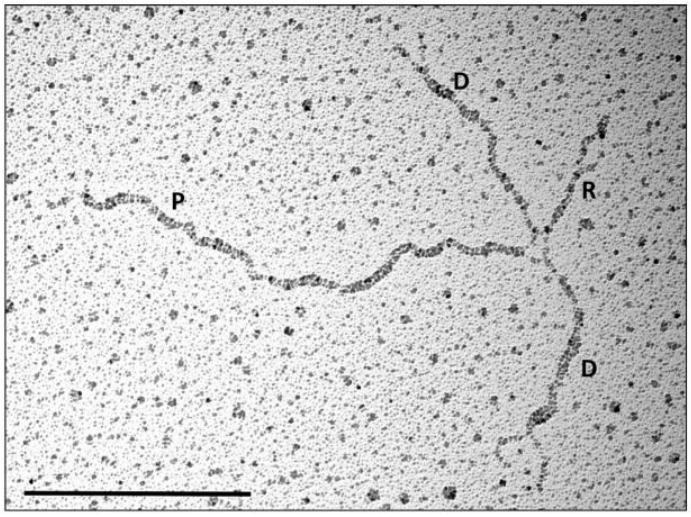

Figure 1.6: Visualisation of a reversed fork structure via electron microscopy (taken from Zellweger *et al*, 2015)[74]**.**
A reversed fork is shown with parental strands (P), daughter strands (D) and the regressed arm (R).

Fork reversal, being a complex pathway, requires the cooperation and involvement of a vast number of factors. In order for the reversal process to occur, so called fork remodellers such as HLTF, ZRANB3 and SMARCAL1 are required[76–78]. In addition to these translocases, Rad51, the well-established homologous recombination factor, was also determined to be a crucial factor for fork remodelling[74]. Fascinating recent studies have shown that Rad51's role lies in the generation of a parental DNA duplex behind the helicase at the stalled forks, which remains bound to the DNA. The parental DNA duplex is subsequently used as a substrate by the above-mentioned DNA translocases to carry out reversal[79].

After the reversal process is completed by the fork remodellers, the final 4-way junction is formed. This acts as a way to stabilize the forks and afford the cells sufficient time to repair potential lesions or take care of sources of stress. However, this structure acts as a double edged-sword, as it resembles one-end of a DSB and when unprotected, can be prone to degradation by nucleases, resulting in degradation of the nascent DNA[73]. Therefore, fork protectors come into play, to ensure the integrity of the reversed forks. Over the past recent years, a substantial number of factors were determined to exert such a protection function. Interestingly, a large subset of these protection factors were originally discovered to be involved in DNA repair pathways such as HR, NHEJ, and Fanconi anemia[72,80,81]. BRCA2, the well-known tumour suppressor that plays an essential role in HR, and WRNIP1, the AAA+ ATPase that interacts with the Werner helicase, are two such examples of protectors of reversed forks[82–84].

Being a protection mechanism against replication stress, fork reversal can produce at least four outcomes that promote genome stability. Firstly, a converging fork from a nearby origin can take over replication from the stalled fork, in order for the DNA to be completely replicated. Second, the process of fork reversal could also be a way to give the cells sufficient time to remove lesions in the template DNA ahead of the fork by excision repair. Third, the re-annealing of the nascent DNA strands could lead to a template switching mechanism to replicate past the source of stress. Finally, recombination-mediated repair can be carried out as another means to resolve the encountered stress[80,85].

As numerous factors have been suggested to be involved in the protection of reversed forks, the natural and curious question arose of why such a number is needed. Findings on WRNIP's role in fork protection came to light and contributed to answering this question. The novel model proposed that BRCA2 protects the regressed arm of the reversed fork from degradation by the MUS81 and MRE11 nucleases, while WRNIP1 protects the junction of the reversed fork from degradation by the SLX4 and DNA2 nucleases (Figure 1.7)[83]. Nevertheless, further research is needed to determine how the various fork protectors cooperate with each other, to achieve a better understanding of the important genome stability-promoting fork reversal pathway.

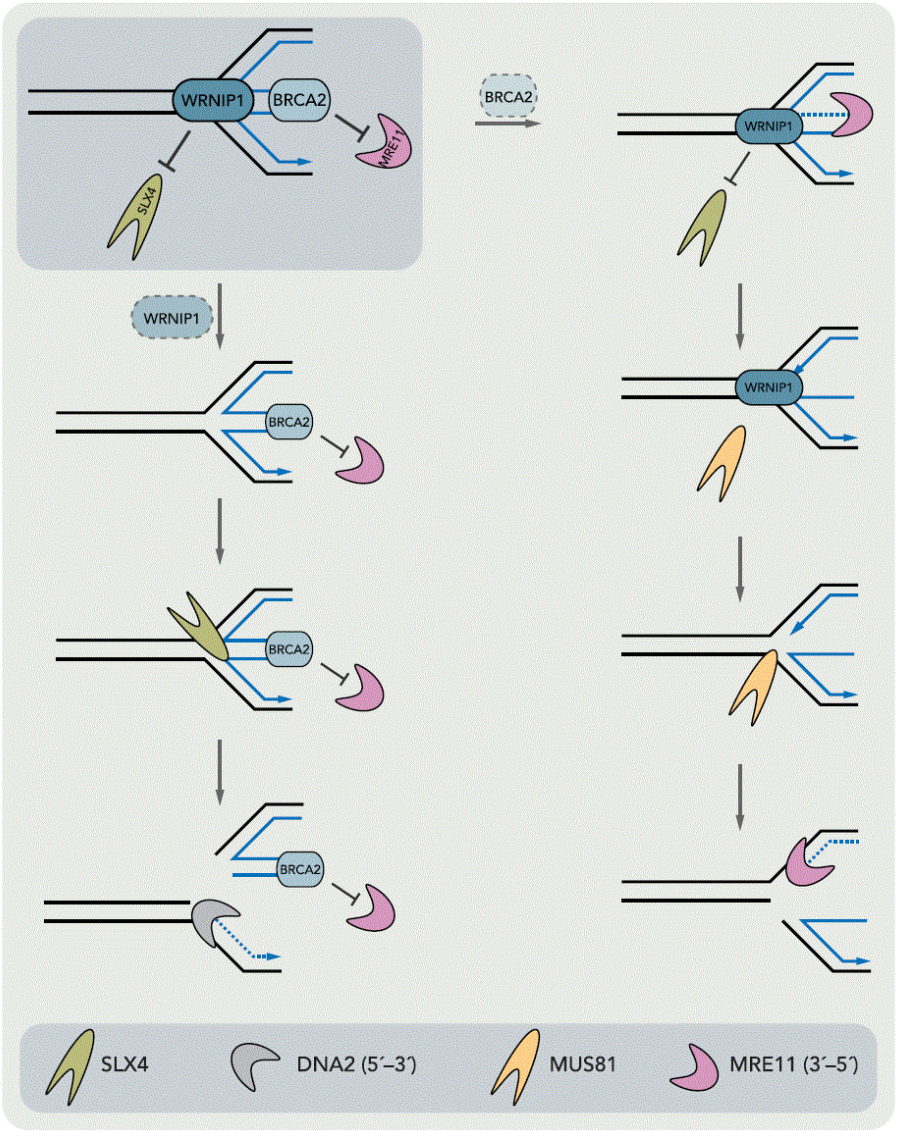

Figure 1.7: Proposed model of two different branches of reversed forks protection (taken from Porebski *et al*, 2019)[83]**.**

BRCA2 is proposed to protect the regressed arm of reversed forks from MUS81/MRE11-mediated degradation while WRNIP1 is proposed to protect the junction of reversed forks from SLX4/DNA2-mediated degradation.

1.1.2.4 Pathway choice for the resolution of replication stress

Similar to the repair of DSBs, cells also face the choice of resolution pathways upon encountering replication stress. Influencing factors include the genetic background, the type of lesion/stress, extent of stress etc[68]. For instance, a cisplatin treatment in cells depleted of the fork reversal remodeller, SMARCAL1, results in PRIMPOL-dependent generation of ssDNA, indicative of re-priming when fork reversal is impaired[86]. A similar observation was made in cells depleted of another fork remodeller, HLTF[77]. PRIMPOL-

dependent re-priming was additionally suggested to occur when cells encounter lesions too bulky for the TLS polymerases[87]. Interestingly, treatments with different concentrations of the same stress-inducing agent give rise to different scenarios. While a high concentration of hydroxyurea (HU) in BRCA1 or BRCA2-depleted cells leads to degradation of forks that have undergone fork reversal[82,88,89], a lower concentration of HU in BRCA-deficient cells results in ssDNA gaps that suggest a shift in preference of re-priming over fork reversal in such conditions[90,91]. To fully understand which pathway the cells favour in which circumstance would be highly beneficial for developing novel therapies in cancer treatment[68].

1.2 The cytoskeleton and its cellular functions

Highly important cellular processes such as cell division, endocytosis, cell mobility, and intra-cellular transport, are just a fraction of the diverse functions carried out by the cytoskeleton[92,93]. Majorly contributing to providing structure and shape to cells, the cytoskeleton is an integral part of the cellular system. It is comprised of a complex meshwork of filaments that includes intermediate filaments, microtubules and actin filaments[94,95].

1.2.1 Intermediate filaments

Intermediate filaments, one of the three components of the cytoskeleton, are highly conserved and comprise of proteins encoded by 73 genes[96,97]. Their functions include the stabilisation of cell shape, cell mechanics, anchorage of organelles, and signal transduction[97,98]. Mutations in proteins that make up intermediate filaments can lead to diseases such as skeletal myopathies, hair disorders etc[96].

1.2.2 Microtubules

Microtubules, formed by heterodimers of globular α- and β-tubulin, take the shape of rigid hollow cylinders. They participate in cellular processes such as cell division, cell motility and intracellular transport[99,100]. Microtubules are dynamic structures that assemble and disassemble. They consist of a plus-end that exposes β-tubulin and a minus-end that exposes α-tubulin[101]. Motor proteins kinesin and dynein assist in the transport of cargo along microtubules in the direction of the plus- and minus-ends respectively[102,103]. Mutations in tubulin have been correlated with brain malformation, cognitive functions impairment, bleeding disorders and infertility[104,105].

1.2.3 Actin filaments

Actin filaments (F-actin), also referred to as microfilaments, is the main source of force generation in cells. This force is used for muscle contraction, cytokinesis, cell migration and intracellular transport[106,107]. F-actin, like microtubules, is also dynamic and undergoes polymerisation as well as de-polymerisation. Generation of the filaments is the result of the polymerisation of globular actin (G-actin) monomers, which creates a plus-end (barbed end) and a minus-end (pointed end). Although G-actin can be added to both ends to elongate the filaments, the polymerisation happens considerably faster at the plus-end[106,108]. Regulators of the polymerisation process include profilins, which

promote actin polymerisation, and the actin de-polymerising factor (ADF)/cofilin family, which promote disassociation of actin monomers from the filament (Figure 1.8)[106,109,110].

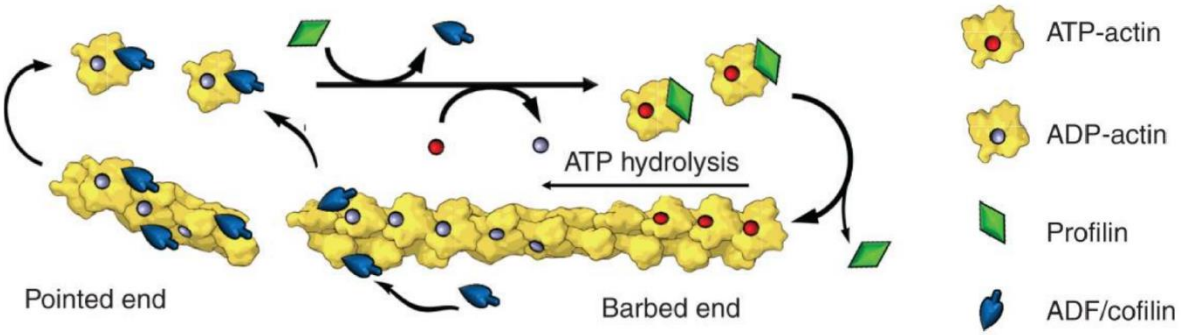

Figure 1.8: **The dynamic polymerisation and de-polymerisation of actin filaments** (adapted from Svitkina, 2018)[106]**.**
Actin filaments consist of a plus-end (barbed end) and a minus-end (pointed end). Polymerisation of actin is promoted by profilins, while de-polymerisation of actin is promoted by ADF/cofilins.

Additional factors, termed actin nucleators, are required for the *de novo* polymerisation of actin. They are categorized into three major classes: the Arp2/3 complex, formins, and the Spire proteins[111]. Of these, Arp2/3, promotes the initiation of branched actin filaments, while formins and the Spire proteins promote unbranched filament nucleation[112,113].

1.2.3.1 Actin filaments in the nucleus and its nuclear functions

Although the functions of cytoplasmic F-actin have been researched in-depth and are well-accepted, the existence and functionality of nuclear F-actin were controversial for a long time[114]. A main cause of this is the extremely high abundance of cytoplasmic actin. Research methods such as microscopic approaches to detect nuclear actin filaments were hindered by the strong cytoplasmic signal. Cell fractionations to separate the different cellular compartments was difficult to accomplish due to contamination of the nuclear fraction by the large cytoplasmic pool of actin. In addition, genetic manipulation of actin could result in modifications of both cytoplasmic and nuclear actin, rendering distinction of the functions of the two compartments arduous[115,116].

An important further development in the nuclear actin field was the development of a new tool to visualise nuclear actin. This tool, from hereon termed actin chromobody, consists of an anti-actin single chain antibody with a GFP tag and nuclear localisation

signal (NLS). The NLS targets the probe to the nucleus, where actin is bound by the chromobody, which is visualised via the GFP tag[117]. With this novel tool, functions of nuclear F-actin were clearly revealed in DSB repair (Figure 1.9)[118] as well as the replication stress response[119–121]. In the fruit fly *Drosophila melanogaster*, it was shown to be required for the re-localization of DSBs in heterochromatin to the nuclear periphery to promote and carry out repair by HR[119]. In human cells, nuclear F-actin was also demonstrated to promote HR for the repair of DSBs. Not only is it involved in the resection step of HR, but its polymerization also mobilizes a subset of DSBs to form clusters that could act as repair domains[120]. A short while after these findings came to light, research in human cells showed the importance of nuclear F-actin in the increase of nuclear volume and sphericity upon replication stress, to prevent deformation of the nuclei. Interestingly, under such conditions, F-actin was additionally found to be involved in the mobility of stressed-replication foci, similar to the described mobility of DNA breaks in *Drosophila melanogaster*[119,121].

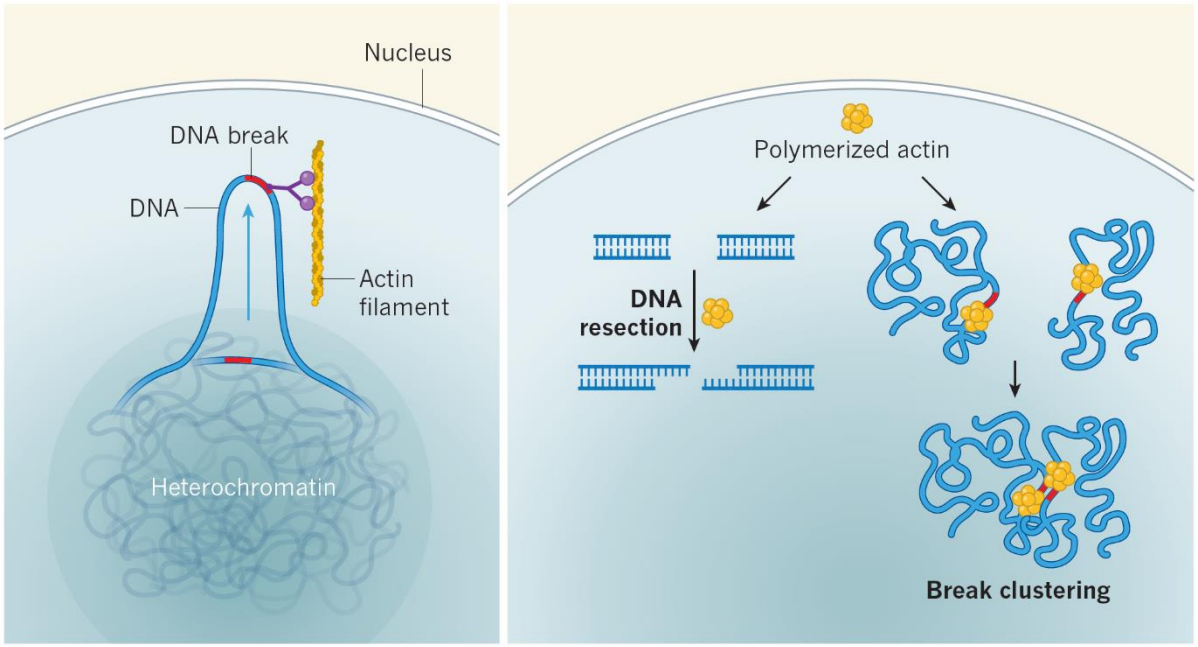

Figure 1.9: **The functions of nuclear F-actin in DSB repair** (adapted from Roukos, 2018)[118]**.** Left: In *Drosophila melanogaster*, F-actin re-localizes DSBs in heterochromatin to the nuclear periphery. Right: In human cells, F-actin is involved in DSB repair by promoting resection in the HR pathway and additionally drives clustering of a subset of the breaks.

1.2.4 Actin-based motor proteins

While actin exerts a large variety of functions within the cell, it does not work alone. It is supported by motor proteins, myosins, which move along the actin filaments,

supporting its role in force generation and various cellular processes[122]. The filaments provide a track for the myosins, on which they transport cargo such as vesicles, organelles, other cellular components, or carry out their anchoring function[123].

1.2.4.1 The superfamily of myosins

The structure of myosins typically includes a motor domain for its interaction with actin, a neck region (also referred to as the lever arm) for amplification of movement and a tail domain that is involved in cargo-binding[124,125]. In addition to containing an actin-binding site, the motor domain harbours an ATP-binding site that hydrolyses ATP as the energy source to power the movement of the myosin. It is highly conserved among the more than 40 classes of myosins discovered so far[122,123]. The tail domains, on the other hand, are vastly diverse, varying in lengths and sequences among the different myosins[125].

The numerous classes of myosins are categorized into conventional myosins and unconventional myosins. The class II muscle myosin group belongs to the conventional myosins group and as the name suggests, plays an essential role in muscle contraction[126]. Extensive research have been carried out on the functions of unconventional myosins and they have been well-established to be involved in a large number of cellular processes in the cytoplasm such as cargo trafficking, as mentioned above. Although the notion of nuclear myosins was initially controversial, several myosins, nuclear myosin I, non-muscle myosin II, myosin Va and b, myosin VI, myosin X, myosin XVI, and finally myosin MVIII have been identified and characterised[127,128].

Over the past years, diverse functions of the nuclear myosins have gradually emerged. Examples of such include the role of nuclear myosin I in transcription, the role of both nuclear myosin I and myosin V to drive the re-localisation of DSBs in heterochromatin on actin filaments and the involvement of myosin V in viral replication[119,129,130].

1.2.4.2 Myosin VI: the only minus-end directed motor protein

Like the other myosins, myosin VI (myo6) comprises of a motor domain, a neck region, and a tail domain (Figure 1.10)[131]. However, it stands out in its uniqueness of being the only myosin discovered so far to walk towards the minus-end of actin filaments. This is due to an insertion in the neck region of the myosin that acts as a reverse gear[132,133]. In the neck region, there is also an IQ domain that binds calmodulin. Following the neck region, contained within the tail domain, is a bundle of three α-helices (3HB), a

single α-helix (SAH), two ubiquitin-binding domains (MIU and MyUb), and the cargo-binding domain (CBD) (Figure 1.10)[131].

The 3HB takes either the folded form or the extended form, which provides myo6 with the ability to take large steps on actin filaments. It was revealed that dimerisation of myo6 monomers occurs between Leu913 (last residue of the three helix bundle) and Arg940[134]. The dimerisation of myo6 is regarded as necessary for its motor activity, upon which it can walk on F-actin in a "hand-over-hand" fashion (Figure 1.11)[135]. The dimer consists of two "heads" of myo6, one of which is considered the leading head and the other the lagging head. The stepping cycle begins with binding of ATP to one myo6 motor, the leading head, releasing it from actin. This is followed by ATP hydrolysis that drives the power stroke, resulting in an approximately 72 nm displacement of the head. The final step is the re-binding of the myo6 head to actin, after which this leading head becomes the lagging head, leading to the next round of the cycle[135,136].

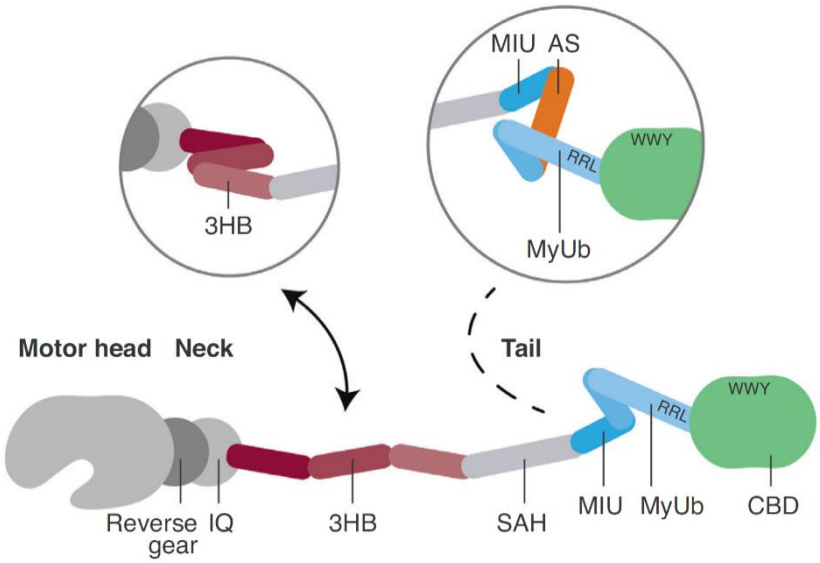

Figure 1.10: **The structure of myo6** (adapted from Magistrati and Polo, 2021)[131]**.**
Myo6 comprises of a motor head, a neck region that contains its reverse gear and a tail domain that harbours two ubiquitin-binding domains as well as interaction sites for its binding partners (RRL and WWY).

Between the 3HB and the CBD lie the two ubiquitin binding domains, MIU and MyUb, the latter of which was shown to preferentially bind to K63-linked polyubiquitin chains[137]. Intriguingly, an alternatively spliced (AS) region is located between the two ubiquitin-binding domains, which leads to the production of the long-isoform and short-isoform of myo6. The splicing involves the inclusion or exclusion of an α-helix and creates a

slight conformational difference in the structure of the isoforms, which leads to the binding of different interaction partners of the long and short isoforms[138]. Binding of other various interactors can also be achieved via the RRL and WWY motifs, both located within the tail domain (shown in the blue and green regions of Figure 1.10)[131,139].

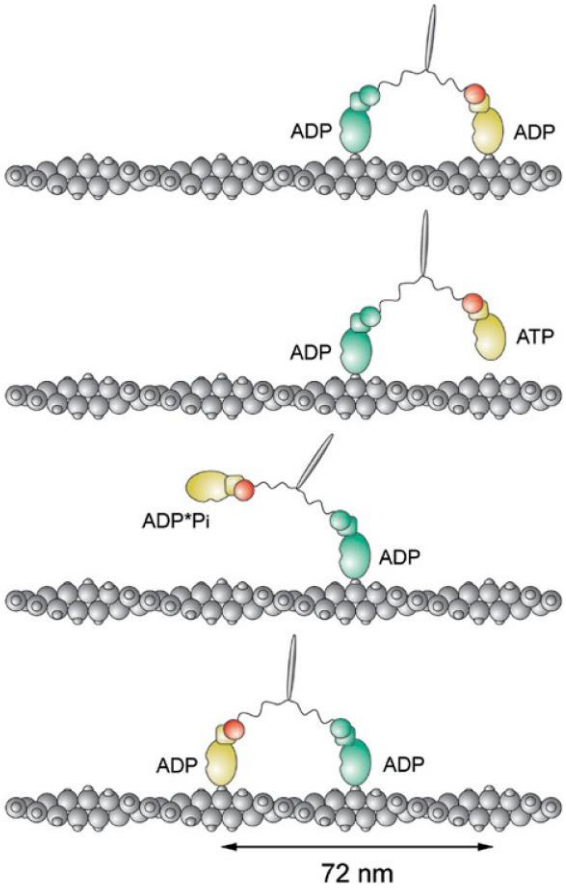

Figure 1.11: **The hand-over-hand model of myo6 walking on actin filaments** (adapted from Ökten *et al*, 2004)[135]**.**

The cycle begins with the binding of ATP to one myo6 head. This leading head is released from actin, after which it hydrolyses ATP for its power stroke. The cycle ends with re-binding of the leading head to actin, after which it becomes the lagging head, to restart the cycle.

1.2.4.3 The functions of myosin VI

The numerous diverse interaction partners of myo6 provide it with the ability to be involved in various cellular functions such as endocytosis, autophagy, cell migration, and differentiation of cochlear hair cells[140–143]. Maintaining a balance of myo6 expression levels in cells is of high importance, as mutations in myo6 are associated with deafness[144], while its overexpression has been found in ovarian and prostate cancers[145,146]. Down-regulation of myo6's expression resulted in impaired migratory

abilities of the cancer cell lines[145,146]. Interestingly, upon DNA damage, its expression level is either up regulated in a p53-dependent manner or down regulated, which varies among different types of cancer cells[147,148].

Similar to actin, the cytoplasmic functions of myo6 have been well-characterised, while its functions in the nucleus, except for its role in transcription, remain largely elusive. It was shown that myo6 interacts with RNA polymerase II (RNAPII) and enhances its activity[149,150]. Recent findings determined myo6 to act as an anchor that maintains RNAPII in clusters, uncovering a clearer understanding of myo6's role in gene expression[151]. Nevertheless, further research needs to be undertaken to unveil other nuclear functions of myo6.

We have discovered two more nuclear function of myo6. One is the function of myo6 in DSB repair, in which we propose myo6 to promote HR, by assisting in the removal of the Ku heterodimer from DSBs. The other function of myo6 is to protect reversed forks[152]. We found myo6 to cooperate with WRNIP1 in the protection of reversed forks from DNA2-mediated degradation and propose a potential mechanism where myo6 ensures proper localisation of WRNIP1 to the reversed forks for protection. Both areas of research will be discussed in detail in the results section of this thesis.

1.3 Tools for the detection and manipulation of target proteins

Antibodies have long dominated as binders for target proteins, and still remain an invaluable tool for many cell biology and biochemistry applications. Fluorescently-labelled antibodies play a crucial role in immunofluorescence microscopy, to determine the localisation and abundance of proteins of interest. Furthermore, there is a high usage of antibodies in biochemical techniques such as ELISA and Western blotting, as well as flow cytometry, for the detection of proteins[153]. While antibodies have been widely used and provided great assistance in numerous techniques, as described above, limitations are nevertheless present. These include their big size, difficulty in penetrating solid tissues, and complex and expensive manufacturing procedures[154–156]. This has led to the development of novel binding molecules such as nanobodies and DARPins.

1.3.1 Nanobodies

Antibodies comprise of two heavy chains and two light chains, resulting in a relatively high molecular weight of approximately 150 kDa, in the case of IgG antibodies. Some time ago, a discovery of IgG-like molecules was made in animals belonging to the Camelidae family. They do not contain light chains but only heavy chains that include a variable region (VHH) for binding antigens, and were thus named heavy chain only antibodies (HCAb)[157]. Although the size of HCAbs are significantly smaller than antibodies, at approximately 90 kDa, they were shown to be highly capable in binding antigens. Further research determined the even smaller VHH domain, at approximately 15 kDa, to bind to a wide range of antigens alone. In this manner, nanobodies were established (Figure 1.12)[158]. Currently, not only are nanobodies used for immunofluorescence microscopy, structural biology, to name a couple of research techniques, but they have also entered the diagnostics and therapeutics fields[158–160]. There is ongoing clinical investigation into a number of nanobodies designed for treating diseases such as inflammation, infectious diseases, breast cancer, brain tumours etc[155]. The wide range of important applications of nanobodies highlight their value as a newly emerged technology.

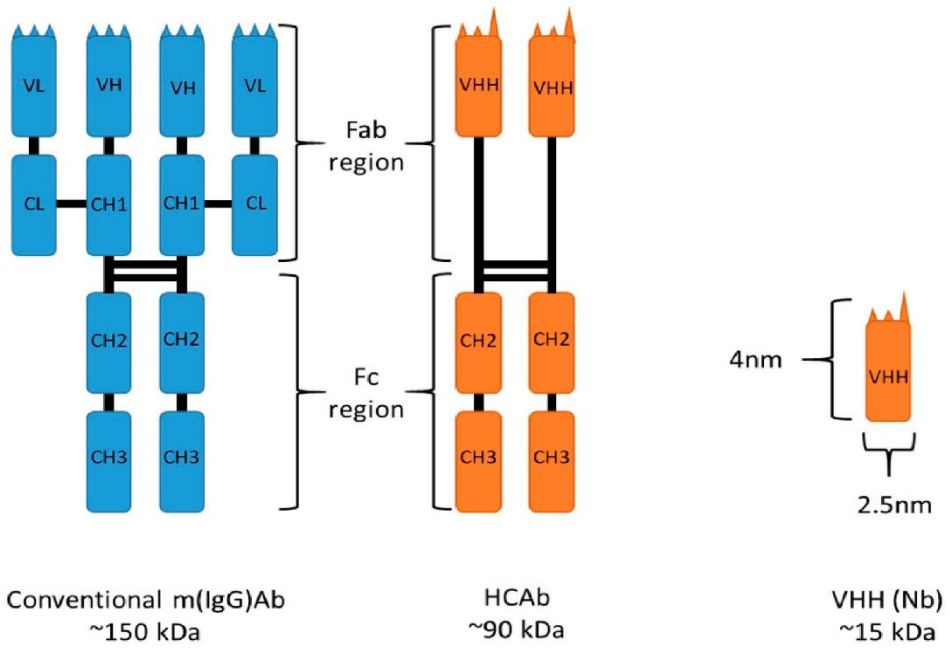

Figure 1.12: **Schematic of the structures of conventional antibodies, heavy chain only antibodies (HCAb) and nanobodies (VHH)** (adapted from Jin *et al*, 2023)[158]**.**
Conventional antibodies consist of two heavy chains and two light chains with variable domains and constant domains in both chain types. HCAb consists only of heavy chains that include variable domains and constant domains. Nanobodies are derived from HCAbs, consisting only of a VHH domain. VL: Variable domain in light chain, VH: Variable domain in heavy chain, CL: Constant domain in light chain, CH: Constant domain in heavy chain, FC: fragment crystallisable region, Fab: fragment antigen-binding region.

1.3.2 DARPins

Another group of small molecule binders have emerged, in the form of repeat protein scaffolds. These repeat proteins come in a diverse variety and have been found in many protein-protein interactions in nature. Examples include the leucine rich repeat (LRR), the tetratrico peptide repeat (TPR) and the ankyrin repeat[161–163]. The repeat proteins typically comprise of repeats of 20-50 amino acids, resulting in stacked motifs that constitute a stable elongated structure and have the potential for a large binding area to target proteins[154].

DARPins (designed ankyrin repeat proteins), as evident from the name, consist of ankyrin repeats and are derived from natural proteins that contain such repeats[156]. The ankyrin repeats typically come in the number of two or three and generally sit between N- and C- capping motives at both ends (Figure 1.13)[164]. This creates a small proteins with a molecular weight of 14-21 kDa[156]. Libraries of DARPins have been generated,

the most common method of which is ribosome display. The process starts with a DNA library that is subjected to polymerase chain reactions (PCRs), after which *in vitro* transcription and translation are carried out, resulting in a ternary complex of mRNA, a ribosome and the translated protein (DARPin). The binding ability of this complex is then tested against the immobilized target protein. If binding is achieved, the DNA of the DARPin is recovered via reverse transcription PCR (RT-PCR). A library size of 10^{12}-10^{14} candidates can be screened through this method[156,165].

The diverse applications of DARPins include their usage as inhibitors of target proteins, as chaperones to assist with crystallography, as binding partners for small proteins in cryoelectron microscopy to name a few[166,167]. Moreover, they have become promising in treating macular degeneration diseases and as antiviral, antitumor candidates, indicating their high potential in the therapeutics field, where new drugs and therapies are continuously sought-after[166,168,169].

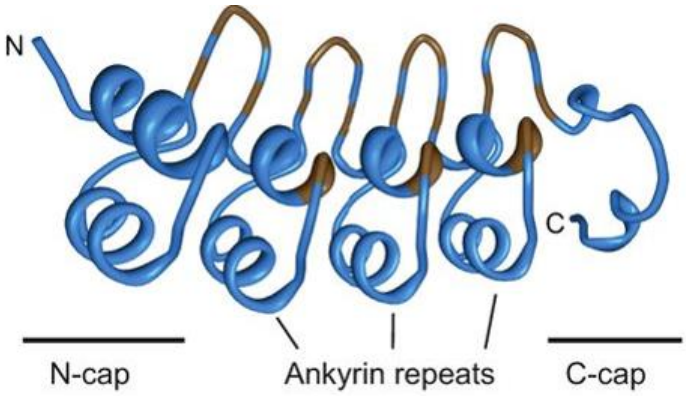

Figure 1.13: **Schematic of a DARPin** (adapted from Harmansa and Affolter, 2018)[164]**.** DARPins generally consist of two to three ankyrin repeats, capped at both N- and C- terminals. They typically have a molecular weight of 14-21 kDa.

Chapter 2

Material and methods

2.1 Reagents

2.1.1 Chemicals

Table 1: A list of the most important used chemicals in this thesis.

Chemical	Source	Catalogue no.
Amersham ECL Prime Western Blotting Detection Reagent	VWR International	RPN2236
Amersham ECL Select Western Blotting Detection Reagent	VWR International	RPN2235
Bovine serum albumin (BSA)	Sigma-Aldrich	A7906
Camptothecin (CPT)	Sigma-Aldrich	C9911
CK-666	Sigma-Aldrich	SML0006
Dimethyl sulfoxide (DMSO)	Fisher Scientific	15605470
DNA2 inhibitor C5	Aobious	AOB9082
Doxycycline hydrochloride (DOX)	Sigma-Aldrich	D3447
Hydroxyurea (HU)	Sigma-Aldrich	H8627
MG-132	Enzo Life Sciences	BML-PI102-0025
MRE11 inhibitor Mirin	Sigma-Aldrich	M9948
Prestained protein ladder	Fisher Scientific	11822124
ProLong Diamond Antifade Mountant	Fisher Scientific	15205739
5-Chloro-2′-deoxyuridine (CldU)	Sigma-Aldrich	C6891
5-Iodo-2-deoxyuridine (IdU)	Sigma-Aldrich	I7215

2.1.2 Antibodies

Table 2: A list of the primary antibodies used in this thesis.

Dilution of the antibodies refers to Western blotting experiments, unless otherwise specified.

Antibody	Species	Source	Catalogue no.	Dilution
alpha-Tubulin	Rabbit pAb	CST	2144	1:1000
BrdU (BU1/75)	Rat mAb	Abcam	ab6326	1:50 (DNA fibre assay)

BrdU (B44)	Mouse mAb	BD Biosciences	347580	1:50 (DNA fibre assay)
GAPDH	Goat pAb	Novus Biologicals	NB300-320	1:1000
GFP	Mouse mAb	Roche	11814460001	1:1000
Histone H2B (53H3)	Mouse mAb	CST	2934	1:1000
Myo6	Rabbit pAb	Wollscheid *et al*[138]	-	1:1000
Phospho-RPA32 (T21)	Rabbit pAb	R&D Systems	AF6654	1:1000
Phospho-RPA32 (S33)	Rabbit pAb	Biomol	A300-246A	1:1000

Table 3: A list of the secondary antibodies used in this thesis.

Dilution of the antibodies refers to Western blotting experiments, unless otherwise specified.

Antibody	**Species**	**Source**	**Catalogue no.**	**Dilution**
Rabbit HRP	Goat	Dako	P044801-2	1:10000
Mouse HRP	Goat	Dako	P044701-2	1:10000
Goat HRP	Rabbit	Dako	P044901-2	1:10000
Camelid VHH	Rabbit	GenScript	A01861	1:5000
Mouse Alexa Fluor 647	Goat	Life	A-21236	1:100 (DNA fibre assay) 1:1000 (immunofluorescence)
Rat Alexa Fluor 488	Goat	Invitrogen	A-11006	1:100 (DNA fibre assay) 1:1000 (immunofluorescence)

2.2 Media and solutions

2.2.1 Media

E.coli cells were grown either in Luria Broth (LB) medium or LB-plates. 100 µg/ml ampicillin or 30 µg/ml kanamycin were added to the LB medium, the LB-plates already contained the respective antibiotic. LB medium, LB-plates and antibiotics were provided by IMB's Media Laboratory.

Human A549, U2OS and HEK293 cells were cultured in Dulbecco's Modified Eagle Medium (DMEM) supplemented with 2 mM L-glutamine, 100 U/ml penicillin, 100 µg/ml

streptomycin and 10% (v/v) fetal bovine serum (FBS). U2OS FlpIn cells were cultured under the same conditions, but with the addition of 150 µg/ml hygromycin.

2.2.2 Solutions

IMB's Media Laboratory provided the following solutions: 10x SDS running buffer, 10x TBE buffer, 5x PBS, 1 M Tris-HCl pH 7.5, 1 M KCl, 2 M $MgCl_2$, 0.5 M EDTA pH 8.0, 5 M NaCl. Other solutions used in this thesis are listed below.

Table 4: A list of solutions used in this thesis.

Solution	Composition
Blocking buffer (Western blot)	5% (w/v) skim milk powder in PBST
Blocking buffer (DNA fibre assay)	2% (w/v) BSA in PBST
Blocking buffer (Immunofluorescence staining)	3% (w/v) BSA in PBS
Cell fractionation buffer A	10 mM HEPES pH 7.5, 10 mM KCl, 1.5 mM $MgCl_2$, 0.34 M sucrose, 10% (v/v) glycerol with freshly supplemented 1x SIGMAFAST Protease Inhibitors EDTA-free (Sigma-Aldrich) and 1mM DTT
Cell fractionation buffer B	20 mM HEPES pH 7.5, 3 mM EDTA, 125 mM potassium acetate, 10% (v/v) glycerol 1.5 mM $MgCl_2$, 0.5% (v/v) IGEPAL, with freshly supplemented 1x SIGMAFAST Protease Inhibitors EDTA-free (Sigma-Aldrich) and 1 mM DTT
Cell lysis buffer (DNA fibre assay)	200 mM Tris-HCl pH 7.4, 50 mM EDTA, 0.5% SDS
Fixation solution (Immunofluorescence staining)	4% (v/v) formaldehyde (Sigma-Aldrich) in PBS
PBST	1x PBS, 0.1% (v/v) Tween 20
PI staining buffer	1x PBS, 20 µg/ml RNAse A (Sigma Aldrich), 100 µg/ml propidium iodide (PI)
Ponceau S staining solution	0.1% (w/v) Ponceau S in 5% (v/v) acetic acid
RIPA buffer	50 mM Tris-HCl pH 7.5, 150 mM NaCl, 1% IGEPAL CA-630, 0.5% sodium deoxycholate, 0.1% SDS, 2.5 mM $MgCl_2$
Trans-Blot Turbo buffer	1x Trans-Blot Turbo buffer (Bio-Rad), 20% ethanol

2.3 DNA oligos

Table 5: A list of the DNA oligos used in this thesis.

ID is the oligo number in the Ulrich lab database.

ID	Oligo	Sequence
5593	M6G4 for_HINDIII	CCCAAGCTTATGGACCTGGGTAAGAAACTGCTGG
5594	M6G4 rev_NHEI	CTAGCTAGCTAGCAGATTTCTGCAGAACTTCAGCG
5597	EGFP for_HINDIII	CCCAAGCTTATGGTGAGCAAGGGCGAGGA
5612	FLAG_SalI_fwd	ACGCGTCGACGATTACAAGGATGACGACGATAAGG
5613	SPOP_NotI_rev	ATAAGAATGCGGCCGCTCATGGGGGTCCCAGAAAAG
5640	M6G4 rev_XhoI	CCGCTCGAGTAGCAGATTTCTGCAGAACTTCAGCG
5641	3xNLS for_KpnI	GGGGTACCCCATGGGGGCCCAG
5642	Puro resistance for_HinDIII with flag sequence	CCCAAGCTTATGGATTACAAGGATGACGACGATAAGAC CGAGTACAAGCCCAC
5643	Puro resistance rev_BsrGI	TGTACAAGGCACCGGGCTTG
5688	E3_5 rev_NheI	CTAGCTAGCTTGCAGGATTTCAGCCAGGTC

2.4 Plasmids

Table 6: A list of the plasmids created during this study.

ID is the plasmid number in the Ulrich lab database.

ID	Plasmid	Construction	Use
4912	pCDNA5 FRT TO EGFP-M6G4-2xRING	PCR amplification of pHU4009 using oHU5597 and oHU5594. Cloning into pHU4758 digested with HINDIII and NHEI.	Targeted degradation of myosin VI
4913	pCDNA5 FRT TO EGFP-M6G4-1xRING	PCR amplification of pHU4009 using oHU5597 and oHU5594. Cloning into pHU4757 digested with HINDIII and NHEI.	Targeted degradation of myosin VI
4956	pENTR4-SPOP-E3_5	PCR amplification of pHU4475 using oHU5612 and oHU5613. Cloning into 3957 digested with SalI and NotI.	Gateway cloning
4957	pENTR4-SPOP-M6G4	PCR amplification of pHU4476 using oHU5612 and oHU5613. Cloning into 3957 digested with SalI and NotI.	Gateway cloning
4958	pDEST-TO-YFP-FRT-E3_5	Gateway cloning. Recombination of pHU4674 into 1803 using recombinase from PPCF	Recombination into FlpIn cells

4959	pDEST-TO-YFP-FRT-M6G4	Gateway cloning. Recombination of pHU4673 into 1803 using recombinase from PPCF	Recombination into FlpIn cells
4960	pDEST-TO-YFP-FRT-SPOP-E3_5	Gateway cloning. Recombination of pHU4956 into 1803 using recombinase from PPCF	Recombination into FlpIn cells
4961	pDEST-TO-YFP-FRT-SPOP-M6G4	Gateway cloning. Recombination of pHU4957 into 1803 using recombinase from PPCF	Recombination into FlpIn cells
5052	pENTR4-NLS-E3_5	PCR amplification of pHU4050 using oHU5641 and oHU5360. Cloning into 1788 digested with KpnI and XhoI.	Gateway cloning
5053	pENTR4-NLS-G4	PCR amplification of pHU3952 using oHU5641 and oHU5640. Cloning into 1788 digested with KpnI and XhoI.	Gateway cloning
5054	pDEST-TO-YFP-FRT-NLS-E3_5	Gateway cloning. Recombination of pHU5052 into 1803 using recombinase from PPCF	Recombination into FlpIn cells
5055	pDEST-TO-YFP-FRT-NLS-G4	Gateway cloning. Recombination of pHU5053 into 1803 using recombinase from PPCF	Recombination into FlpIn cells
5056	pCDNA5 FRT TO EGFP-E3_5-2xRING	PCR amplification of pHU4008 using oHU5597 and oHU5688. Cloning into pHU4758 digested with HINDIII and NHEI.	Control DARPin for targeted degradation of myosin VI

Table 7: A list of the plasmids generated by others and used in this thesis.

ID is the plasmid number in the Ulrich lab database.

ID	Plasmid	Use	Source
2527	p3xFlag-CMV-7.1 expression _vector	Mammalian expression of N-terminal Flag fusion protein	[redacted]
2535	pEGFP-C1	Mammalian expression of N-terminal EGFP fusion protein	[redacted]
2905	pEGFP-MyosinVI-FL-iso2	overexpression of GFP-Myo6 in mammalian cell culture	[redacted]
2908	pEGFP-MyosinVI-Tail-iso2	overexpression of GFP-Myosin VI-Tail domain isoform 2 in mammalian cell culture	[redacted]

3819	pCMV-NES-3G61(GFP-DARPin)-SNAP	overexpression in mammalian cell culture	[redacted]
3920	pmCherry-C1-R62D actin-3XNLS-P2A	overexpression of the polymerization-dead actin mutant in the nucleus	Addgene #58477
3952	pCMV 3xNLS-M6G4-mRUBY	overexpression in mammalian cell culture system - sensor/trap for nuclear Myosin VI	[redacted]
4050	3xNLS-E3_5-mRUBY	Overexpression of E3_5 control DARPinin mammalian cell culture	[redacted]
4475	E3_5-SPOP	Control DARPin for DOX induced nuclear degradation system	[redacted]
4476	M6G4-SPOP	Myosin VI-G4 DARPin for DOX induced nuclear degradation of myosin VI in mammalian cells	[redacted]
4636	pcDNA5/FRT/TO	Genomic integration vector for tetracycline-inducible expression of proteins in mammalian cells.	[redacted]
4757	pCDNA5 FRT TO GNb-1xRING	Targeted degradation of GFP-tagged proteins	[redacted]
4758	pCDNA5 FRT TO GNb-2xRING	Targeted degradation of GFP-tagged proteins	[redacted]
5356	pEGFP Myo6 Tail iso2 AAA	overexpression in mammalian cell culture	[redacted]
5358	pEGFP Myo6 Tail iso2 A1013G, I1104A	overexpression in mammalian cell culture	[redacted]
5383	pEGFP Myo6 Tail iso2 WLY	overexpression in mammalian cell culture	[redacted]
5498	pEGFP Myo6 Tail iso2 DNA bdg mut	overexpression in mammalian cell culture	[redacted]
5453	p3xFlag-CMV_YFP_NES_Myo6_tail	overexpression studies in mammalian cell culture	[redacted]
5463	p3xFlag-CMV_YFP_3xNLS_Myo6_tail	overexpression studies in mammalian cell culture	[redacted]

2.5 siRNAs

Table 8: A list of the siRNAs used in this thesis.

siRNA	Source	Catalogue no.
Allstars negative control siCtrl	Qiagen	SI03650318

siBRCA2 FlexiTube GeneSolution GS675	Qiagen	GS675
siHLTF Silencer Select	Thermo Fisher Scientific	s13137
siMyo6 FlexiTube #5	Qiagen	SI03142692
siMyo6 FlexiTube #7	Qiagen	SI04243351
siMyo6 FlexiTube #8	Qiagen	SI04370737
siMyo6 FlexiTube #10	Qiagen	SI04998749
siRad51 Silencer Select	Thermo Fisher Scientific	s531930
siRad51 Silencer Select	Thermo Fisher Scientific	s11734
siSMARCAL1 FlexiTube #1	Qiagen	SI00103180
siSMARCAL1 FlexiTube #3	Qiagen	SI00103194
siWRNIP1 FlexiTube GeneSolution GS56897	Qiagen	GS56897
siZRANB3 Silencer Select	Thermo Fisher Scientific	s38488
siZRANB3 Silencer Select	Thermo Fisher Scientific	s224929

2.6 Strains and cell lines

2.6.1 Bacterial strains

Table 9: A list of the bacterial strains used in this thesis.

ID is the strain number in the Ulrich lab database.

ID	Strain	Use	Source
14	Top Ten	F– mcrA Δ(mrr-hsdRMS-mcrBC) φ80lacZΔM15 ΔlacX74 recA1 araD139 Δ(ara-leu)7697 galU galK λ– rpsL(StrR) endA1 nupG	Cloning

2.6.2 Mammalian cell lines

Table 10: A list of the mammalian cell lines used in this thesis.

ID is the cell line number in the Ulrich lab database.

ID	Cell line	Antibiotics	Source
1	HEK 293	-	CR-UK Cell Services
31	U2OS	-	CR-UK Cell Services
42	A549	-	[redacted]
94	U2OS_Traffic Light Reporter	1 µg/ml puromycin	[redacted]
119	A549 CRISPR knockout Myosin VI	-	[redacted]
169	Flp-In U2OS TREX	10 µg/ml blasticidin	[redacted]

279	U2OS Flp-In TREX EGFP-M6G4-1xRING	10 µg/ml blasticidin + 100 µg/ml hygromycin	This study
280	U2OS Flp-In TREX EGFP-M6G4-2xRING	11 µg/ml blasticidin + 100 µg/ml hygromycin	This study
289	U2OS Flp-In SPOP-E3_5	12 µg/ml blasticidin + 100 µg/ml hygromycin	This study
290	U2OS Flp-In SPOP-M6G4	13 µg/ml blasticidin + 100 µg/ml hygromycin	This study
297	U2OS Flp-In TREX EGFP-M6G4-2xRING #8	14 µg/ml blasticidin + 100 µg/ml hygromycin	This study
299	U2OS Flp-In TREX NLS-E3_5	15 µg/ml blasticidin + 100 µg/ml hygromycin	This study
300	U2OS Flp-In TREX NLS-M6G4	16 µg/ml blasticidin + 100 µg/ml hygromycin	This study

2.7 DNA manipulation

2.7.1 DNA concentration measurement

DNA concentration was measured with the Nanodrop 2000 spectrophotometer (Thermo Scientific) or Multiskan GO Mikrotiterplatten-Spektralphotometer (Thermo Scientific).

2.7.2 Agarose gel electrophoresis

Agarose gels were prepared by dissolving 1% (w/v) agarose in 1x TBE buffer, which was subsequently supplemented with SYBR Safe DNA stain (Invitrogen). DNA was mixed with the 6x DNA loading dye at a 1:5 ratio, after which the mix was loaded onto the gel. The gel was run at 100 V for 30 min. For determination of the size of the DNA constructs, 100 bp or 1 kb DNA ladders (New England Biolabs) were used as the size standard.

2.7.3 Polymerase chain reaction

Polymerase chain reactions (PCR) were performed for the amplification of DNA. Typically, 100-200 ng DNA was mixed with 10 µl of 5x HF buffer, 1 µl of 10 mM dNTPs, 2.5 µl of 10 µM forward and reverse oligos, 0.5 µl of the Phusion HF polymerase, and adjusted with water to a total volume of 50 µl. PCRs were performed in a Professional TRIO cycler (Biometra). The protocol included an initial denaturation step at 98°C for 30 s, followed by 30 cycles of 98°C for 10 s (denaturation), 50-72°C (depending on the melting temperature of the oligos) for 30 s (annealing) and 72°C for 30 s/kb (Phusion

polymerase) of the amplified DNA fragment (extension). The protocol was completed with a final extension step at 72 °C for 10 min.

2.7.4 DNA sequencing

400-700 ng of plasmid DNA was mixed with 1 µl of 10 µM DNA primer and adjusted with water to a total volume of 7 µl, and subsequently sent for sequencing to StarSEQ GmbH.

2.8 Protein manipulation

2.8.1 Western blotting

SDS polyacrylamide gel electrophoresis was first performed with 4–15% Criterion™ TGX Stain-Free™ protein gels (Bio-Rad) in a 1x SDS buffer. Prior to being loaded onto the gel, the protein samples were mixed with 4x NUPAGE LDS sample buffer (+1 mM DTT) at a ratio of 1:3 and boiled for 10 min at 95°C. For determination of the molecular weight of the proteins, a Pre-stained PageRuler protein ladder (Thermo Fisher Scientific) was used as the size standard. The gels were run at 200 V for 40-90 min, after which transfer of the proteins from the acrylamide gel to a nitrocellulose membrane (Bio-Rad) was performed using the Trans-Blot Turbo System (Bio-Rad), according to the manufacturer's instructions. After the transfer was completed, the membrane was incubated with the Western blot blocking buffer for 1 h, followed by three PBST washes for 5 min each. The membrane was subsequently incubated with primary antibodies at a dilution of 1:1000 (Table 2) overnight at 4°C. On the following day, the membrane was washed with PBST three times for 5 min each, followed by incubation with HRP-conjugated secondary antibodies at a dilution of either 1:5000 or 1:10,000 (Table 3) for 1 h, after which another three PBST washes were performed for 5 min each. Visualisation of the proteins on the membrane was achieved using the ECL Prime or Select Western blotting detection reagent (Amersham) and a Fusion FX7 system (Vilber Lourmat S.A).

2.9 Methods for *E.coli*

2.9.1 Cultivation of bacterial cells

E.coli cells were cultured in LB medium or on LB plates with the respective antibiotic at 37 °C.

2.9.2 Transformation of *E.coli* competent cells

Competent *E. coli* Top Ten cells were thawed on ice and subsequently mixed with 100-500 ng plasmid DNA for 20 min on ice. This was followed by a 45 s heat shock at 42°C, after which the cells were transferred back to the ice. The cells were diluted with 1 ml of LB medium and shaken at 900 rpm for 1 h at 37°C. As a final step, the cells were plated on LB plates with the respective antibiotic.

2.9.3 Extraction of DNA

To isolate plasmid DNA, a single bacterial clone was inoculated in LB medium with the respective antibiotic and grown overnight at 37°C, shaken at 200-220 rpm. Plasmid DNA was isolated the following day using the GeneJET Plasmid Miniprep kit (Thermo Scientific), according to the manufacturer's instructions.

2.10 Methods for mammalian cells

2.10.1 Cultivation of mammalian cells

Frozen cells that were previously stored at -150°C were rapidly thawed in a 37°C water bath, after which they were centrifuged at 300 g for 5 min, before being plated and grown in DMEM (this term will hereon be used, see section 2.2.1 for composition).

Cells were cultured in DMEM and passaged when confluency reached 80-90%. The passaging process involved one wash with PBS, after which the cells were subjected to trysinisation, for detachment from the culturing plate. Trypsinisation was carried out with 0.05% Trypsin-EDTA-Phenol red (Gibco) for approximately 7 min at 37°C, before DMEM was added to stop the trypsinisation process. The cells were subsequently transferred to a new culturing plate at a suitable dilution.

When necessary, cells were frozen for long-term storage. The cells were first trypsinised with 0.05% Trypsin-EDTA-Phenol red (Gibco) for approximately 7 min at 37°C, after which DMEM was added and the mix was centrifuged at 300 g to obtain a cell pellet. The pellet was re-suspended in freezing medium (90% DMEM and 10% DMSO) and initially frozen at -80°C in cryovials. The cryovials were transferred to -150°C the next day for long-term storage.

2.10.2 Harvesting cells

Cells were washed twice with ice cold PBS, after which they were scraped off the plates and collected in 1 ml of PBS. The cells were subsequently centrifuged at 4,500 g for 1 min, to obtain a cell pellet, which was frozen at -20°C until further processing.

2.10.3 Transfection of mammalian cells

Cells were counted with the TC20 Automated Cell Counter (Bio-Rad) and plated at $2x10^6$ cells/10 cm plate (U2OS cells) or $4x10^6$ cells/10 cm plate (HEK293 cells) to prepare for transfection the next day.

U2OS cells were transfected with 5 µg DNA using Lipofectamine 2000 (Thermo Fisher Scientific), according to the manufacturer's instructions. The transfection mix was incubated with the cells at 37°C for 4-6 h, before it was replaced with DMEM.

HEK293 cells were transfected with 10 µg DNA using polyethyleneimine (PEI). In short, 10 µg DNA, 2 ml DMEM without FBS (with antibiotics and glutamine, see section 2.2.1) and 40 µl PEI were fixed and incubated at room temperature for 10 min. 6 ml DMEM was added to the mix to generate the transfection mix. The transfection mix was incubated with the cells at 37°C overnight, before it was replaced with fresh DMEM.

2.10.4 siRNA mediated knockdown

Cells were plated at $1.2x10^6$ cells/10 cm plate (U2OS cells) to prepare for the knockdown the next day. The cells were transfected with 20 nM siRNA using Lipofectamine RNAiMAX (Thermo Fisher Scientific) according to the manufacturer's instructions. The transfection mix was incubated with the cells at 37°C for 4 h, before it was replaced with DMEM.

2.10.5 Generation of stable cell lines

U2OS FlpIn cells were plated at $2x10^6$ cells/10 cm plate to prepare for the transfection the next day. 1 µg of the target plasmid, 9 µg of the Flp-recombinase pOG44 (pHU1809) and 30 µl FuGene HD (Promega) were mixed in 1 ml Opti-MEM medium. The mix was incubated for 10 min at room temperature, after which it was added to cells in DMEM. The transfection mix was incubated with the cells at 37°C for 24 h, before it was replaced with fresh DMEM. 100 µg/ml hygromycin was added after another 24 h for selection. The culturing medium was replaced every 2 days with fresh DMEM and 100 µg/ml hygromycin. Hygromycin-resistant colonies appeared and grew for approximately 2 weeks before they were trypsinised, pooled and cultured as described in section 2.10.1.

2.10.6 Traffic light reporter assay

Cells were co-transfected with 20 nM siRNA, 3.3 µg GFP-Donor (pHU3500), and 6.7 µg SCE-I nuclease plasmid (pHU3499) using Lipofectamine 2000 on 10 cm plates (see section 2.10.2). 48 h post transfection, the cells were transferred from the 10 cm plate

to a 15 cm plate. 24 h after transfer of the cells to a 15 cm plate, cells were trysinised (see section 2.10.1) and DMEM was added to stop the trypsinisation process. The cell suspension was subsequently centrifuged at 300 g for 5 min, after which the pellet was re-suspended in 2 ml PBS, of which 1 ml was used for flow cytometry analysis and if needed, the other 1 ml was used for Western blot analysis. Flow cytometry analysis was carried out with the BD LSRFortessa SORP instrument (BD Biosciences) and data analysis was carried out with the Flow Jo software. Western blot analysis was carried out as described in section 2.8.1.

2.10.7 DNA fibre assay

Cells were labelled with 50 µM CldU (Merck) for 20 min and 50 µM IdU (Merck) for 20 min respectively. An additional 4 mM HU treatment was given for 5 h when indicated in the figures. Alternatively, cells were labelled with 50 µM CldU (Merck) for 20 min and 50 µM IdU (Merck) for 40 min respectively, with or without the addition of 1 µM CPT together with the IdU pulse. Cells were subsequently trypsinised, re-suspended in PBS, and diluted to 1.75×10^5 cells/ml. Labelled cells were mixed with unlabelled cells at a ratio of 1:1. Cell lysis was carried out on microscopy slides, on which 4 µl of the cells was mixed with 7.5 µl of the DNA fibre assay lysis buffer. After a 9 min incubation, the slides were tilted at an angle of 15-45° to stretch the DNA fibres on the slides. The fibres were subsequently fixed in methanol/acetic acid (3:1) overnight at 4 °C. After fixation, the fibres were denatured in 2.5 M HCl for 1 h, washed with PBS and blocked with 2%BSA/PBST for 40 min. The fibres were incubated with primary antibodies against CldU and IdU (Table 2) for 2.5 h, washed with PBST and incubated with secondary antibodies labelled with Alexa Fluor 488 and Alexa Fluor 647 (Table 3) for 1 h. Following the antibody incubations, the slides were mounted in ProLong™ Diamond Antifade Mountant (Thermo Fisher Scientific). Images of the fibres were acquired using a Leica Thunder widefield microscope and analysis was carried out using Fiji ImageJ. To assess overall replication speed for the 20 min CldU plus 20 min IdU assays, only the fibres that contained two tracks of equal length were measured. To assess fork asymmetry (IdU/CldU ratio) in those assays, fibres with shorter IdU tracks were also analysed. All final figures for the fibre assays were created with GraphPad Prism 8.4.0.

2.10.8 Flow cytometry based cell cycle analysis

A549 cells were plated at $1.5x10^6$ cells/15 cm plate. On the following day, the cells were treated with 100 nM CPT for 24 h, after which they were released into fresh

medium and harvested at different time points. The cells were harvested by trysinisation (see section 2.10.1) and normal growth medium was added to stop the process. The cell suspension was subsequently centrifuged at 300 g for 5 min, after which the pellet was re-suspended in 1 ml ice cold 70% ethanol (EtOH) for fixation. Fixation was carried out at 4 °C for 1 h before proceeding with further steps or at -20 °C for up to several weeks until further processing. Following fixation, staining of DNA with propidium iodide (PI) was carried out. Cells were centrifuged at 1000 g for 10 min to remove the EtOH and washed once with PBS. All supernatant was discarded and the cell pellet was re-suspended in 0.5-1 ml PBS containing 80 µg/ml PI and 20 µg/ml RNAse A. Flow cytometry analysis was carried out with the BD LSRFortessa SORP instrument (BD Biosciences) and data analysis was carried out with the Flow Jo software.

2.10.9 Immunofluorescence staining

Cells were fixed on coverslips with 4% paraformaldehyde (Merck) for 10 min, permeabilised with 0.3% Triton X-100/PBS for 5 min and blocked with the immunofluorescence blocking buffer for 1 h, followed by three PBST washes for 5 min each. The coverslips were subsequently incubated with primary antibodies at a dilution of 1:1000 (Table 2) overnight at 4°C. On the following day, the coverslips were washed with PBST three times for 5 min each, followed by incubation with secondary antibodies at a dilution of 1:1000 (Table 3) for 1 h, after which another three PBST washes were performed for 5 min each. Subsequently, cells were incubated with 5 µg/ml Hoechst (VWR) for 5 min, for detection of the nuclei. Coverslips were mounted with ProLong™ Diamond Antifade Mountant (Thermo Fisher Scientific). Images of the cells were acquired using a Leica Thunder widefield microscope and analysis was carried out using Fiji ImageJ.

2.10.10 Cell fractionation

Cells were harvested (see section 2.10.2) to obtain a cell pellet, which was re-suspended carefully in 200 µl cell fractionation buffer A. This was incubated on ice for 15 min, before 30 µl was taken and further treated with 0.5% IGEPAL and 1 µl Sm nuclease (125 units) for 1 h, to obtain the whole cell extract (WCE) fraction. The cell suspension solution was centrifuged at 1300 g, 4 °C for 5 min. The supernatant was taken and transferred to a new tube, to obtain the cytoplasmic fraction. The cell pellet, which contained the nuclei, was washed twice with 500 µl cell fractionation buffer A (without protease inhibitor, DTT and Triton X-100). The nuclei were lysed with cell

fractionation buffer B on ice for 1 h, after which the sample was centrifuged at 21,000 g for 15 min. The supernatant was taken and transferred to a new tube, to obtain the nuclear soluble fraction. The cell pellet was re-suspended in 150 µl 2x LDS, to obtain the nuclear insoluble fraction. All obtained fractions were subsequently subjected to Western blotting (see section 2.8.1).

Chapter 3

Results

3.1 Determination of the potential role of myo6 in the HR pathway

To determine novel potential functions of myo6 in the nucleus, [redacted] collaborated with the lab of [redacted] to perform SILAC-based quantitative mass spectrometry following pulldown assays with either GST control or a GST-MyUb construct, which was identified as an ubiquitin-binding domain of myo6[137]. The results showed a surprisingly large number of nuclear factors, of which many have roles in DNA repair and DNA replication, indicating these as potential unidentified functions of myo6. Out of the numerous DNA repair factors, we identified various proteins to be part of the repair machinery for DSBs. After we obtained the mass spectrometry results, two papers were published that showed nuclear F-actin to be involved in the HR pathway[119,120]. Taking together the mass spectrometry results and the new insights on F-actin, we decided to first pursue myo6's potential involvement in DSB repair.

3.1.1 Depletion of myo6 results in a decrease in repair by the HR pathway

Firstly, in order to determine whether myo6 does indeed play a role in the general repair of DSBs, we made use of the flow cytometry-based "Traffic light reporter (TLR)" assay developed by Certo *et al* (Figure 3.1A)[170]. This assay determines the usage of HR and NHEJ by cells after generation of a double strand break. The cells have an integrated gene that contains a target site for the SceI nuclease, transfection of which generates a double strand break that can be repaired either by HR or by NHEJ. Repair by HR would involve the utilization of an exogenous GFP donor template and lead to the translation of the GFP protein and generate green fluorescence that can be visualized by flow cytometry. On the other hand, repair by NHEJ would cause a frameshift that leads to the translation of the mCherry protein, generating red fluorescence[170].

As positive controls for HR and NHEJ, we performed siRNA-mediated knockdowns of CtIP and Ku70, as they are well established to be proteins involved in HR and NHEJ respectively[171,172]. Unfortunately, we did not observe a decrease in utilisation of the NHEJ pathway upon depletion of Ku70 (result not shown) and thus did not make any

conclusions regarding repair by NHEJ in this assay. In addition, we wanted to see if we could reproduce the results from Schrank *et al* on F-actin in our assay[120], and therefore used an Arp2/3 inhibitor, CK666, that inhibits the polymerization of actin filaments, as a second positive control. Both the knockdown of CtIP and inhibition of Arp2/3 resulted in a decrease in the HR efficiency. With our positive controls for HR having worked, we moved on with the knockdown of myo6 and also observed a decrease in the HR efficiency, similar as what we observed for the positive controls. This gave us the first indication that myo6 is involved in DSB repair by HR and led us to investigate further into its potential function in the pathway.

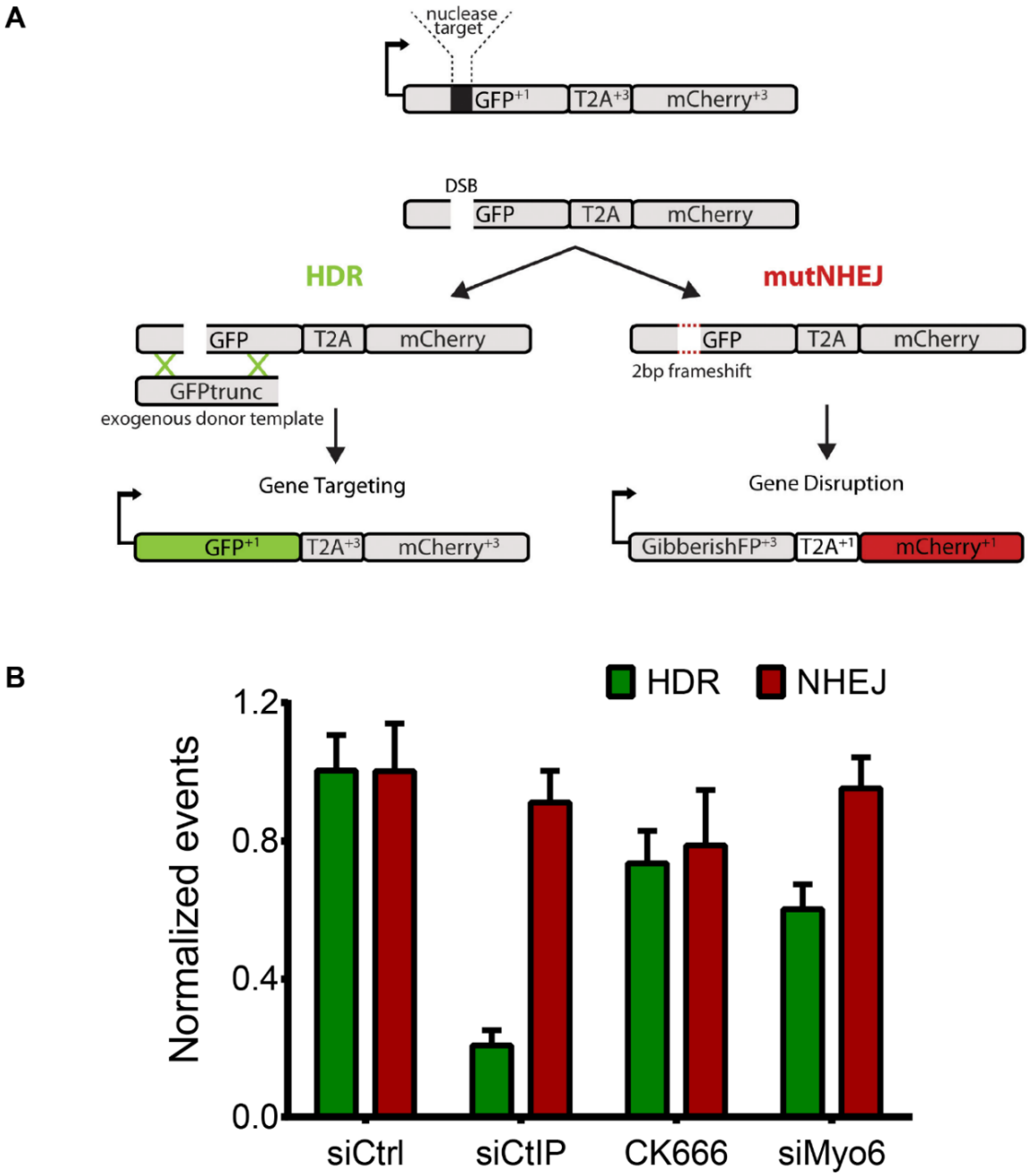

Figure 3.1: Depletion of myo6 results in decreased HR efficiency.

(A) Schematic of the TLR assay (adapted from Certo *et al*, 2011)[170]. **(B)** The TLR assay was performed in U2OS cells stably integrated with the construct as shown in (A). siRNA-mediated knockdowns of CtIP and Myo6 (final concentration 20 nM) were performed 72 h before the assay was performed. 50 μM CK666 was also added 72 h before the assay was performed. Flow-cytometry based analyses was carried out to determine the efficiency of HR and NHEJ repair by determining the percentage of GFP and mCherry cells. Here HR is referred to as HDR (homology-directed repair).

3.1.2 Myo6 KO cells show lower RPA phosphorylation levels after DNA damage

With the first indication of myo6 to play a role in HR, we next aimed to find out in which step or steps of the pathway myo6 is involved in. As F-actin was shown to be involved in the resection step of the HDR pathway [120], we wondered whether this is also true for myo6. Upon resection of the damaged DNA, RPA, a DNA-binding protein, rapidly coats the single-stranded DNA. This leads to its phosphorylation by the kinases ATM, ATR, DNA-PK and CDK2, which in turn triggers a cascade of the recruitment of different factors respectively throughout numerous downstream steps to carry out HR [43]. Therefore, a way to determine a potential role of a protein in resection is to analyse the phosphorylation levels of RPA.

To generate DNA damage in the form of DSBs, we treated the cells with camptothecin (CPT). CPT is a topoisomerase I (TOP1) inhibitor, which traps TOP1 on DNA, inducing DNA damage upon replication or transcription conflicts [173,174]. After the CPT treatment, we compared the phosphorylated RPA (pRPA) levels between A549 *wildtype* (WT) and myo6 CRISPR *knockout* (KO) cells, both of which were obtained from [redacted] (IFOM). In addition, we treated the cells with CK666, to determine the effect of actin polymerization inhibition. KO cells and CK666-treated cells have decreased levels of pRPA compared to the controls upon CPT treatment (Figure 2A). This result was to some extent expected for the CK666-treated cells, as F-actin has been implicated in the resection step of HR [120], but it additionally indicates myo6 to be involved. This results further strengthens the hypothesis of myo6 playing a role in HR.

My colleagues [redacted] and [redacted] have further confirmed myo6's function in the HR pathway. In addition to pRPA level analysis, they have further shown the involvement of myo6 in the resection step of the HDR pathway by BrdU resection assays and RPA foci analysis. Recruitment of myo6 to the sites of DNA damage was also observed by using laser tracks and live-cell imaging. Further downstream steps were also impacted upon the depletion of myo6. Compared to *wildtype* cells, myo6-depleted cells showed an impairment in Rad51 foci formation. Additionally, with a collaboration with the lab of [redacted] (TU Darmstadt), we used live-cell time-lapse microscopy to follow the mobility of DSBs through analysing Rad52 foci after the generation of DSBs. Similar to what was previously shown for CK666-treated cells by Schrank *et al*[120], we observed a similar phenotype for myo6-depleted cells, in which Rad52 mobility was impaired in comparison to control cells. This is an indication of myo6 having an additional role in homology search, as one of

the later downstream steps in the HR pathway, similar to what had been discovered for F-actin[120] (Figure 2B).

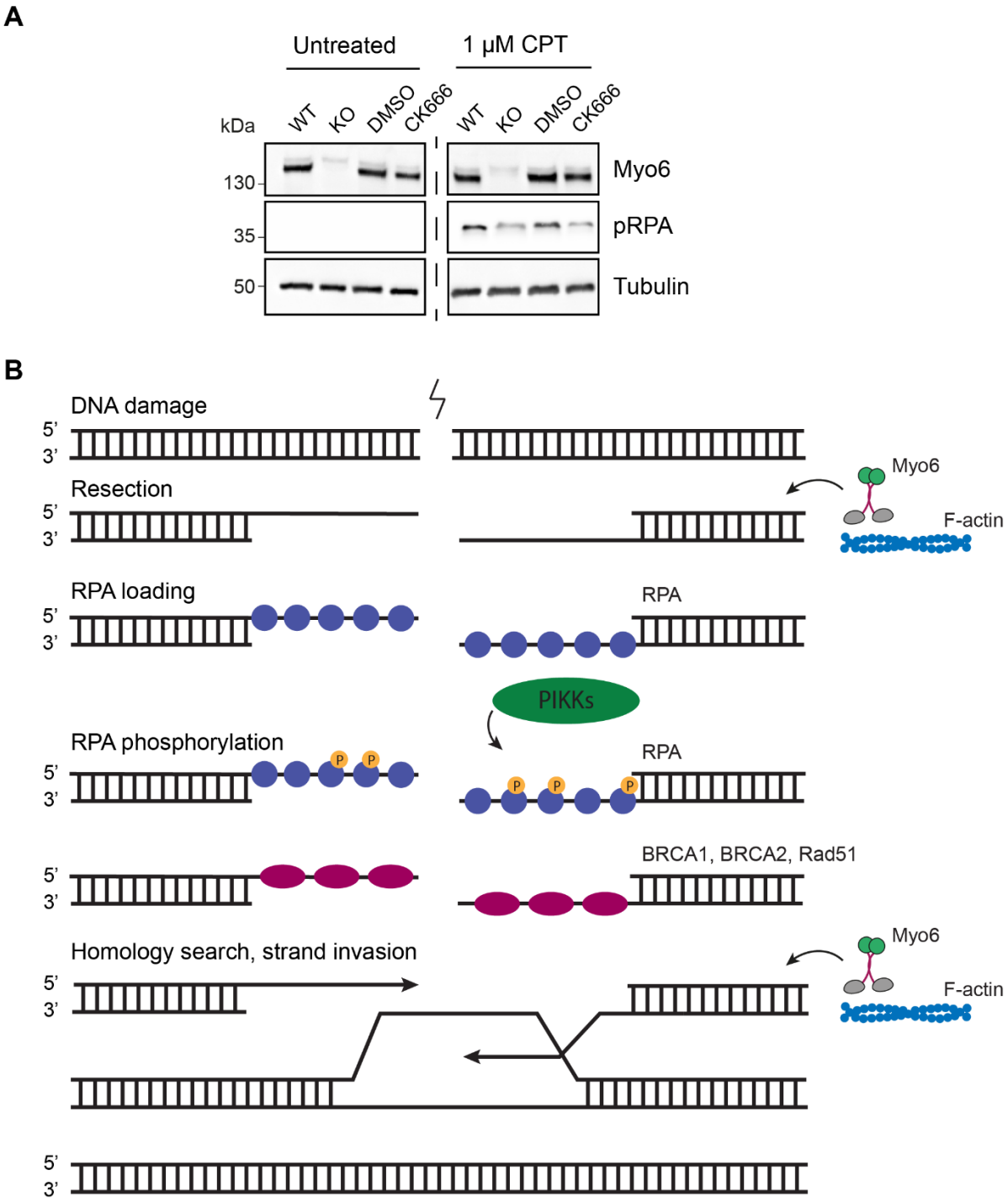

Figure 3.2: KO cells have less phosphorylation of RPA after DNA damage induction.
(A) Western blot analyses of WT and KO cells after a 1 h treatment with 1 µM CPT. Pre-treatment with DMSO or 100 µM CK666 were performed 2 h prior to the CPT treatment to determine the effect of inhibition of actin polymerization. Tubulin serves as the loading control. **(B)** Depicted model of the potential involvement of myo6 in the HR pathway in the resection and homology search steps.

3.2 Characterisation of myo6's role in replication during and after DNA damage

As mentioned previously, we identified not only DNA repair proteins in our mass spectrometry experiments but also factors involved in DNA replication. Results shown in the previous section indicate myo6 to play a role in DNA repair, specifically of DSBs. Due to myo6's potential role in both DNA repair and DNA replication, we wanted to determine whether myo6 plays a role in unperturbed replication as well as replication progression upon and after DNA damage.

3.2.1 Myo6 KO cells do not slow down replication in the presence of DNA damage

To compare replication speed between WT and KO cells, I made use of the well-established DNA fibre assay. The cells were given two different thymidine analogues respectively (CldU and IdU), in order to label the newly synthesized DNA. To generate DNA damage, I used CPT once more, which was given together with IdU. The two labels could be visualized with fluorescent antibodies by microscopy, in red and green respectively (schematic shown in Figure 3.3A). For comparison of the replication speed, the length of the second label IdU was measured.

The results show that in unperturbed conditions, WT and KO cells replicate at a similar speed. Upon DNA damage on the other hand, WT cells slow down replication while KO cells do not (Figure 3.3B). Interestingly, the replication slow-down upon such a treatment had previously been associated with induction of fork reversal by Zellweger *et al*[74]. I wanted to investigate if the absence of replication slow-down could also be observed in WT cells treated with CK666, to determine whether F-actin is also involved in replication slow-down upon the CPT treatment, similar to myo6. Similarly to what was observed for WT and KO cells, in unperturbed conditions, cells treated with either DMSO or CK666 replicated at a similar speed. Upon DNA damage however, DMSO-treated cells slowed down replication, while CK666 did not (Figure 3.3C). This phenotype was also recently shown in a similar experimental setup in a publication by Palumbieri *et al*, in which the authors showed nuclear F-actin to play a role in the fork reversal process[175]. As we observed a similar phenotype for KO cells, it would be worthwhile investigating further into the connection between myo6 and fork reversal.

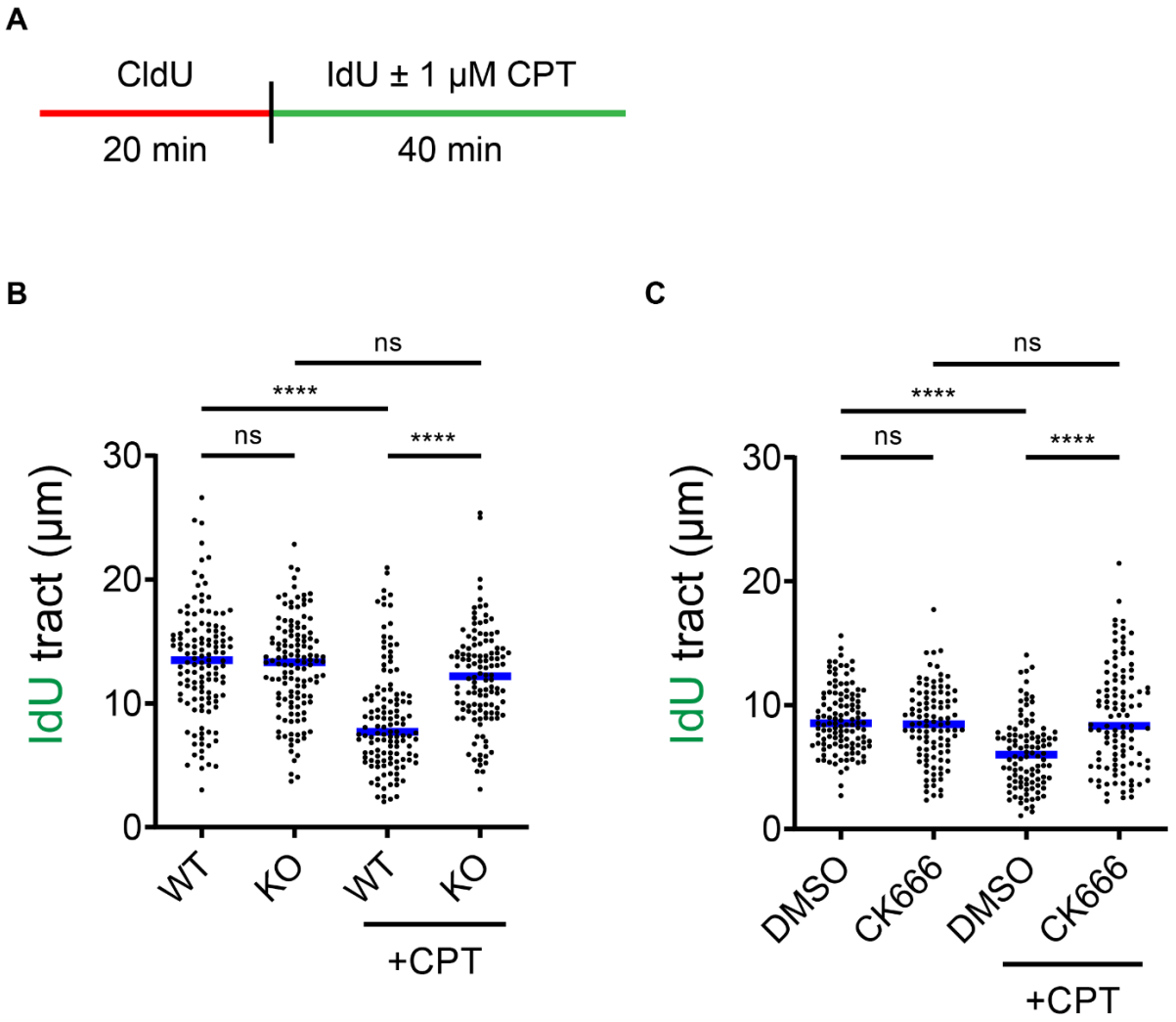

Figure 3.3: KO of myo6 affects replication slowdown during the presence of DNA damage.

(A) Schematic of the fibre assay to measure unperturbed replication and replication in the presence of DNA damage. **(B)** The DNA fibre assay as shown in (A) is performed in WT and KO cells. Replication speed was compared by measuring the length of the IdU tract. A minimum of 100 fibres were analysed for each sample. Significance was determined by the Mann-Whitney test where ns= $p>0.05$, ****= $p<0.0001$. **(C)** The DNA fibre assay as shown in (A) was performed in DMSO- and CK666-treated cells. Replication speed was compared by measuring was length of the IdU tract. A minimum of 100 fibres were analysed for each sample. Significance was determined by the Mann-Whitney test where ns= $p>0.05$, ****= $p<0.0001$.

3.2.2 Myo6 is involved in replication progression or recovery after DNA damage

Having observed that myo6 plays a role in replication progression during DNA damage, we next wanted to find out if it would in addition be involved in replication progression or recovery after release from DNA damage. Therefore, I set up a flow

cytometry-based assay to analyse cell cycle profiles after the release from a 24 hour CPT treatment. As the CPT treatment in this experiment was significantly longer than the one in the experiment described in the previous section (section 3.2.1), the concentration used was also significantly lower. Time points up until 24 hours after the release were taken (Figure 3.4A). Figure 4B shows that WT and KO cells were synchronized in S-phase after the CPT treatment (0 h time point). Upon release, WT cells gradually recovered cell cycle progression and at the 24 h time point, it could be observed that most of the cells progressed into G2-phase. A small G1-phase peak could also be observed, indicating the start of the next cell cycle. The KO cells on the other hand, after being blocked in S-phase, did not recover cell cycle progression and were still observed to be stuck in S-phase 24 hours after release from DNA damage.

The results from this section show that not only does myo6 play a role in replication slow-down during DNA damage but it also seems to be important for cell cycle recovery or progression after DNA damage.

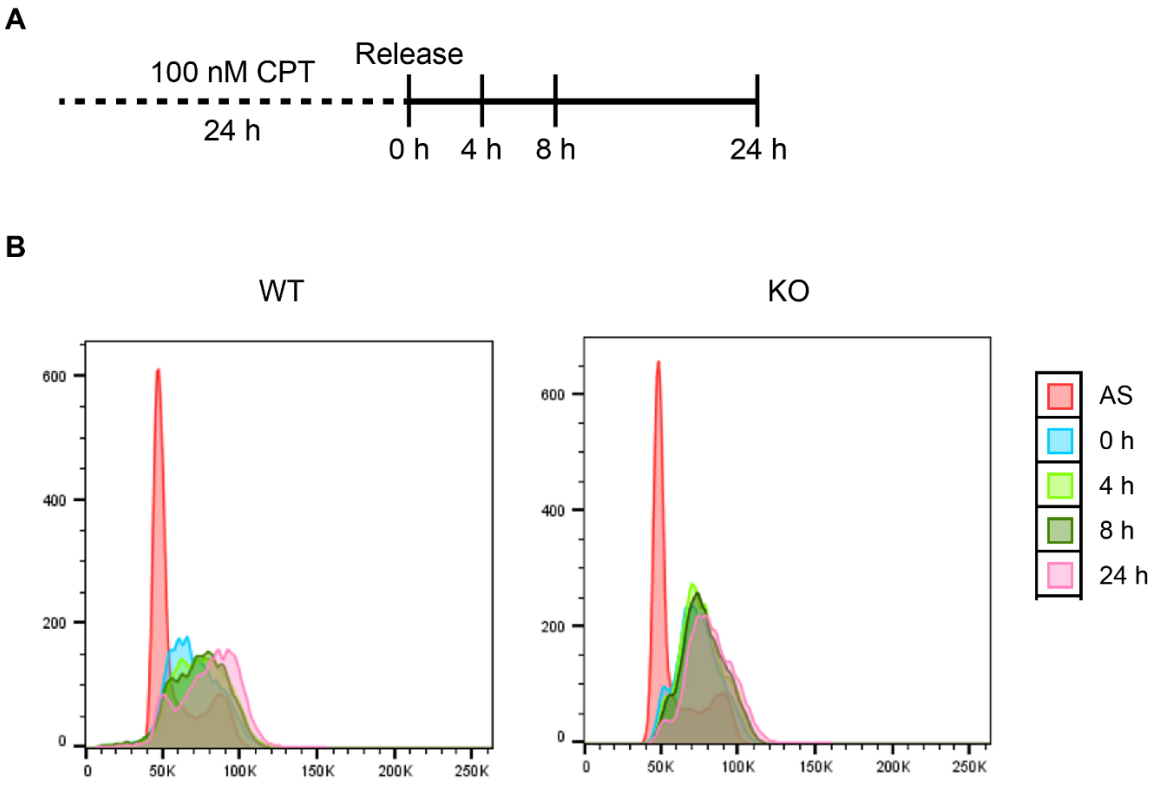

Figure 3.4: KO of myo6 affects replication recovery after release from CPT treatment. **(A)** Schematic of the assay to determine replication recovery/progression after a 100 nM CPT treatment for 24 h. **(B)** Flow cytometry analyses of the cell cycles of WT and KO cells, via DNA staining by 80 µg/ml PI, generated from the experimental setup as shown in (A). Analysis was carried out in FlowJo. AS stands for asynchronous cells, which were not subjected to the CPT treatment.

3.3 Determination of myo6's potential role in the replication stress response

Results from Chapter 3.2 (Figure 3.4) showed the impaired replication recovery in KO cells after a CPT-mediated S phase arrest. One explanation for this could be problematic fork restart upon the depletion of myo6, hinting at a potential role of myo6 in the replication stress response that we decided to investigate further into.

3.3.1 Myo6 KO cells show lower RPA phosphorylation levels after replication stress

We had previously shown that myo6 depleted cells have lower levels of phosphorylated RPA after a CPT treatment compared to WT cells. As CPT creates DNA damage as well as replication stress[173], we decided to treat cells with hydroxyurea (HU), which creates replication stress by depleting dNTPs[176]. In this way, we could create a scenario that mainly focussed on replication stress. In parallel to using KO cells, I also treated the cells with CK666 to compare the effect of myo6-depletion with the inhibition of ARP2/3-driven actin polymerization. As seen in Figure 3.5, KO and CK666-treated cells have decreased levels of pRPA compared to their respective controls upon HU treatment. This result indeed supported our hypothesis that myo6 is involved in the replication stress response. As the next step, we wanted to further investigate myo6's contribution to the replication stress response, particularly which pathway it could specifically be involved in.

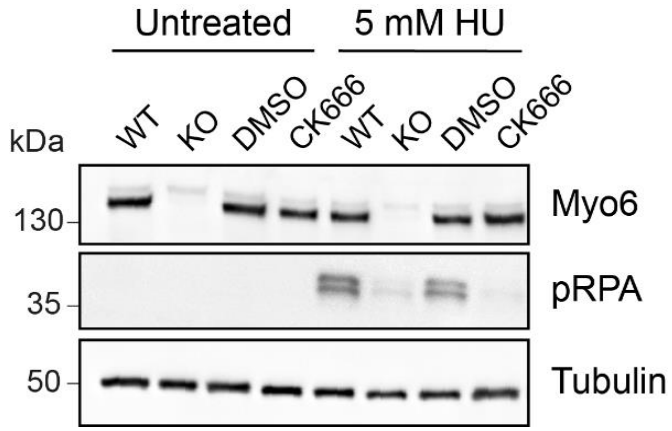

Figure 3.5: KO cells show decreased phosphorylation of RPA after replication stress induction.

Western blot analyses of WT and KO cells after a 1 h treatment with 5 mM HU. Pre-treatment with DMSO or 100 µM CK666 were performed 2 h prior to the HU treatment to determine the effect of inhibition of actin polymerization. Tubulin serves as the loading control.

3.4 Investigation of myo6's role in fork protection

Previous results have indicated myo6 to play a role in the replication stress response (Figure 3.5). As a further indication of this, we scored a number of potential interactors of myo6 in the mass spectrometry such as the Bloom syndrome helicase (BLM), Claspin (CLASPN), WRNIP1, which are involved in the replication stress response[152].

One of the factors from our mass spectrometry results, WRNIP1, is a well-established player in the fork reversal pathway, as a protector of reversed forks[83]. We first wanted to determine if WRNIP1 and myo6 indeed interact with other. We confirmed by proximity ligation assays (PLA), immunoprecipitation experiments with cell lysate and in vitro pulldown experiments with purified proteins that WRNIP1 and myo6 directly interact with each other (results shown in Shi *et al*[152]). Having observed their interaction, we set out to investigate whether myo6, same as WRNIP1, also protects reversed forks.

3.4.1 Myo6 plays a role in fork progression

To determine whether myo6 plays a role in fork protection, I performed a commonly-used fork protection assay[82,177] together with siRNA-mediated depletion of established fork protectors, BRCA2 and WRNIP1, as positive controls. For better comparison with the positive controls, instead of using the myo6 KO cell line, I performed siRNA-mediated depletion of myo6 (siMyo6). I first wanted to reproduce the unperturbed replication result with the WT and KO cells that I previously obtained (Figure 3.3) in the siMyo6 cells. Therefore I carried out the unperturbed replication fibre assay and measured the entire length of the fibres (CldU+IdU) and subsequently divided it by the time of incubation, to obtain the speed (kb/min) (Figure 3.6A).

I was surprised to observe that siMyo6 cells resulted in a lower replication speed compared to control cells (Figures 3.6B and 3.6C), as previous experiments with the KO cells did not indicate the depletion of myo6 to affect replication speed and could be explained by adaptation of the KO clone. The slower replication speed could be due to slower replication progression in general, the result of increased fork stalling or impaired recovery after stalling, as observed from Figure 3.4. Therefore, to further analyse the data obtained from this experiment, I measured the lengths of the CldU and IdU tracts separately and plotted the ratio of IdU/CldU (Figure 3.6D). Compared to the control cells, siMyo6 cells showed a lower IdU/CldU ratio, indicating more fork stalling or potentially impaired recovery after stalling. As forks undergo spontaneous fork reversal during replication, this could also indicate defective protection of

spontaneously reversed forks. To differentiate among the different scenarios, I proceeded with the fork protection fibre assay, to determine whether myo6 is involved in fork protection, like its interaction partner WRNIP1.

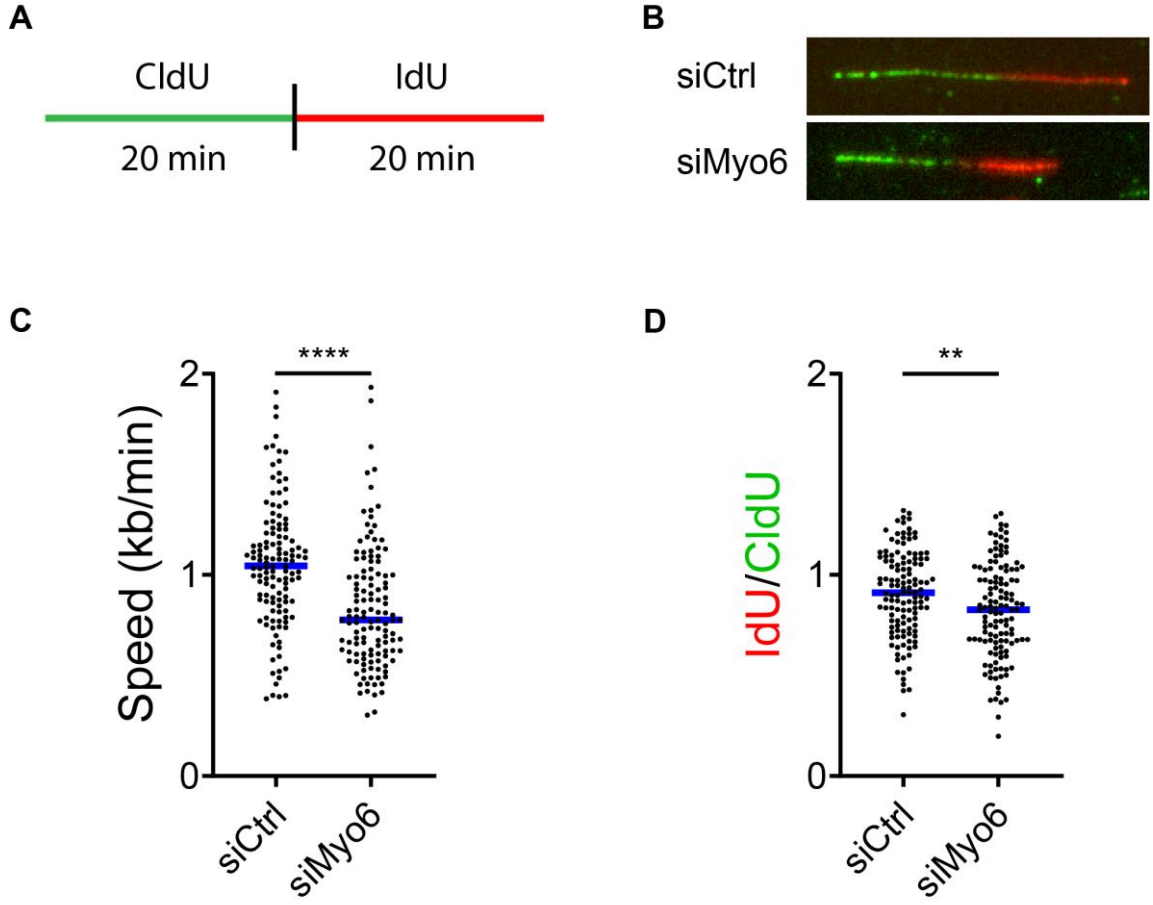

Figure 3.6: siRNA-mediated depletion of myo6 results in a defect in fork progression. **(A)** Schematic of the fibre assay to measure unperturbed replication. **(B)** Representative images of siCtrl and siMyo6 cells subjected to the DNA fibre assay as shown in (A). **(C)** Quantification of the DNA fibre assay, shown as the speed of replication (kb/min). siRNA-mediated knockdown of Myo6 in U2OS cells was performed 72 hr prior to the assay. A minimum of 100 fibres were analysed for each sample. Significance was determined by the Mann-Whitney test where ****= $p<0.0001$. **(D)** Quantification of the DNA fibre assay, shown as the ratio of IdU/CldU. A minimum of 100 fibres were analysed for each sample. Significance was determined by the Mann-Whitney test where **= $p<0.01$.

3.4.2 Myo6 is involved in fork protection downstream of fork reversal

The fork protection fibre assay was performed according to Figure 3.7A. HU was added after the two labels of CldU and IdU as replication stress, to stall the forks, after which a portion of the forks would reverse. If the forks were sufficiently protected, no degradation of the second IdU tract was expected (Figure 3.7B left). On the other hand, if a protein were important for fork protection and depleted in the cells, degradation of the IdU tract was expected (Figure 3.7B right). If the ratio of IdU/CldU were plotted, degradation would be indicated by a ratio of less than 1, while no degradation would result in a ratio of approximately 1.

As my positive controls in the experiment, I used siRNA-mediated depletion of the well-known protectors of the reversed forks- BRCA2 and WRNIP1. As expected, depletion of either protein resulted in degradation of the second tract and an IdU/CldU ratio of approximately 0.8, lower than the ratio of approximately 1 of control cells (Figures 3.7C and 3.7D). Upon depletion of myo6, I observed degradation of the DNA to a similar extent as depletion of the two positive controls, indicating myo6 to indeed play a role in fork protection. Interestingly, by using the PLA, we observed an enhanced PLA signal between myo6 and WRNIP1 when we subjected the cells to the same HU treatment that was used for the fork protection fibre assays[152], further indicating the involvement of myo6 in fork protection and a potential cooperation with WRNIP1 in the pathway, which called for further investigation.

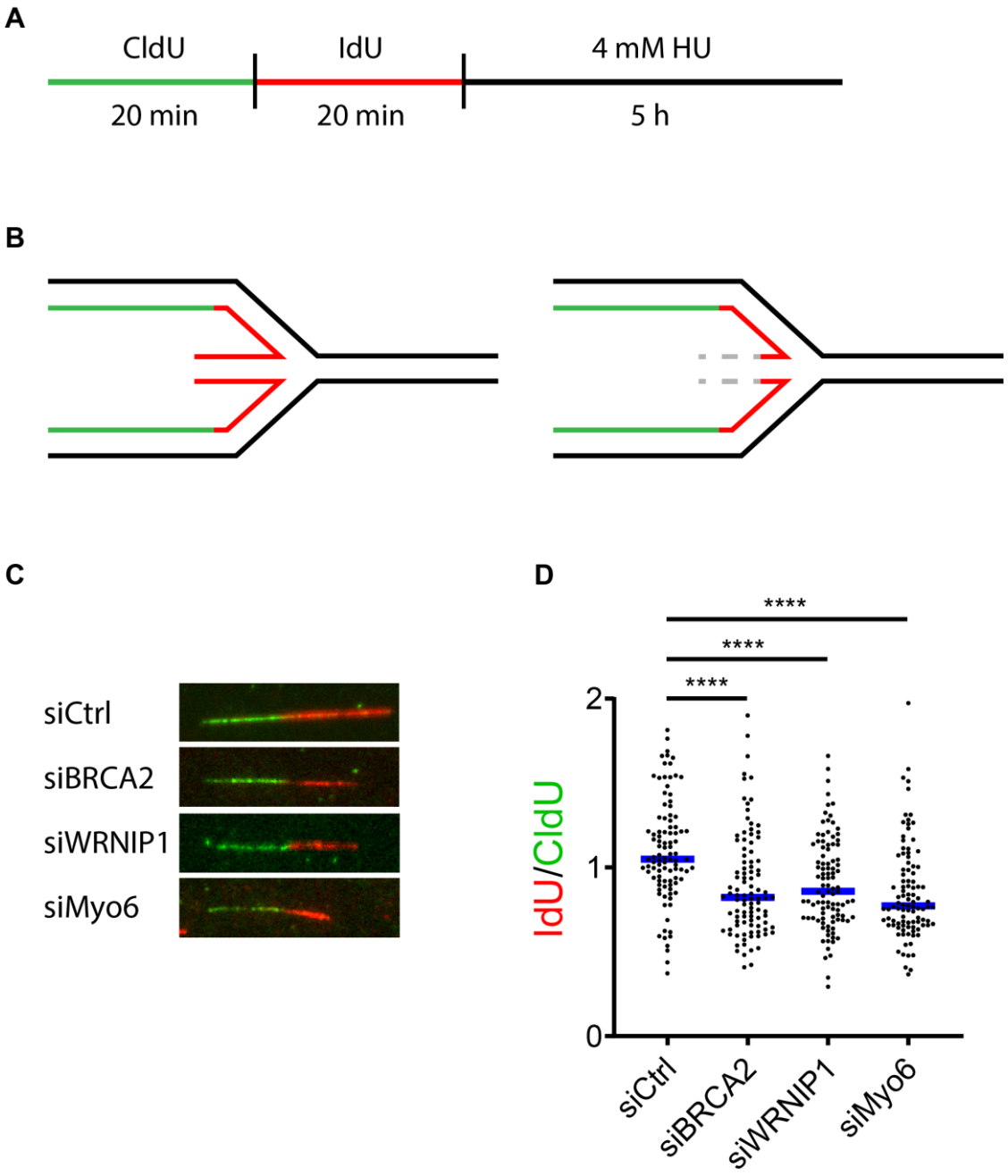

Figure 3.7: Myo6 is involved in fork protection.

(**A)** Schematic of the fibre assay to determine fork protection. **(B)** Representation schematic of a protected fork (left) and a degraded fork (right) as two possible results from assays as shown in (A). **(C)** Representative images of siCtrl, siBRCA, siWRNIP1, siMyo6 cells subjected to the DNA fibre assay as shown in (A). **(D)** Quantification of the DNA fibre assay, shown as the ratio of IdU/CldU. siRNA-mediated knockdowns in U2OS cells were performed 72 h prior to the assay. A minimum of 100 fibres were analysed for each sample. Significance was determined by the Mann-Whitney test where ****=p<0.0001.

To show that the degradation phenotype specifically comes from the depletion of myo6 and not an off-target effect from the siRNA-mediated knockdown, I made use of a U2OS cell line that inducibly expresses siRNA-resistant YFP-myo6 (hereon named U2OS FlpIn YFP-myo6) upon the addition of doxycycline (DOX). Figure 3.8A shows the knockdown efficiency of endogenous myo6 and the expression of ectopic YFP-myo6 in the DOX-treated samples. Clear expression of YFP-myo6 could be observed, as the top band in the myo6 blot. Figure 3.8B shows that depletion of myo6 in this cell line results in nascent strand degradation, in line with the phenotype shown previously (Figure 3.7). Upon expression of YFP-myo6, I observed a rescue of the degradation, which showed that the observed degradation phenotype is specific for myo6.

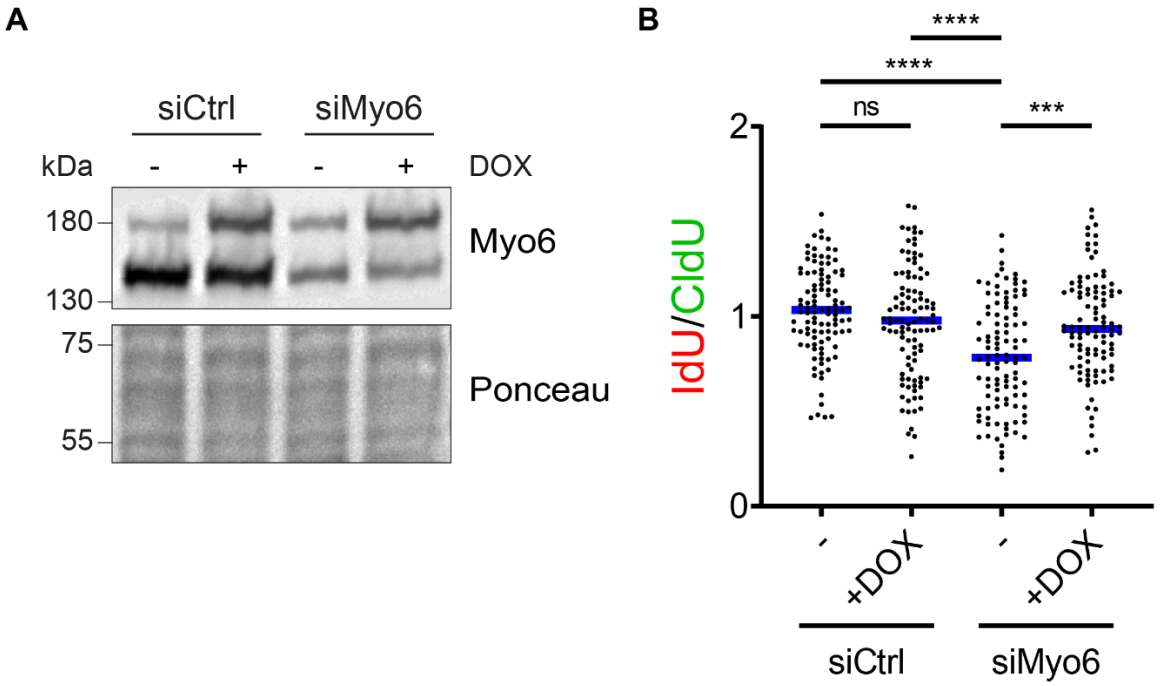

Figure 3.8: Re-expression of YFP-myo6 in myo6-depleted cells rescues the degradation of forks.

(A) Western blot analysis of the knockdown efficiency of myo6 and expression of YFP-myo6 in U2OS FlpIn YFP-myo6 cells. U2OS cells harbouring DOX-inducible YFP-myo6 were siRNA-transfected 72 h prior to the assay (siRNA #10 targeting myo6) and treated −/+ 20 ng/ml DOX 24 h prior to the assay. **(B)** A DNA fibre assay was performed with samples from (A), according to Figure 3.7A. Quantification of the DNA fibre assay was shown as the ratio of IdU/CldU. A minimum of 100 fibres were analysed for each sample. Significance was determined by the Mann-Whitney test where ns= $p>0.05$ and ****= $p<0.0001$.

To confirm that the degradation of the DNA resulted from fork reversal and consecutive impaired protection of the reversed forks in siMyo6 cells, I depleted the fork remodellers in addition to myo6 (Figure 3.9A), to determine whether the degradation can be rescued due to the absence of fork reversal. While the single depletion of myo6 resulted in nascent strand degradation, co-depletion of any one of the fork remodellers Rad51, HLTF, ZRANB3 and SMARCAL1 together with myo6, rescued the degradation phenotype and restored the IdU/CldU ratio back to 1 (Figure 3.9B). This result indicates myo6 to protect forks that have been reversed from degradation. However, alternative fork structures generated by the above-mentioned remodellers cannot be ruled out.

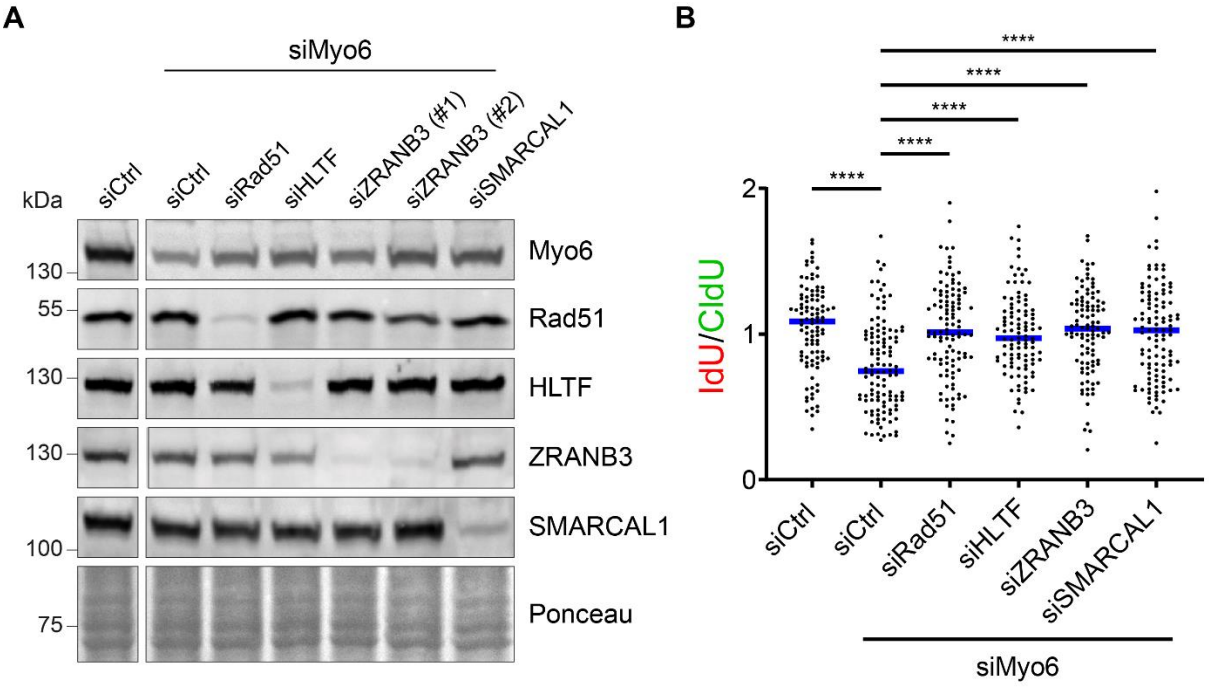

Figure 3.9: Co-depletion of fork remodellers in myo6-depleted cells rescues the degradation of forks.

(A) Western blot analysis of the knockdown efficiency of myo6 and the fork remodellers. siRNA-mediated knockdowns were performed 72 h prior to the assay. The final siRNA concentration was 40 nM for each sample. **(B)** A DNA fibre assay was performed with samples from (A), according to Figure 3.7A. Quantification of the DNA fibre assay was shown as the ratio of IdU/CldU. A minimum of 100 fibres were analysed for each sample. Significance was determined by the Mann-Whitney test where ****= p<0.0001.

3.4.3 Myo6 and WRNIP1 act in the same branch of the fork protection pathway

Although many factors have been established to play a role in fork protection, it has been proposed that the different factors inhibit different nucleases that could degrade the reversed forks[177–180]. In addition, it was proposed by Porebski *et al* that BRCA2 protects the arms of the reversed forks from MRE11-mediated degradation while WRNIP1 protects the junction of the reversed forks from SLX4 and DNA2-mediated degradation (Figure 3.10A)[83]. After having determined myo6 to protect reversed forks from degradation, the next question we wanted to address was which pathway of reversed fork protection myo6 functions in. Is it working together with BRCA2 to protect the arms of the reversed forks or is it working together with WRNIP1 to protect the junction of the reversed forks?

To answer this question, I first carried out a co-depletion of myo6 and WRNIP1 (Figure 10B), to determine if there would be a further reduction in the IdU/CldU ratio, which would indicate the two proteins acting in different pathways. While the results showed no further reduction in the ratio (Figure 3.10C), during the experiments, I came to the conclusion that it would be difficult to see an additive effect with this assay. Furthermore, although Porebski *et al* observed that BRCA2 and WRNIP1 inhibit different nucleases, and proposed the two proteins to localize to different parts of the reversed fork, they did not see a further decrease in the IdU/CldU ratio[83]. Therefore, this approach remained inconclusive and I moved on to an alternative approach of using inhibitors for the different nucleases.

I performed the fork protection assay, in which I depleted WRNIP1 and myo6 (Figure 3.10D), and treated the cells with Mirin, an MRE11 inhibitor or C5, a DNA2 inhibitor. The results showed that the nascent strand degradation in WRNIP1-depleted cells could only be fully rescued by the addition of C5 and not Mirin (Figure 3.10E), which reproduced the published data[83]. In the Myo6-depleted cells, I observed a very similar phenotype, where the degradation could be rescued slightly by the Mirin treatment and only rescued fully by the C5 treatment. This indicates myo6 to be in the same fork protection pathway as WRNIP1 and protect the reversed forks from DNA2, distinct from the BRCA2 protection branch.

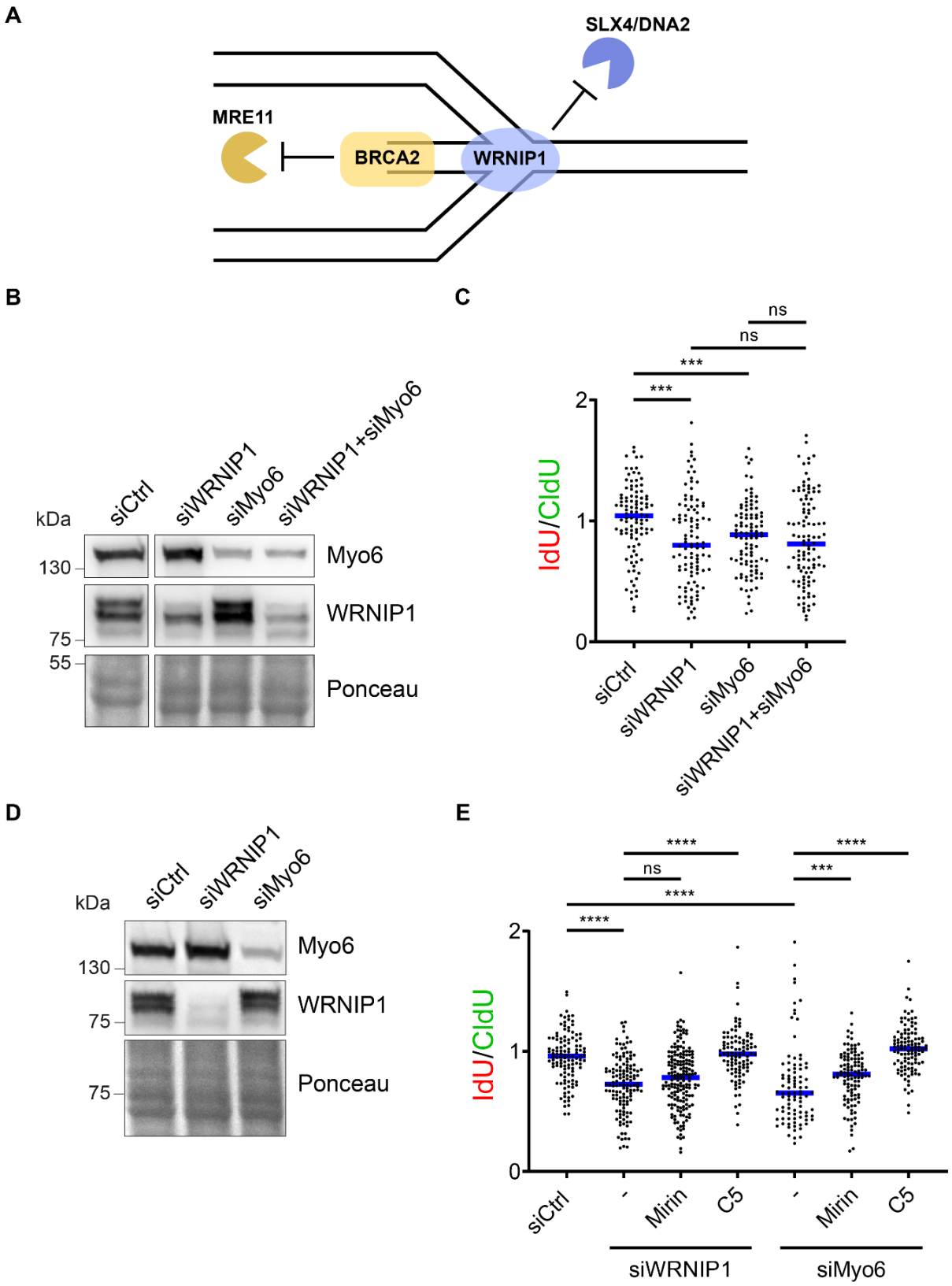

Figure 3.10: Myo6 protects reversed forks from DNA2-mediated degradation, same as WRNIP1.

(A) Proposed model of BRCA2 and WRNIP1 localised to different parts of the reversed fork and inhibiting different nucleases (adapted from Porebski *et al*, 2019)[83]. **(B)** Western blot analysis of the knockdown efficiency of WRNIP1 and myo6. siRNA-mediated knockdowns

were performed 72 h prior to the assay. The final siRNA concentration was 40 nM for each sample. **(C)** A DNA fibre assay was performed with samples from (B), according to Figure 3.7A. **(D)** Western blot analysis of the knockdown efficiency of WRNIP1 and myo6. siRNA-mediated knockdowns were performed 72 h prior to the assay. **(E)** A DNA fibre assay was performed with samples from (D), according to Figure 3.7A. Mirin (final concentration 25 μM) and C5 (final concentration 50 μM) were added for 5 h, together with the 4mM HU treatment, after the IdU label. **(C, E)** Quantification of the DNA fibre assay was shown as the ratio of IdU/CldU. A minimum of 100 fibres were analysed for each sample. Significance was determined by the Mann-Whitney test where ns= $p>0.05$, ***= $p<0.001$ and ****= $p<0.0001$.

3.4.4 The motor domain of myo6 is essential for its fork protection function

The next question we addressed was which domain(s) of myo6 is important for its fork protection function. As myo6 is a motor protein, consisting of a motor domain, helical tail and cargo-binding domain (CBD)[138], it was obvious to start with the essentiality of its motor domain (Figure 3.11A left). Myo6 is a process motor protein that walks on actin filaments in a “hand-over-hand” fashion (Figure 3.11A right). To study the importance of the motor domain of myo6, I overexpressed a motor-deletion mutant of myo6 (TAIL), which would potentially dimerise with endogenous myo6, impairing its “hand-over-hand” walking function in a dominant negative manner (Figure 3.11B). I performed the fork protection assay with untransfected cells (Un), cells transfected with GFP and cells transfected with TAIL (Figure 3.11C). Both untransfected and GFP-transfected cells showed no nascent strand degradation, while cells expressing the myo6 tail showed degradation to a similar extent as when cells were depleted of myo6 via siRNAs (Figure 3.11D). As observed from this result, the motor domain is essential for myo6’s fork protection function.

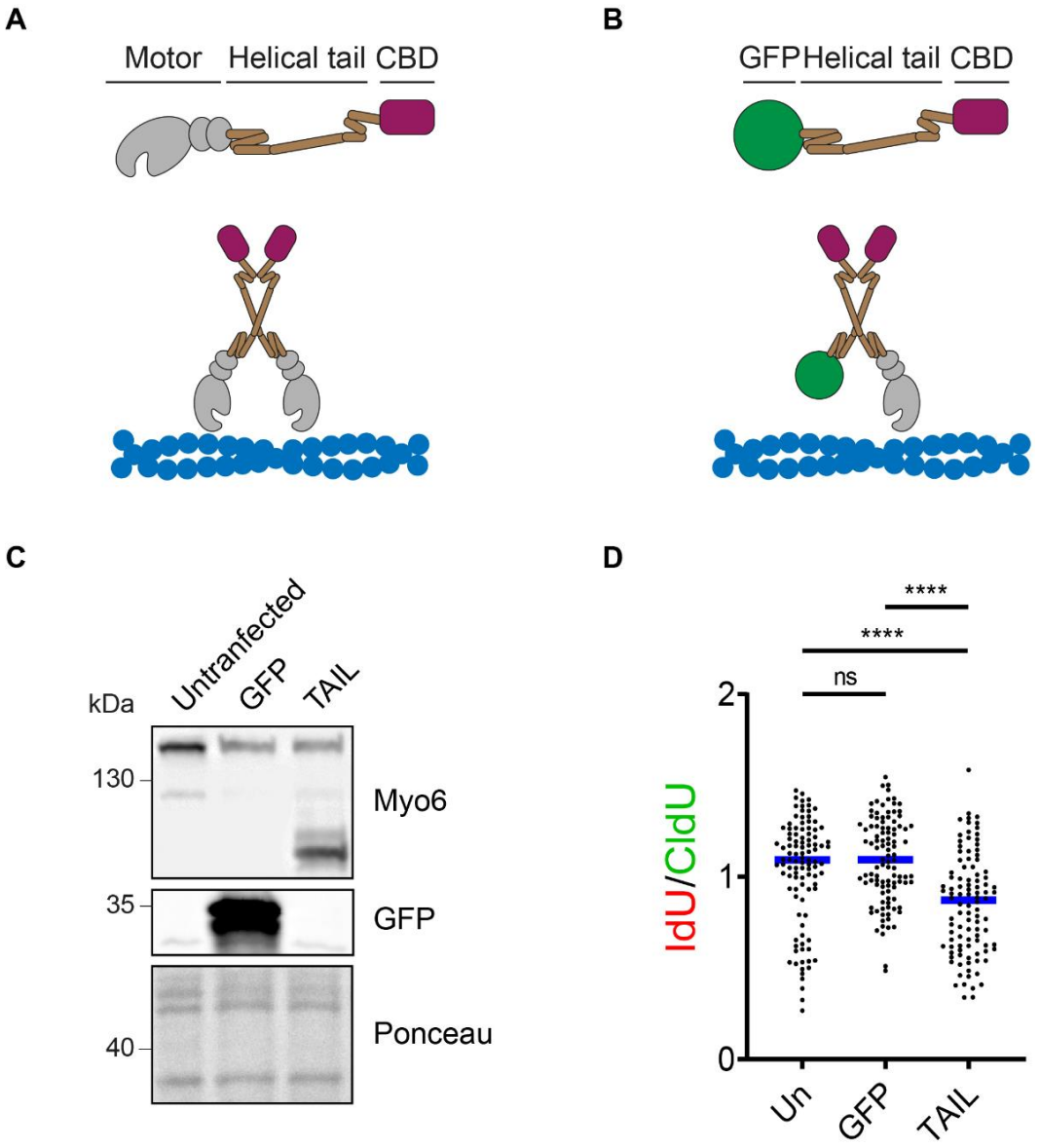

Figure 3.11: The motor domain of myo6 is required for fork protection.

(A) Schematic of a myo6 monomer with its domains (left) and its dimerised form on F-actin (right) (Adapted from Magistrati *et al*, 2021)[131]. **(B)** Schematic of a myo6 monomer with its motor domain replaced by GFP, named TAIL (left) and its "hetero"-dimerised form with endogenous myo6 on actin filaments (right). **(C)** Western blot analysis of the transfection efficiency of GFP and TAIL. Cells were either transfected with 0.5 µg of GFP together with 4.5 µg empty vector or 5 µg of the TAIL plasmid, 48 h prior to the assay. **(D)** A DNA fibre assay was performed with samples from (C), according to Figure 3.7A. Quantification of the DNA fibre assay was shown as the ratio of IdU/CldU. A minimum of 100 fibres were analysed for each sample. Significance was determined by the Mann-Whitney test where ns= $p>0.05$ and ****= $p<0.0001$.

3.4.5 Further analysis of myo6 domain essentiality for fork protection

Having determined the motor domain of myo6 to be essential for its fork protection function, I moved on to investigating which other domains are also potentially required. To investigate into other domains of myo6, I again made use of the dominant negative myo6 tail (in this assay shown as “WT”) containing different mutations that disrupt the MyUb domain (MyUb Struct), ubiquitin-binding (Ub-bdg) by single-point mutations in each UBD, DNA-binding (DNA-bdg) or the WLY-motif within the cargo-binding domain (Cargo-bdg) (Figure 3.12A). As overexpression of the dominant negative tail results in nascent strand degradation, a rescue of the degradation with any tail mutant would indicate the importance of the respective domain.

Upon overexpression of the different tails (Figure 3.12B), I observed nascent strand degradation in the WT tail sample, confirming the results from the previous experiment (Figure 3.12C). The DNA-bdg and Cargo-bdg samples showed a similar ratio as WT, indicating that these domains are not needed for myo6’s fork protection function. On the contrary, the tail with a disrupted MyUb domain did not show degradation, indicating that it is a needed domain for fork protection. This correlates well to previously obtained data, as myo6 interacts with WRNIP1 via its MyUb domain (data shown in Shi *et al*[152]). The ratio of the Ub-bdg was halfway between WT and MyUb Struct, which indicates a contribution of ubiquitin binding to myo6’s function in the fork protection pathway.

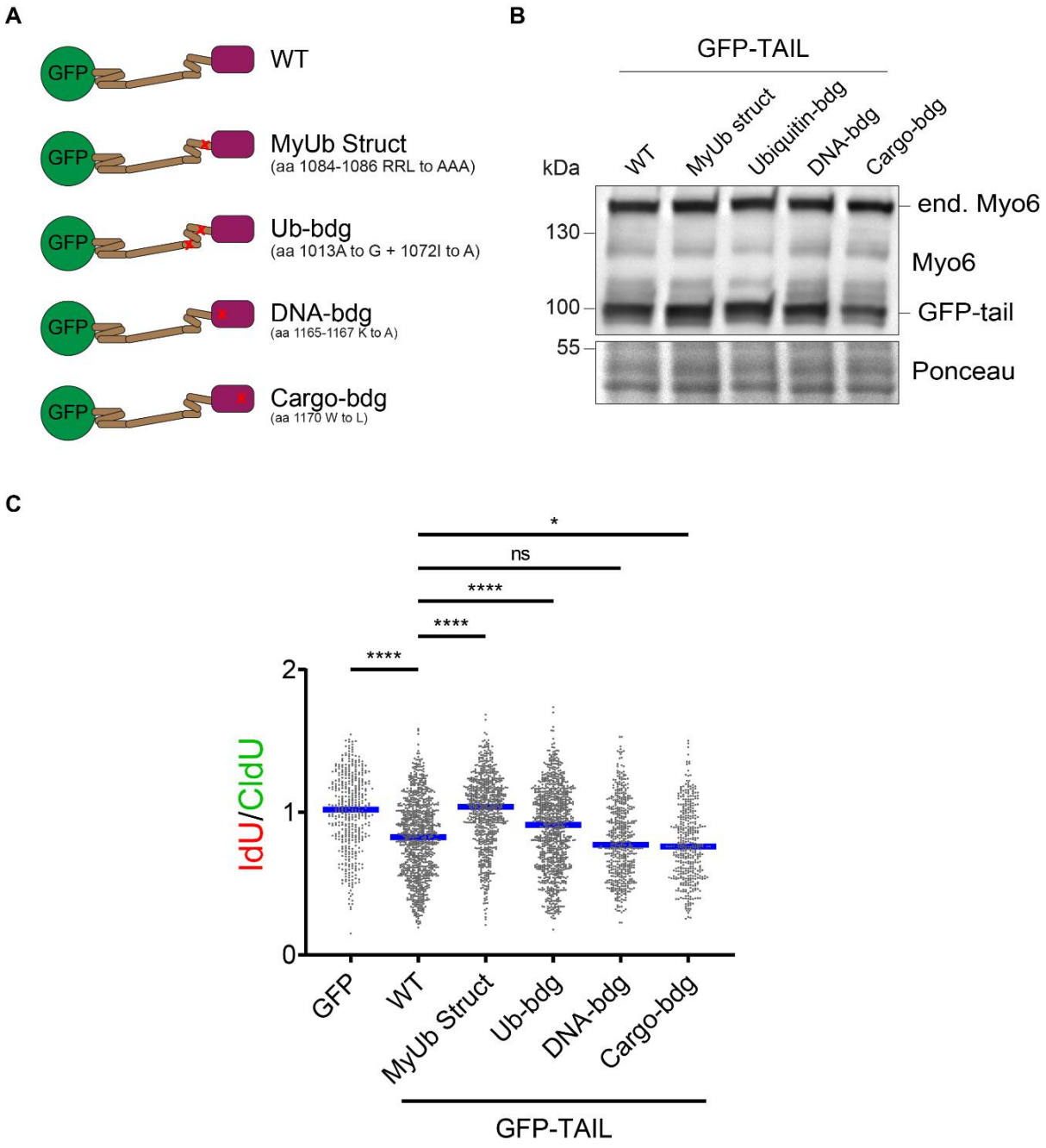

Figure 3.12: The MyUb domain is needed in addition to the motor domain of myo6 for fork protection.

(A) Schematic of myo6 tails with different mutations (adapted from Magistrati *et al*, 2021)[131]. **(B)** Western blot analysis of the transfection efficiency of GFP and GFP-TAILs. Cells were either transfected with 0.5 µg of GFP together with 4.5 µg empty vector or 5 µg of the respective TAIL plasmid, 48 h prior to the assay. **(C)** A DNA fibre assay was performed with samples from (B), according to Figure 3.7A. Quantification of the DNA fibre assays was shown as the ratio of IdU/CldU. A minimum of 300 fibres from at least 3 independent experiments were analysed for each sample and combined to generate the final figure. Significance was determined by the Mann-Whitney test where ns= $p>0.05$, *= $p<0.05$ and ****= $p<0.0001$.

3.4.6 Inhibition of actin polymerization does not lead to de-protection of reversed forks

As myo6 is a motor protein that travels on actin filaments and its motor domain of is needed for fork protection (Figures 3.11D and 3.12C), an obvious question was whether actin filaments also contribute to fork protection. Therefore, I made use of a mutant form of actin (R62D) that cannot polymerise and would inhibit polymerisation of endogenous actin filaments when overexpressed[181]. R62D has been used in a number of publications to demonstrate the importance of nuclear F-actin[119–121]. In this experiment, I used overexpression of the myo6 TAIL-construct as my positive control (Figure 3.13A). Upon overexpression of R62D-3xNLS (specifically inhibiting nuclear F-actin polymerisation), I did not observe any nascent strand degradation (Figure 3.13B), indicating nuclear F-actin filaments to not be involved in fork protection. This was surprising as we had previously observed the motor domain of myo6 that associates with F-actin to be required for fork protection (Figures 3.11D and 3.12C), which hinted at F-actin also having a similar fork protection function as myo6. A recent publication by Palumbieri *et al* has shone light on actin filaments to have a novel function in the remodelling of reversed forks, which is a potential explanation for why I did not observe degradation when I overexpressed the actin mutant[175].

Taken together, the results in this section have shown the novel function of myo6 to protect forks from DNA2-mediated degradation, downstream of fork reversal. The motor and MyUb domains are essential for this function, with an additional contribution from its ubiquitin-binding domain. What is highly sought-after in the cytoskeleton field is the differentiation between the cytoplasmic and nuclear contributions of the cytoskeleton proteins. As myo6 is immensely abundant in the cytoplasm and scarce in the nucleus, a crucial point to investigate is whether it is cytoplasmic or nuclear myo6 that plays a role in fork protection. This part will be addressed in detail in the next section of this thesis.

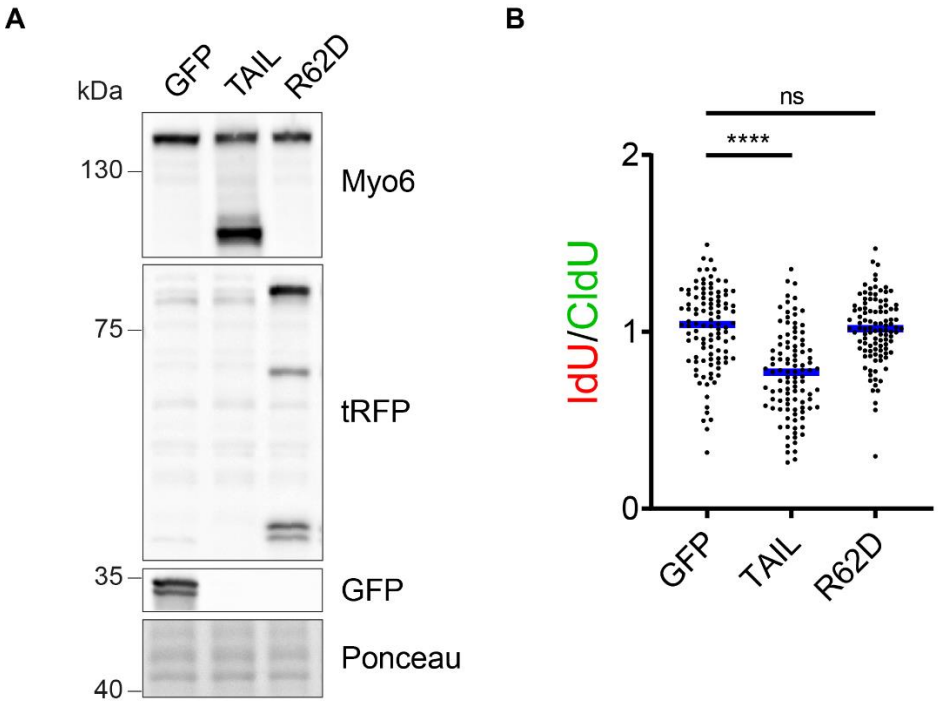

Figure 3.13: Overexpression of non-polymerisable actin does not result in degradation of forks.

(A) Western blot analysis of the transfection efficiency of GFP, TAIL and R62D. Cells were either transfected with 0.5 µg of GFP together with 4.5 µg empty vector or 5 µg of TAIL or R62D, 48 h prior to the assay**. (B)** A DNA fibre assay with samples from (A) was performed according to Figure 3.7A. Quantification of the DNA fibre assay was shown as the ratio of IdU/CldU. A minimum of 100 fibres were analysed for each sample. Significance was determined by the Mann-Whitney test where ns= $p>0.05$ and ****= $p<0.0001$.

3.5 Differentiating nuclear and cytoplasmic myo6

In the previous results section, I have shown the contribution of myo6 to the protection of reversed forks. Nevertheless, as I have not differentiated between the low abundant pool of nuclear myo6 and largely abundant pool of cytoplasmic myo6, this remains a highly important question to address. Due to the immense amount of cytoplasmic myo6, it has been difficult for us to visualize and manipulate endogenous nuclear myo6 using the "classic" approaches of immunofluorescence (IF) microscopy and cell fractionation. Therefore, we have made use of the DARPin technology[166] to facilitate us in the manipulation of myo6, and assign the newly discovered functions of myo6 to either the cytoplasmic pool or the nuclear pool.

3.5.1 DARPins as a tool to manipulate myo6

As we required specific DARPins that target myo6, we collaborated with the lab of [redacted], from whom we received a large number of DARPins raised against myo6, which were obtained via ribosome display. My colleagues have screened the received DARPins and found one DARPin (G4), to bind to myo6 *in vitro* and to be able to deplete myo6 from cell lysate (data shown in Shi *et al*[152]). Further experiments in this thesis are performed with the G4 DARPin. We aimed to degrade myo6 with a functionalised version of our DARPin, on the protein level, specifically in the nucleus, to achieve our goal of differentiating between the contributions of nuclear or cytoplasmic myo6 to fork protection.

3.5.2 Usage of the antibody RING-mediated destruction (ARMeD) system

Although our final goal was to degrade nuclear myo6 specifically, we first wanted to show that the G4 DARPin is able to function intracellularly. To accomplish this, we first made use of a degradation system, the antibody RING-mediated destruction (ARMeD) system that degrades proteins in both the nucleus and cytoplasm simultaneously[182]. The system makes use of a construct that comprises of the RING domain of the E3-ubiquitin ligase RNF4 coupled to a GFP-nanobody that would bind to GFP-tagged proteins. The degradation process begins with binding of the ARMeD construct to the substrate protein, after which ubiquitination of the RING domain as well as the substrate protein is carried out, resulting in targeting the substrate for proteasomal degradation (Figure 3.14A)[182]. While one RING domain is sufficient for degradation of the target protein, the two RING construct is shown to be even more efficient.

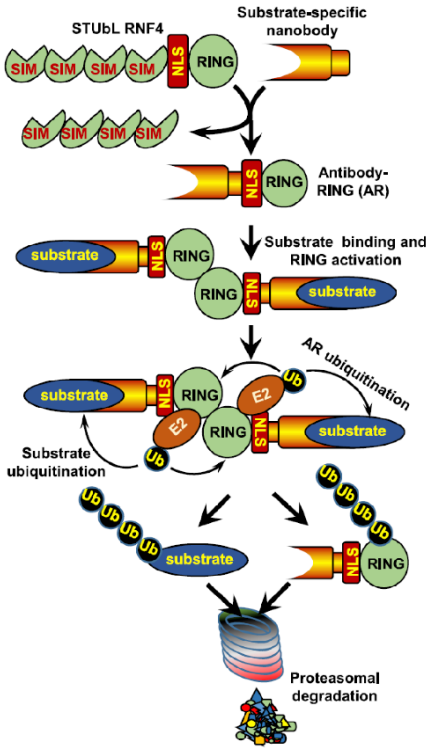

Figure 3.14: The ARMeD system schematic (adapted from Ibrahim *et al*, 2020)[182]**.** Cascade of proteasomal degradation of substrate proteins in both the cytoplasm and the nucleus by the ARMeD system.

3.5.3 Usage of the ARMeD system for degradation of myo6 on the protein level

As an initial try to degrade myo6 with the ARMeD system, I performed a transient overexpression of GFP-myo6 together with either the 1xRING construct or the 2xRING construct (Figure 3.15A). The myo6 Western blot showed the successful transfection of GFP-myo6, seen as the top band, above the endogenous myo6 band. Although the anti-camelid blot showed the expression of the RING constructs, degradation of GFP-myo6 was unfortunately not observed. A possible explanation for this is that the ARMed system cannot counteract the overexpression of a protein but would rather work in an endogenous context. Therefore, we next sought to exchange the GFP-nanobody with the myo6-binding G4 DARPin, in hopes of successfully degrading endogenous myo6 (Figure 3.15B).

Having exchanged the GFP-nanobody for the G4 DARPin, I transfected both the G4-1xRING and G4-2xRING constructs into the cells and took time points every 24 hours until 72 hours after transfection (Figure 3.15C). The constructs contain a GFP-tag, for convenient detection by Western blotting and visualization by microscopy. Although clear expression of the constructs could be detected, degradation of myo6 was

relatively inefficient, and was only observed to be slightly more pronounced towards the later time points in the cells transfected with G4-2xRING.

After obtaining the results from these two experiments, we decided on further optimization by the means of generating stable cells lines that can inducibly express the constructs upon the addition of DOX, as Ibrahim *et al* observed highly efficient protein degradation in this manner[182].

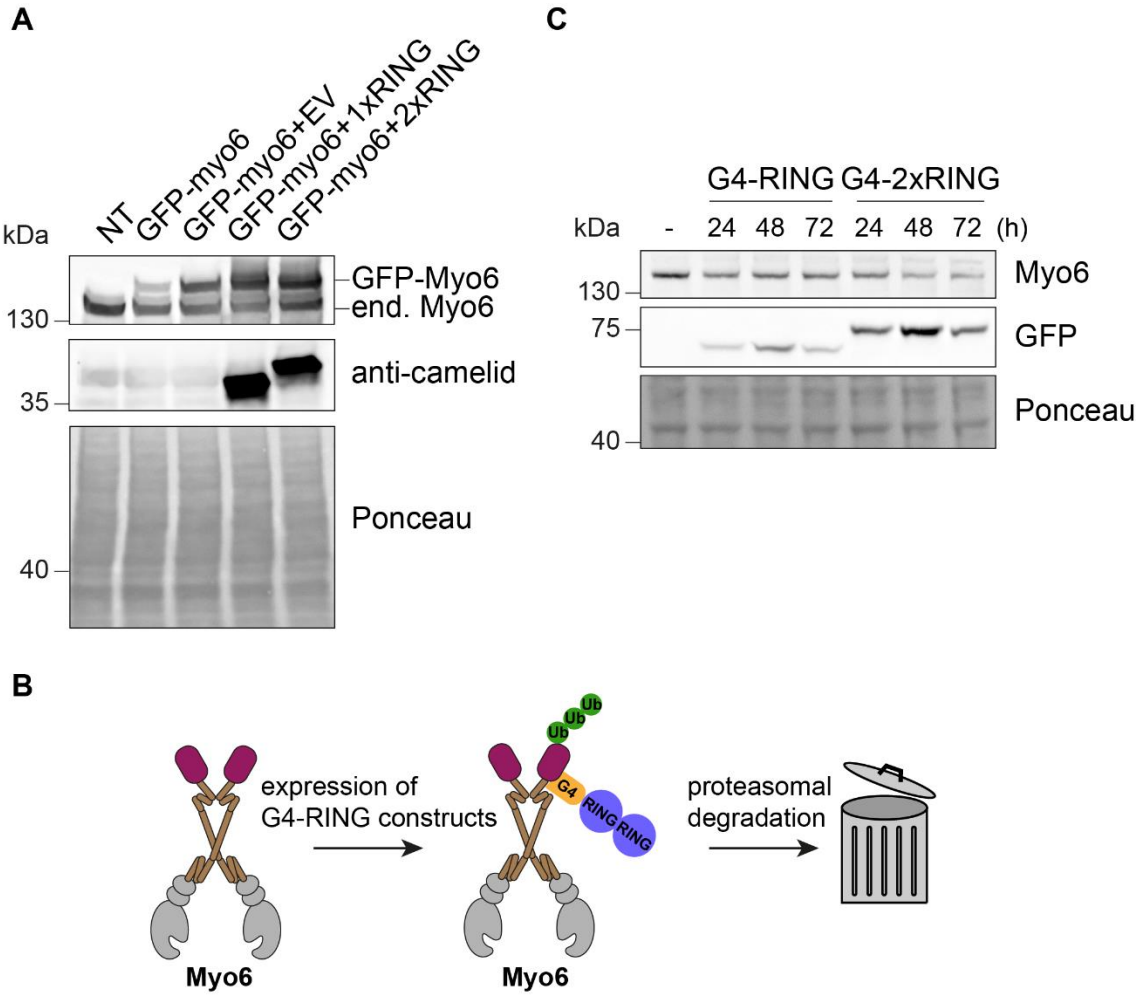

Figure 3.15: Test and modification of the ARMeD system.

(A) Western blot analysis of HEK293 cells either transfected with 3 µg GFP-myo6 together with 7 µg empty vector (EV) or 10 µg ARMeD 1xRING or 2xRING constructs. A non-transfected (NT) sample and a sample transfected with 3 µg GFP-myo6 alone were also included as controls. The cells were harvested for Western blotting 48 h post transfection. **(B)** Schematic of the ARMeD system for degradation of myo6 with the modified DARPin tool. **(C)** Western blot analysis of U2OS cells transfected with 5 µg G4-RING or G4-2xRING constructs with time points up to 72 h after the transfection.

3.5.4 Generation of stable cell lines that inducibly express the RING constructs

To generate stable cell lines that express the RING constructs, I made use of the U2OS FlpIn cells that allows integration of a target gene into a specific locus within the genome via the Flp recombinase[183]. Upon integration, the gene can be inducibly expressed with the addition of DOX.

I created stable cell lines with both the G4-RING and G4-2xRING constructs, after which I treated the cells with DOX to assess expression levels of the constructs and potential degradation of myo6 (Figure 3.16A). While low expression of G4-RING could be observed by Western blot analysis, expression of G4-2xRING was barely detectable. To determine whether the low expression levels of both constructs was a homogenous effect within the entire cellular population or simply rather expression of the constructs in very few cells, I performed IF experiments. The results proved the second hypothesis to be correct, as very few cells showed expression of the constructs (Figure 3.16B). Therefore, to achieve a more homogenous population of cells that express the constructs, I proceeded to generate single cell clones.

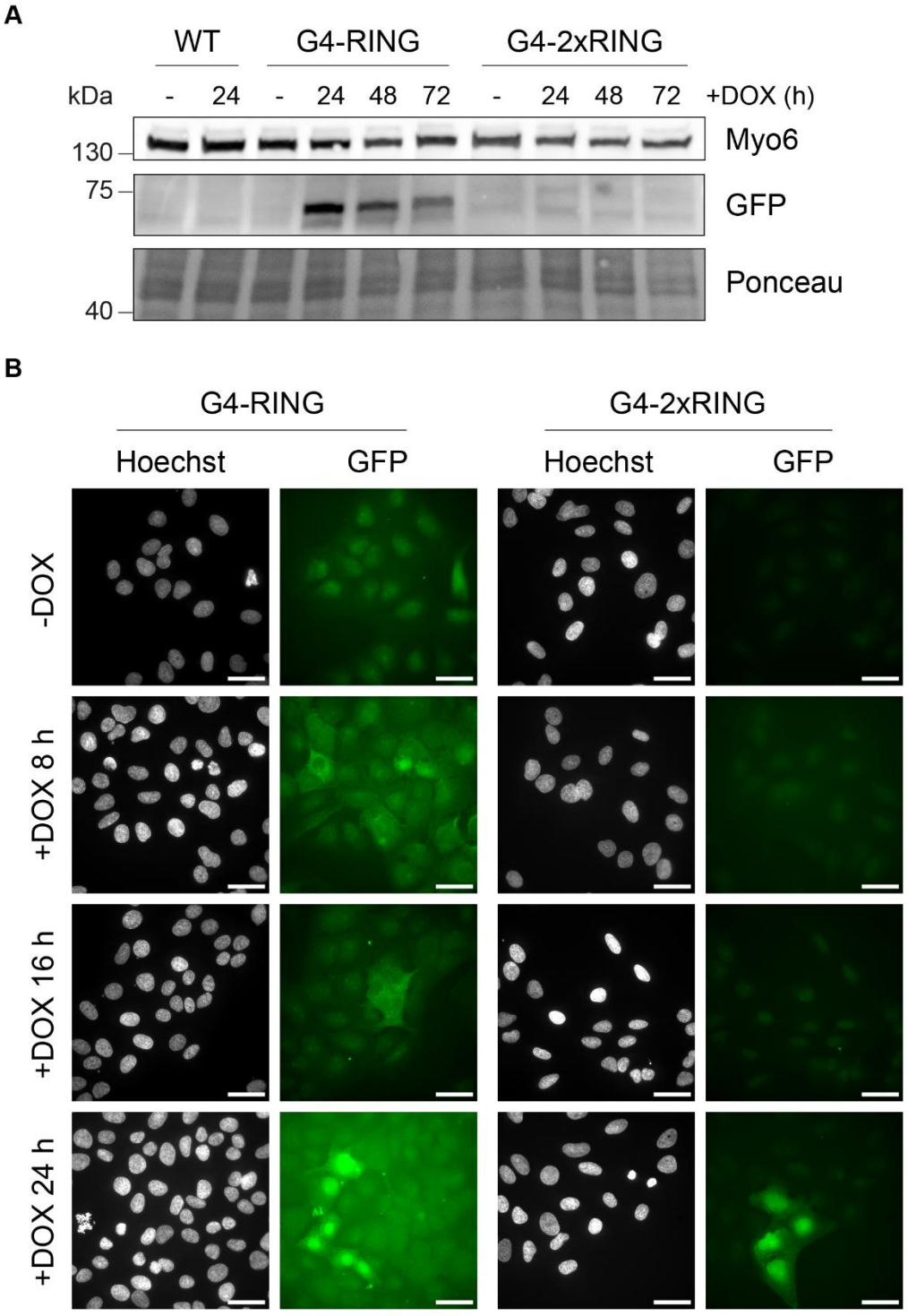

Figure 3.16: Generation of stable cell lines expressing G4-RING and G4-2xRING.
(A) Western blot analysis of U2OS FlpIn cells with stably integrated G4-RING and G4-2xRING constructs that can be inducibly expressed upon DOX. Cells were treated with 20 ng/ml DOX and samples were collected 24, 48 and 72 h post treatment. WT cells served as the control. **(B)** IF analysis of U2OS FlpIn G4-RING and G4-2xRING treated with 20 ng/ml DOX for 8, 16, 24 h. The nuclei were stained with Hoechst, shown in grey and the constructs were visualised via their GFP-tag, shown in green. Scale bars are 40 µm, shown in white in the lower right corner of the images.

3.5.5 Generation of G4-RING and G4-2xRING single cell clones

To generate single cell clones that express the RING constructs, I first performed single cell sorting via flow cytometry with the help of the [redacted]. In total, 191 clones that expressed the constructs were sorted for each cell line. After expansion of these clones, I took 32 clones from each cell line to screen for clones with a good expression level using high throughput microscopy with the help of the [redacted]. Figures 3.17A and 3.17B respectively show the results of G4-RING and G4-2xRING single cell clones from the high throughput microscopy experiment, with the chosen clones for further experiments highlighted with a blue box. The clones were chosen based on their expression levels. While the majority of the clones were chosen based on their high GFP signal, a small number were also chosen based on lower GFP signal intensities, in order to have a diverse mixture of clones for further testing.

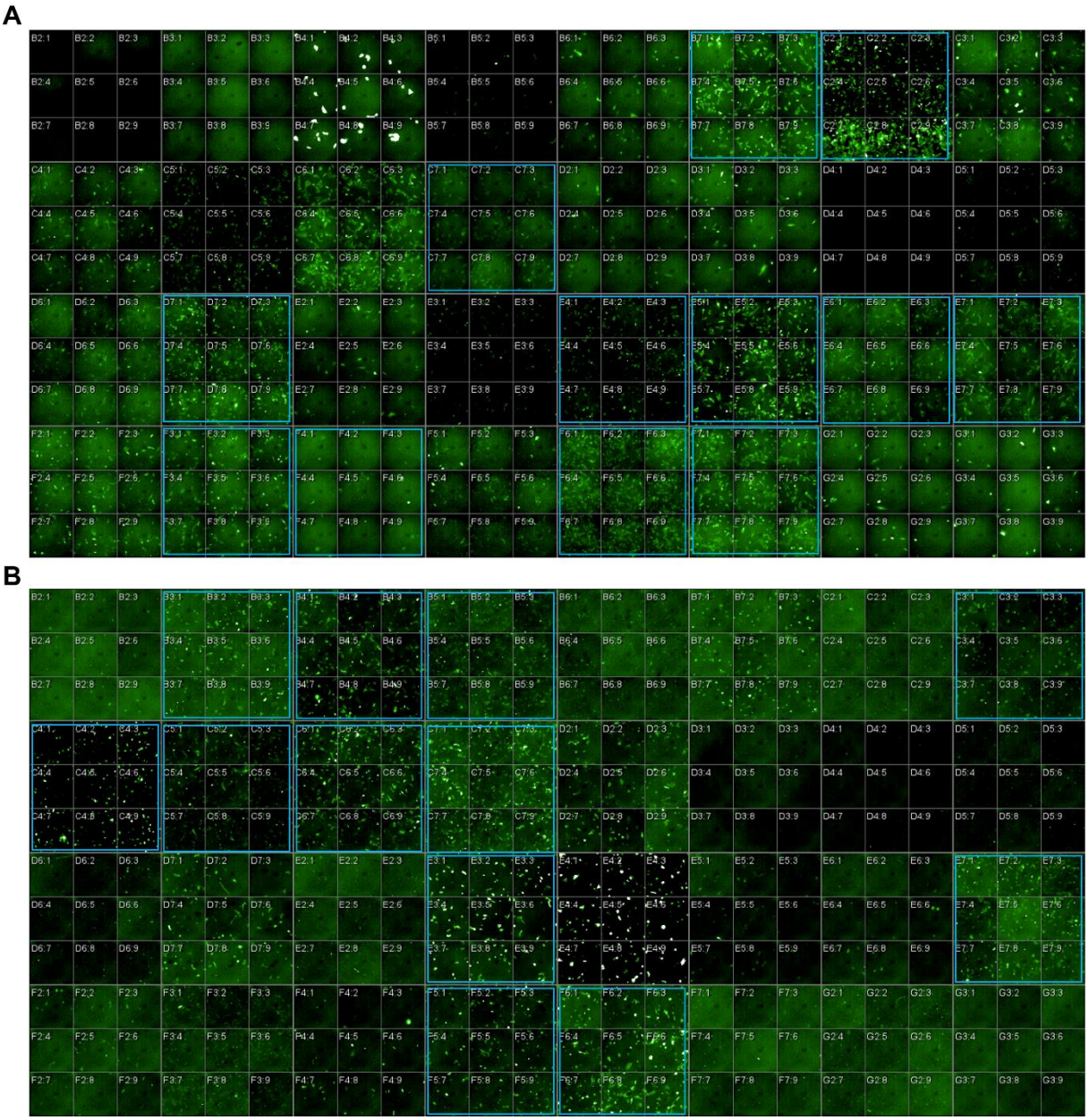

Figure 3.17: Screening of G4-RING and G4-2xRING expression levels in single cell clones.

(A) High throughput screening of U2OS FlpIn single cell clones expressing G4-RING for determination of the construct expression. The clones were treated with 20 ng/ml DOX for 16 h prior to microscopy analysis using the 20x water objective on the Opera Phoenix microscope. Chosen clones for further experiments are highlighted with a blue box. **(B)** High throughput screening of U2OS FlpIn single cell clones expressing G4-2xRING for determination of the construct expression. The clones were treated with 20 ng/ml DOX for 16 h prior to microscopy analysis using the 20x water objective on the Opera Phoenix microscope. Chosen clones for further experiments are highlighted with a blue box.

3.5.6 Screening of myo6 degradation in G4-RING and G4-2xRING single cells clones

The next step after choosing the single cells clones from the high throughput microscopy experiment was to determine whether myo6 could be degraded on the protein level in these clones via Western blot analysis. Although I had previously chosen 24 clones from high throughput screening (Figure 3.17), five of these clones showed impaired growth and were thus not subjected to the Western blot analysis. I therefore performed simple Western blots with eleven clones expressing G4-RING and eight clones expressing G4-2xRING (Figures 3.18A and 3.18B). WT cells not expressing any construct were taken as the control and each clone was treated -/+ DOX. Somewhat unexpectedly, I only observed degradation of myo6 in one out of all the tested clones, #8, which inducibly expresses G4-2xRING, although the expression of the construct in each clone could be observed from the GFP blot. Some clones were observed to already express the construct in the absence of DOX, indicating leakiness of the inducible system.

After a closer inspection of the Western blot result, I noticed that the size of the expressed construct varied among the different clones, with each construct to be far smaller than the expected size of 75 kDa. This indicates that the construct was degraded, suggesting a possible reason for the absence of degradation of myo6. The degradation of the G4-RING construct could have been too rapid and potentially could have occurred prior to it binding to myo6.

By comparison to the other clones, the expression level of G4-2xRING in clone #8 seemed moderate, with no significant amount of leaky expression of the construct observed. This clone will hereon be referred to as 2R#8. Even though the expressed G4-2xRING construct in 2R#8 was also observed to be smaller than the expected 75 kDa, unlike the other clones, it seemed to be capable of also degrading myo6. Further characterisation of 2R#8 will follow in the subsequent experiments.

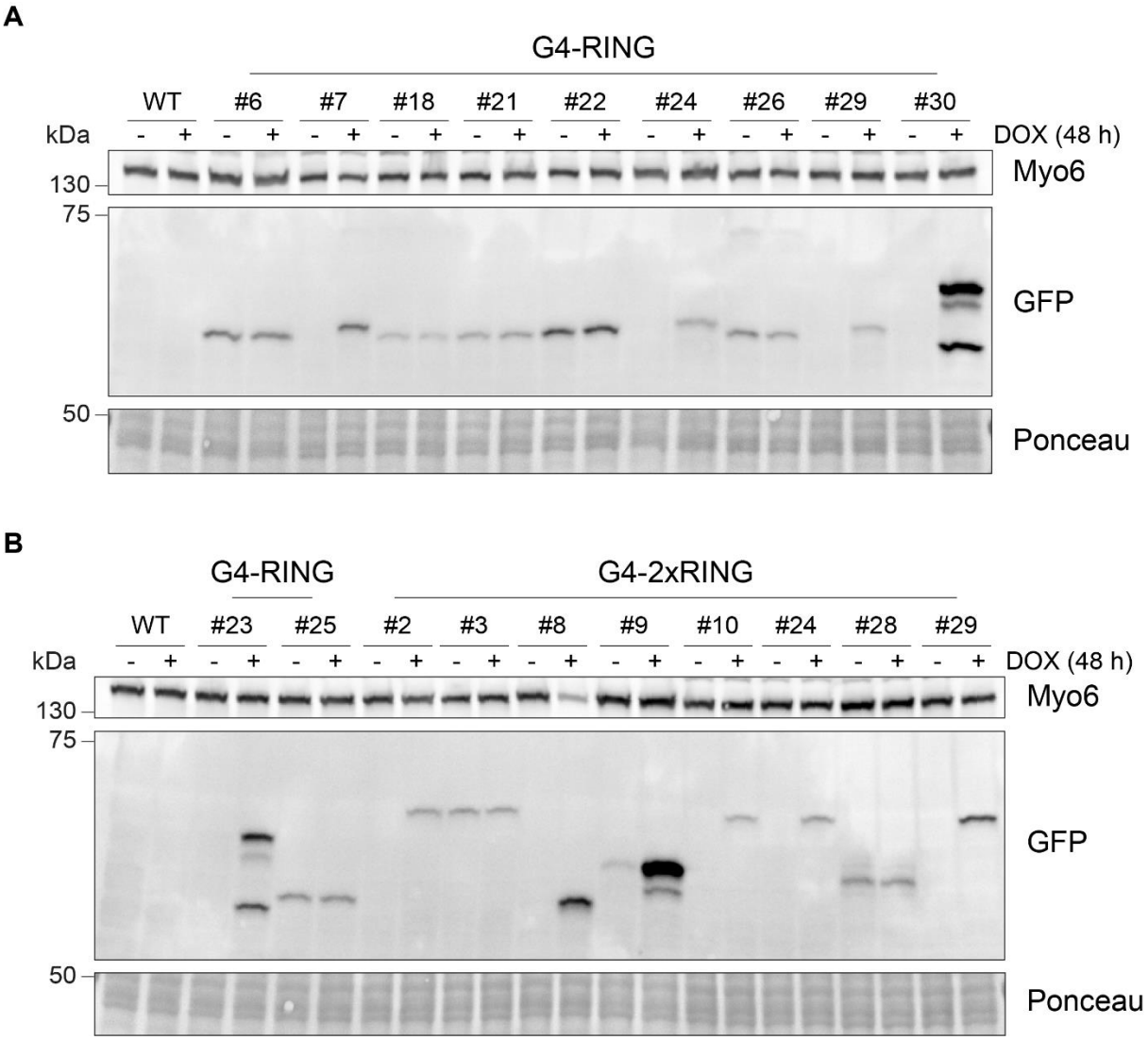

Figure 3.18: Screening of myo6 degradation in G4-RING and G4-2xRING single cell clones.

(A) Western blot analysis of nine U2OS FlpIn single cell clones stably integrated with G4-RING to determine potential degradation of myo6 in the clones. The cells were treated −/+ 20 ng/ml DOX 48 h prior to the assay. WT cells served as the control. Expected size of the construct was approximately 75 kDa. **(B)** Western blot analysis of two U2OS FlpIn single cell clones stably integrated with G4-RING and eight single cell clones stably integrated with G4-2xRING, to determine potential degradation of myo6 in the clones. The cells were treated −/+ 20 ng/ml DOX 48 h prior to the assay. WT cells served as the control. Expected size of the construct was approximately 75 kDa.

3.5.7 Characterisation of 2R#8

Before moving on to using 2R#8 in functional assays, I wanted to characterise the clone in further detail. As it was shown that the ARMeD system is highly efficient and capable of degrading a target protein within 24 hours[182], I also wanted to determine the earliest time point, at which myo6 is degraded in 2R#8. This would provide convenience for further experiments with this clone. Therefore, I treated 2R#8 with DOX and collected time points for up to 24 hours (Figure 3.19A). I observed a gradual decrease in myo6 levels as the cells were treated longer with DOX, with degradation already detectable after 4 hours and peaking at approximately 16-24 hours after the addition of DOX. In another experiment, I also took samples of cells treated with DOX for up until 72 hours, but observed no difference in the extent of degradation among the 24, 48 and 72 h samples (result not shown). Therefore, for all subsequent experiments, I only added DOX for 24 hours to induce expression of the G4-2xRING construct in 2R#8.

As the next step of the characterisation of 2R#8, we asked whether myo6 and G4-2xRING were degraded via the proteasome, as we expected based on Ibrahim *et al*[182]. To determine this, I added DOX to induce expression of the construct and added the proteasomal inhibitor, MG132, prior to harvesting of the samples. As observed previously, the addition of DOX induced degradation of myo6, correlating with the expression of G4-2xRING (Figure 3.19B). Upon the addition of MG132 to the sample treated with DOX in 2R#8, I observed a shift towards a larger band size of G4-2xRING, indicating stabilisation of the construct. The myo6 blot also showed slight stabilisation of myo6 upon the MG132 treatment. These observations suggested that the degradation of myo6 in 2R#8 was indeed proteasome-dependent.

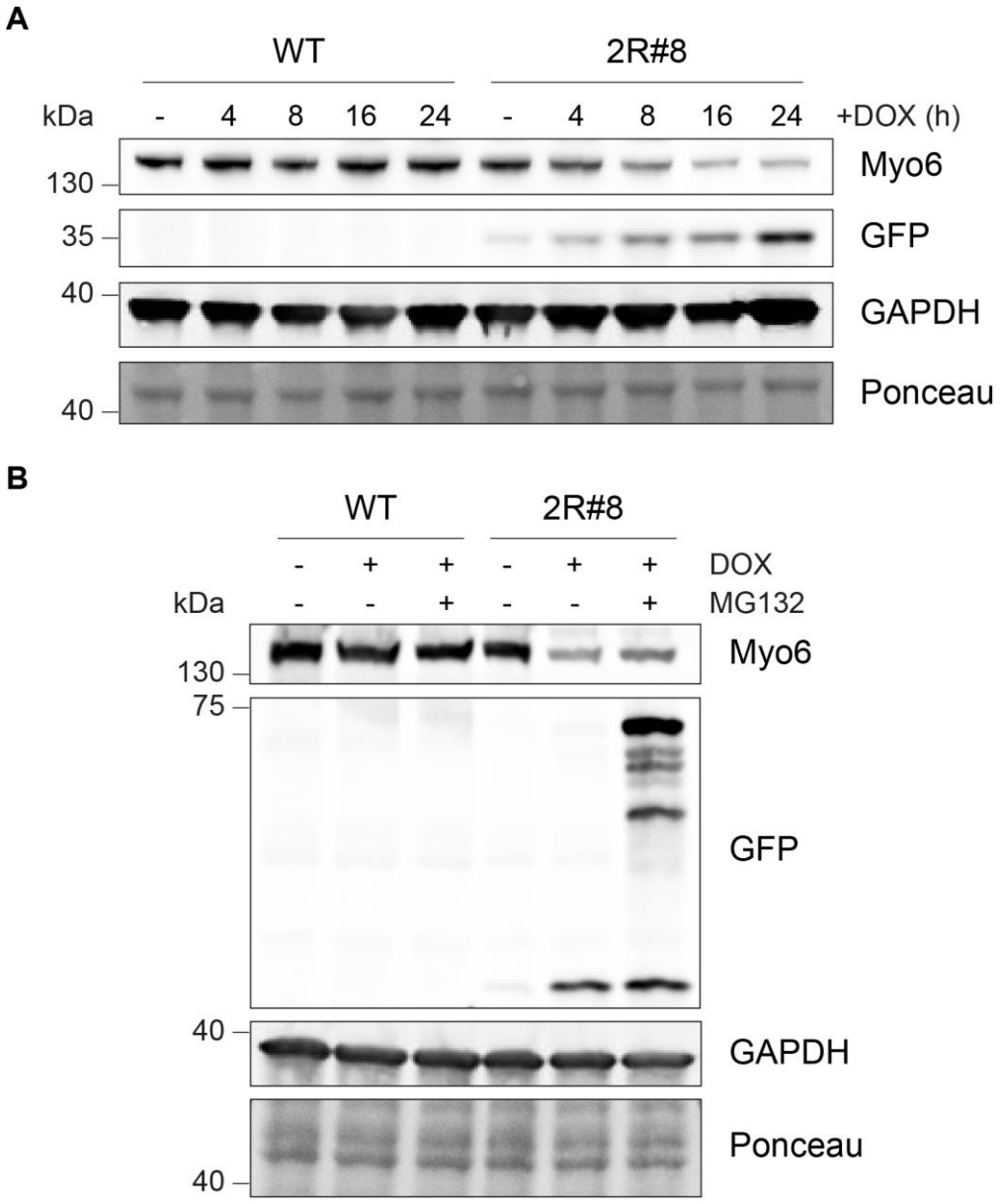

Figure 3.19: Further characterisation of 2R#8.

(A) Western blot analysis of 2R#8 subjected to a DOX treatment time course. The cells were treated with 20 ng/ml DOX and samples were collected 4, 8, 16 and 24 h post treatment. WT cells served as the control. **(B)** Western blot analysis of 2R#8 treated with both 20 ng/ml DOX 24 h prior to the assay and 30 µM MG132 4 h prior to the assay. WT cells served as the control.

Having sufficiently characterised 2R#8 for my purposes, I proceeded to using 2R#8 in functional assays, as the original aim of the DARPin was to manipulate myo6 intracellularly and differentiate between the contribution of either nuclear or cytoplasmic myo6. With the fork protection fibre assay, I had shown that siRNA-mediated depletion of myo6 resulted in nascent strand degradation (Figure 3.7). I next wanted to assess whether degradation of myo6 on the protein level with G4-2xRING

would result in the same phenotype. For comparison of the efficiency of myo6 depletion, I performed siRNA-mediated knockdown of myo6 in 2R#8 or treated 2R#8 with DOX. Western blot analysis of the samples showed that degradation of myo6 on the protein level in 2R#8 was comparable with the siRNA-mediated depletion (Figure 3.20A). I subjected the same samples to the fork protection fibre assay and observed that the sample treated with DOX showed nascent strand degradation to a similar extent as the siMyo6 cells. This not only strengthened the specificity of myo6's contribution towards fork protection, but also made a leap towards differentiating the nuclear and cytoplasmic functions of myo6.

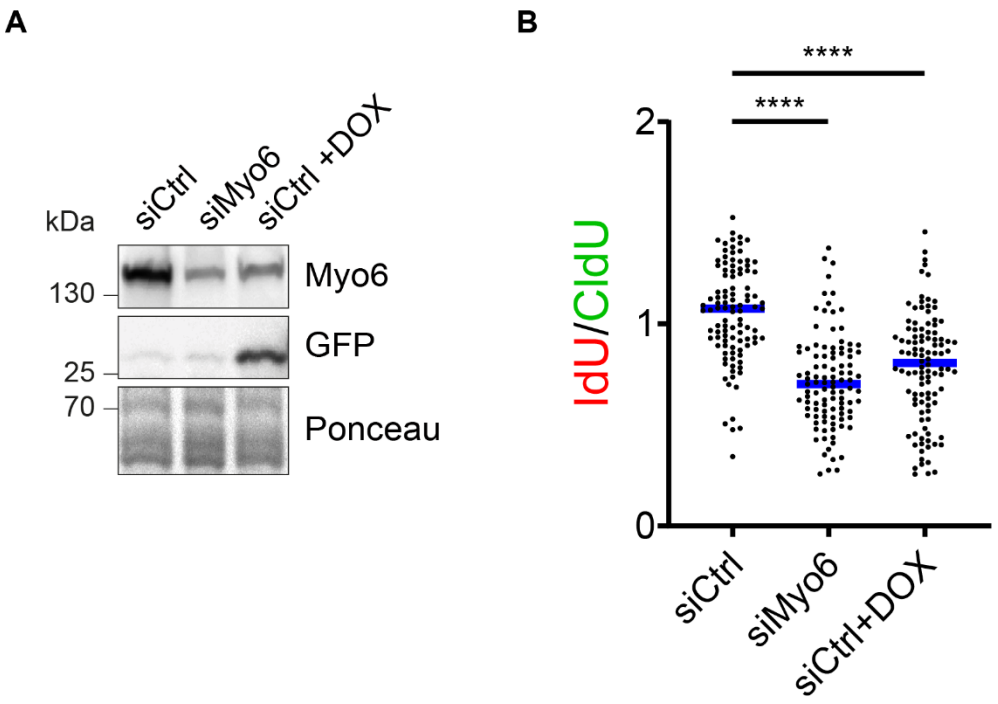

Figure 3.20: Degradation of myo6 on the protein level also results in fork de-protection. **(A)** Western blot analysis of the knockdown efficiency of myo6 and degradation of myo6 in 2R#8. siRNA-mediated knockdowns were performed 72 h prior to the assay and 20 ng/ml DOX was added 24 h prior to the assay. **(B)** A DNA fibre assay was performed with samples from (A), according to Figure 3.7A. Quantification of the DNA fibre assay was shown as the ratio of IdU/CldU. A minimum of 100 fibres were analysed for each sample. Significance was determined by the Mann-Whitney test where ****= p<0.0001.

3.5.8 Usage of the SPOP system

Having determined with the ARMeD system that the G4 DARPin was capable of functioning and manipulating myo6 within cells, I started tackling the next aim of manipulating nuclear and cytoplasmic myo6 separately. Interestingly, there is a system that degrades only the nuclear pool of a target protein[184], which we could make use of to try to degrade nuclear myo6 specifically. This system, hereon referred to as the SPOP system, relies on CUL3, one of the Cullin-RING ubiquitin ligases, as well as the SPOP adapter protein that contains a BTB domain (Figure 3.21A)[184]. The substrate recognition domain of the adaptor protein was exchanged for a GFP-nanobody, thus allowing the complex to bind to GFP-tagged proteins and targeting them for degradation. Figure 3.21B shows that although the SPOP construct is expressed both in the nucleus and the cytoplasm, the targeted protein is only degraded in the nucleus, making this an excellent system to only degrade the nuclear pool of a protein[184]. We therefore took the chance to utilize this system and modified it to target nuclear myo6.

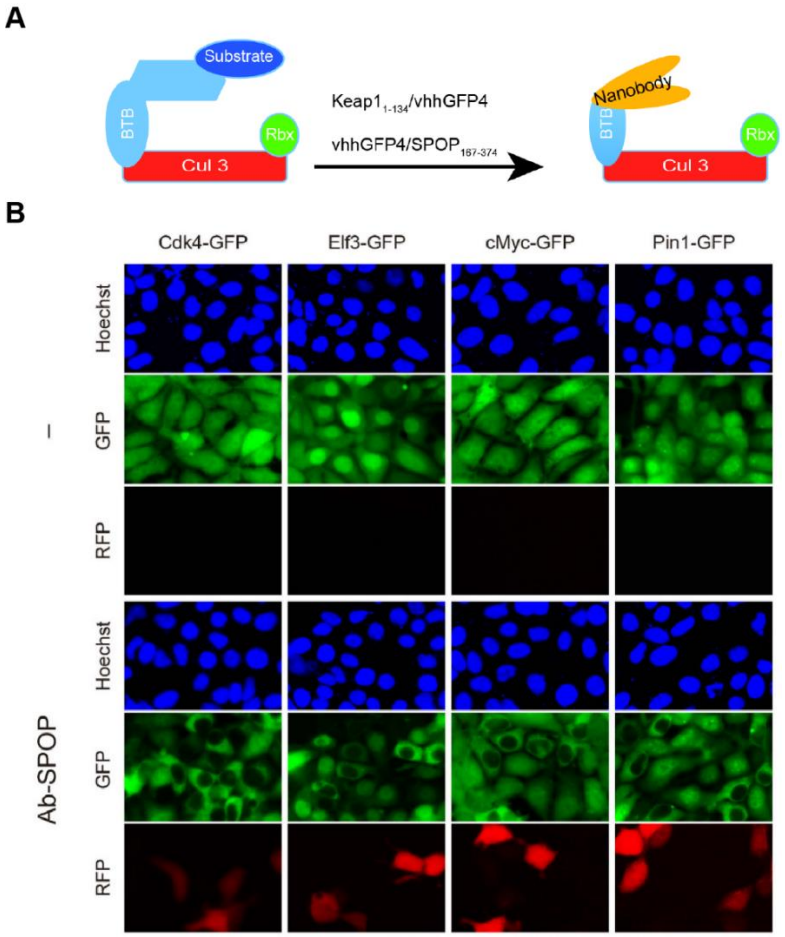

Figure 3.21: The SPOP system (adapted from Shin *et al*, 2015)[184]**.**
(A) Schematic of the SPOP-CUL3 construct. SPOP is depicted as "BTB", as it contains a BTB domain. **(B)** Usage of the SPOP degradation system for the nuclear pool of proteins.

3.5.9 Usage of the SPOP system for degradation of myo6 on the protein level

As I had previous experience with the ARMeD degradation system, I wanted to use a similar pipeline for the SPOP system. As a first step, I exchanged the GFP-nanobody with the G4-DARPin (Figure 3.22). The newly modified construct will be hereon referred to as SPOP-G4. In parallel, I also created a control construct, SPOP-E3_5, of which E3_5 is a control DARPin that does not target a specific protein.

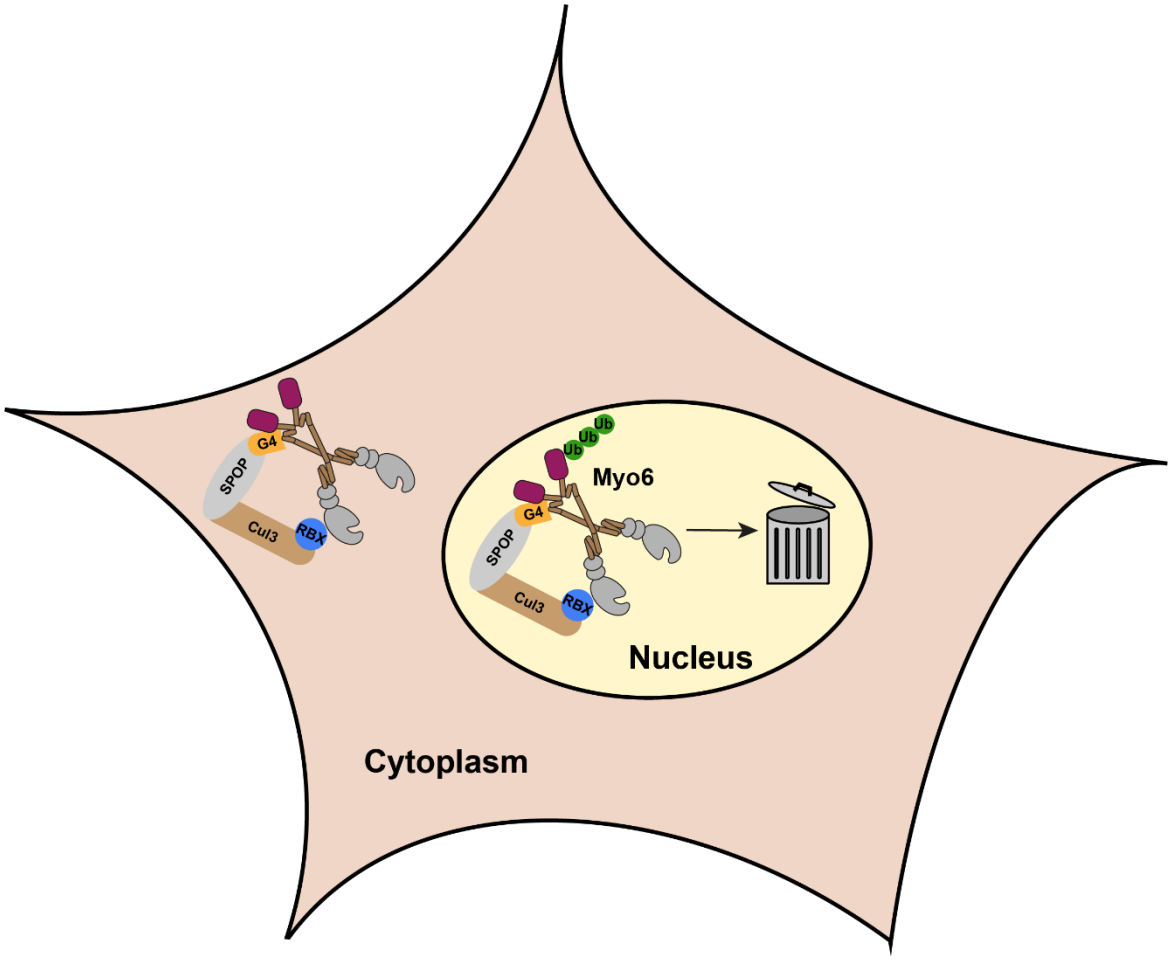

Figure 3.22: Modification of the SPOP system (adapted from Shin *et al*, 2015)[184]**.** Schematic of SPOP-mediated degradation of nuclear myo6 with the GFP-nanobody in the original construct exchanged for the G4 myo6-binding DARPin.

3.5.10 Fractionation of cells to test functionality of SPOP-G4

As mentioned previously in this chapter, the immense amount of cytoplasmic myo6 renders it difficult for us to visualise and manipulate endogenous nuclear myo6 using IF microscopy due to the strong cytoplasmic signal. This rendered using IF of myo6 to test the functionality of SPOP-G4 unfeasible. Another approach that we wanted to test for determining the depletion of the nuclear pool of a protein was cell fractionation. I

transfected cells with SPOP-E3_5 and SPOP-G4 and obtained the whole cell extract (WCE), cytoplasmic (Cyto), nuclear soluble and nuclear insoluble fractions. I used tubulin as the control for the cytoplasmic fraction and histone H2B for the nuclear insoluble fraction. The Ponceau staining served as the general loading control (Figure 3.24). The myo6 blot showed prominent bands in the WCE and Cyto fractions, as expected but very surprisingly showed a similar intensity for the nuclear insoluble fraction. As my colleagues and I had previously performed numerous IF stainings and were barely able to detect the signal of nuclear myo6, the result from this fractionation experiment seemed unrealistic and unreliable. The strong signal in the nuclear insoluble fraction was possibly due to precipitation of myo6 with chromatin, making the cell fractionation approach also unsuitable for testing the SPOP-G4 construct.

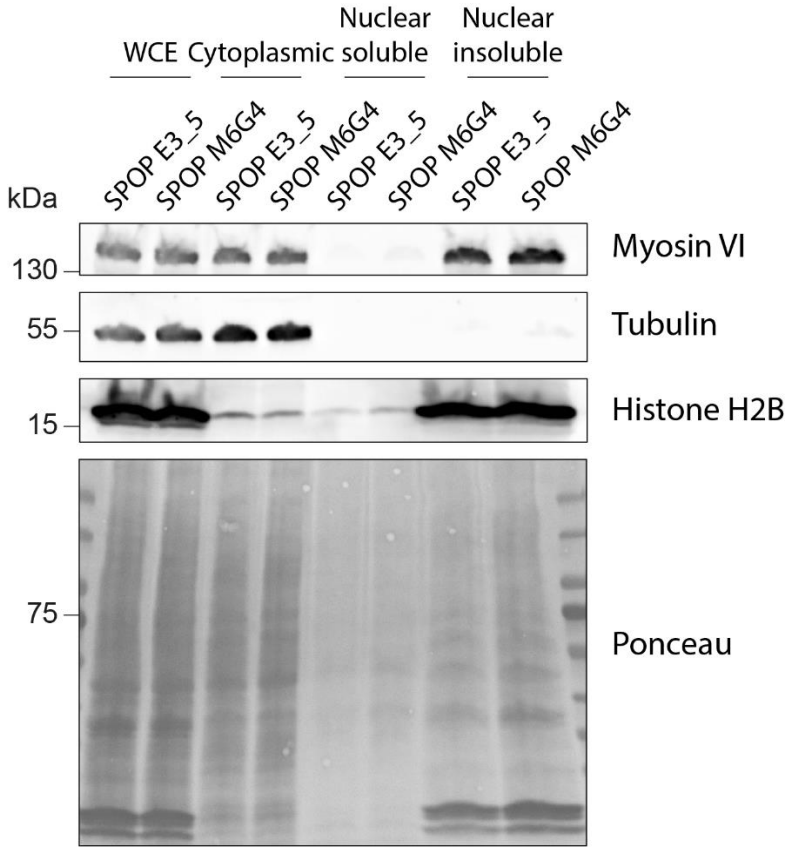

Figure 3.23: Cell fractionation to determine potential degradation of nuclear myo6 with SPOP-G4.

Western blot analysis of HEK293 cells transfected with 5 µg control construct SPOP-E3_5 or SPOP-G4. Cells were harvested 48 h post transfection and fractions for whole cell extract (WCE), the cytoplasm (Cyto), soluble nuclear components and insoluble nuclear components were subjected to SDS-PAGE and analysed by Western blotting. Tubulin was used as the control for the cytoplasmic fraction and histone H2B was used as the control for the nuclear insoluble fraction (chromatin). The Ponceau staining served as the general loading control.

3.5.11 Generation and screening of SPOP single cell clones

Having taken into account that the ARMeD degradation system worked better in cells with G4-2xRING stably integrated, I generated stable cell lines for the SPOP system accordingly. As I previously observed that the bulk population of cells expressing G4-2xRING could not sufficiently degrade myo6, I created single cell clones, after which I found the single cell clone 2R#8 to efficiently degrade myo6 to a similar extent as siRNA-mediated depletion. To minimise the number of unnecessary steps to obtain a fully functional SPOP-G4, I started creating single cell clones out of the bulk population of cells stably integrated with the construct. I used the same FlpIn system[183] to generate the stable cell line, in which the constructs could be induced with DOX.

As microscopic and fractionation approaches had been ruled out as screening methods for the SPOP single cell clones, I needed an alternative way to determine whether the SPOP-G4 system was functional intracellularly. Previous results in sections 3.2 and 3.3 have shown that myo6 depletion results in a decrease in pRPA levels after DNA damage or replication stress induction. Therefore, I decided to use this as a readout for screening of the SPOP clones. Before starting the screening process, I performed an initial test in 2R#8. I treated 2R#8 with DOX for 24 hours to induce expression of G4-2xRING, after which I treated the cells with an acute dosage of UV to create DNA damage as well as replication stress. Western blot analysis of the samples show that upon the DOX treatment in 2R#8, the UV induced phosphorylation of RPA was reduced compared to the cells not treated with DOX (Figure 3.24A). This correlates well with what I observed in KO cells subjected to either DNA damage or replication stress.

Although the pRPA assay does not solve the question of differentiating between the contributions of either nuclear or cytoplasmic myo6, it was a reasonable test for determining whether SPOP-G4 functions intracellularly at all. Having determined this assay to provide a suitable readout, I proceeded to use this for screening of the SPOP clones. I firstly screened five SPOP-G4 clones and took WT cells as the control (Figure 26B). The cells were treated with or without DOX for 48 hours to induce expression of the construct, after which they were subjected to a UV treatment. I detected expression of the construct in all clones and observed a decrease in RPA phosphorylation in clones #3, #4 and #5 when comparing cells treated with and without DOX. I did however also notice a similar trend for the WT cells, albeit to a potentially lesser extent. To determine the reproducibility of the assay, I wanted to repeat the experiment with

the clones that showed promising results, screen more clones and use SPOP-E3_5 clones as the control.

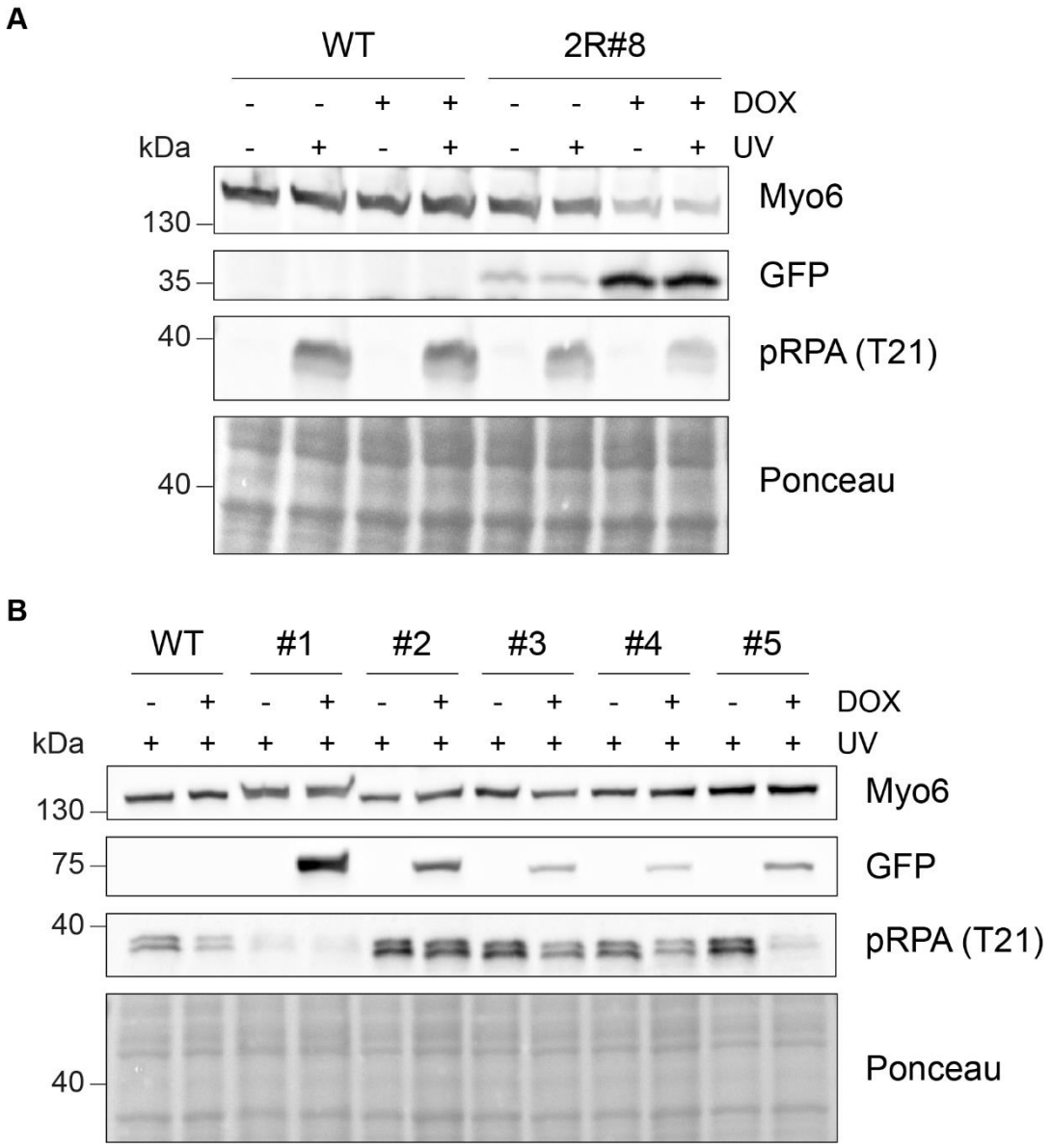

Figure 3.24: Method for screening the functionality of SPOP clones.

(A) Western blot analysis of a UV treatment in 2R#8, to determine pRPA levels. WT and 2R#8 cells were treated with 200 ng/ml DOX 24 h prior to the assay, after which they were subjected to an acute dose of 40 J/m^2 UV. The samples were subsequently recovered in fresh medium for 1 h before harvesting for Western blotting to compare RPA phosphorylation levels between cells treated with and without DOX. **(B)** Five SPOP-G4 clones were subjected to the same assay as described in (A), with WT cells as control. 200 ng/ml DOX was added for 48 h prior to the 40 J/m^2 UV treatment.

Figure 3.25 shows the second round of screening for the SPOP clones. In addition to assessing the phosphorylation level of RPA at phosphorylation site T21, I also

analysed the phosphorylation site S33. I first compared the results of clones #3, #4 and #5 from this experiment to the previous one, to determine whether the previous result could be reproduced. Unfortunately, I observed significantly different results, with the pRPA levels remaining stable or even increasing upon the addition of DOX, which was inconsistent with the decrease that I had observed previously. In addition, I also noticed inconsistency in the change in pRPA level between clones treated with and without DOX among the five SPOP-E3_5 clones. Taken together, the observations from this experiment and a few subsequent ones (data not shown), demonstrate this assay to be inconsistent and unsuitable for further screening of the SPOP clones.

As I had not found a suitable method to determine whether SPOP-G4 could function intracellularly and degrade nuclear myo6, I put this part on hold until a suitable solution could be provided. In the meantime, I investigated into other different methods to differentiate between nuclear and cytoplasmic myo6.

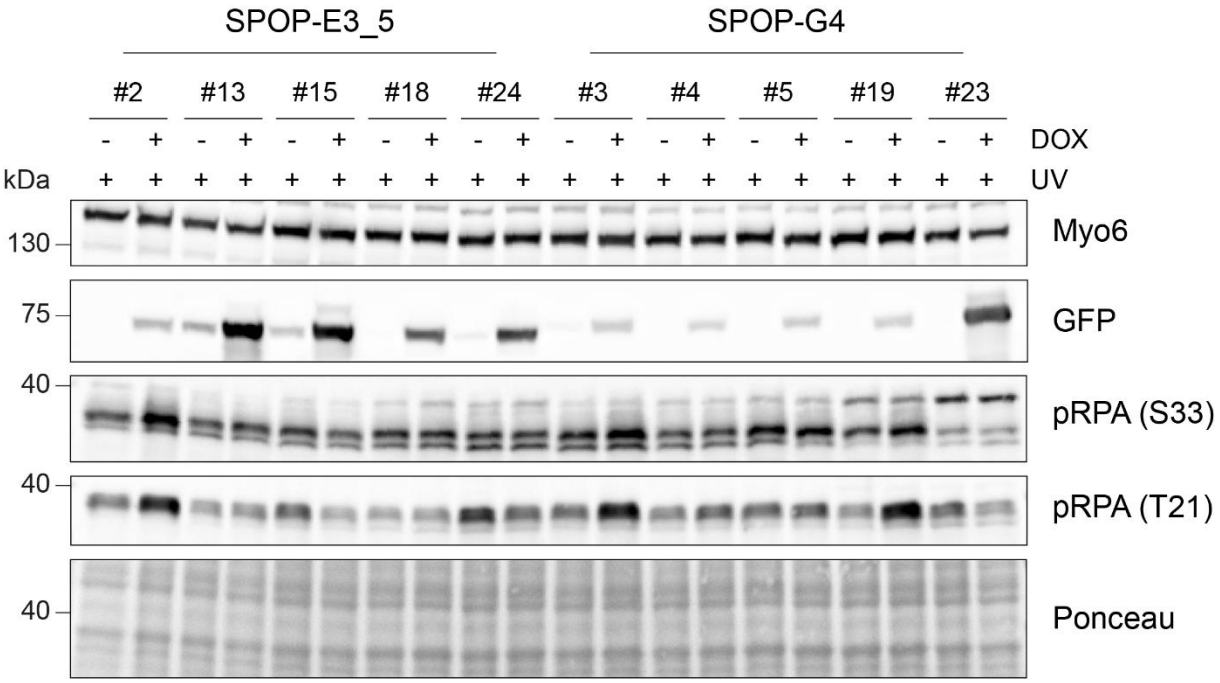

Figure 3.25: Screening of SPOP-E3_5 and SPOP-G4 clones round #2.

Western blot analysis of a UV treatment in SPOP-E3_5 and SPOP-G4 clones, to determine pRPA levels. SPOP-E3_5 and SPOP-G4 clones were treated with 200 ng/ml DOX for 48 h prior to the assay, after which they were subjected to an acute dose of 40 J/m^2 UV. The samples were subsequently recovered in fresh medium for 1 h before harvesting for Western blotting to compare RPA phosphorylation levels between cells treated with and without DOX.

3.5.12 Re-localisation of nuclear myo6 with NES-G4

As another approach to deplete only the nuclear pool of myo6 with the G4-DARPin, we decided to try to re-localize myo6 from the nucleus to the cytoplasm by fusing a nuclear export signal (NES) to the DARPin, hereon referred to as NES-G4. We envisioned the DARPin to enter the nucleus and bind to myo6, after which it would re-localise myo6 to the cytoplasm with the NES tag (Figure 3.26A). However, the problem of visualising nuclear myo6 had not yet been solved, due to the highly abundant cytoplasmic pool (Figure 3.26B left), and it would have been unclear whether NES-G4 would indeed function in the way that we imagined. Therefore, to prove that the concept of a NES-DARPin would be capable of re-localising nuclear target proteins, I first proceeded to test the system on a protein that is mainly expressed in the nucleus, as an easy readout. As GFP is mainly present in the nucleus (Figure 3.26B right), I used this protein for proof of concept.

An initial experiment with a co-transfection of GFP and a NES-GFP-binding DARPin showed the DARPin to localise mainly to the nucleus and GFP to remain in the nucleus (data not shown). This potentially indicated that the excessive amount of expressed GFP was too much for the DARPin to export from the nucleus. As a solution, I performed a titration of the DARPin against GFP (Figure 3.27). As expected, transfected GFP alone was significantly more abundant in the nucleus than the cytoplasm. The DARPin, in different titrations, localised at times more abundant in the nucleus and at times more abundant in cytoplasm. Despite the different compartment localisations of the DARPin, GFP remained in the nucleus. Although this proof of concept experiment did not work as expected, I nevertheless attempted an experiment with myo6 and NES-G4. Not only was it difficult to visualise nuclear myo6, as expected, but the expression level of NES-G4 was also extremely low, rendering the NES system unsuitable for manipulation of nuclear myo6.

Although visualisation of nuclear myo6 is a challenging task, visualisation of cytoplasmic myo6 on the other hand, is extremely straightforward. Therefore, instead of manipulating nuclear myo6 to determine the effects of nuclear myo6 depletion, manipulating and depletion of cytoplasmic myo6 was a significantly easier approach that would allow us to answer whether cytoplasmic myo6 is responsible for its fork protection function.

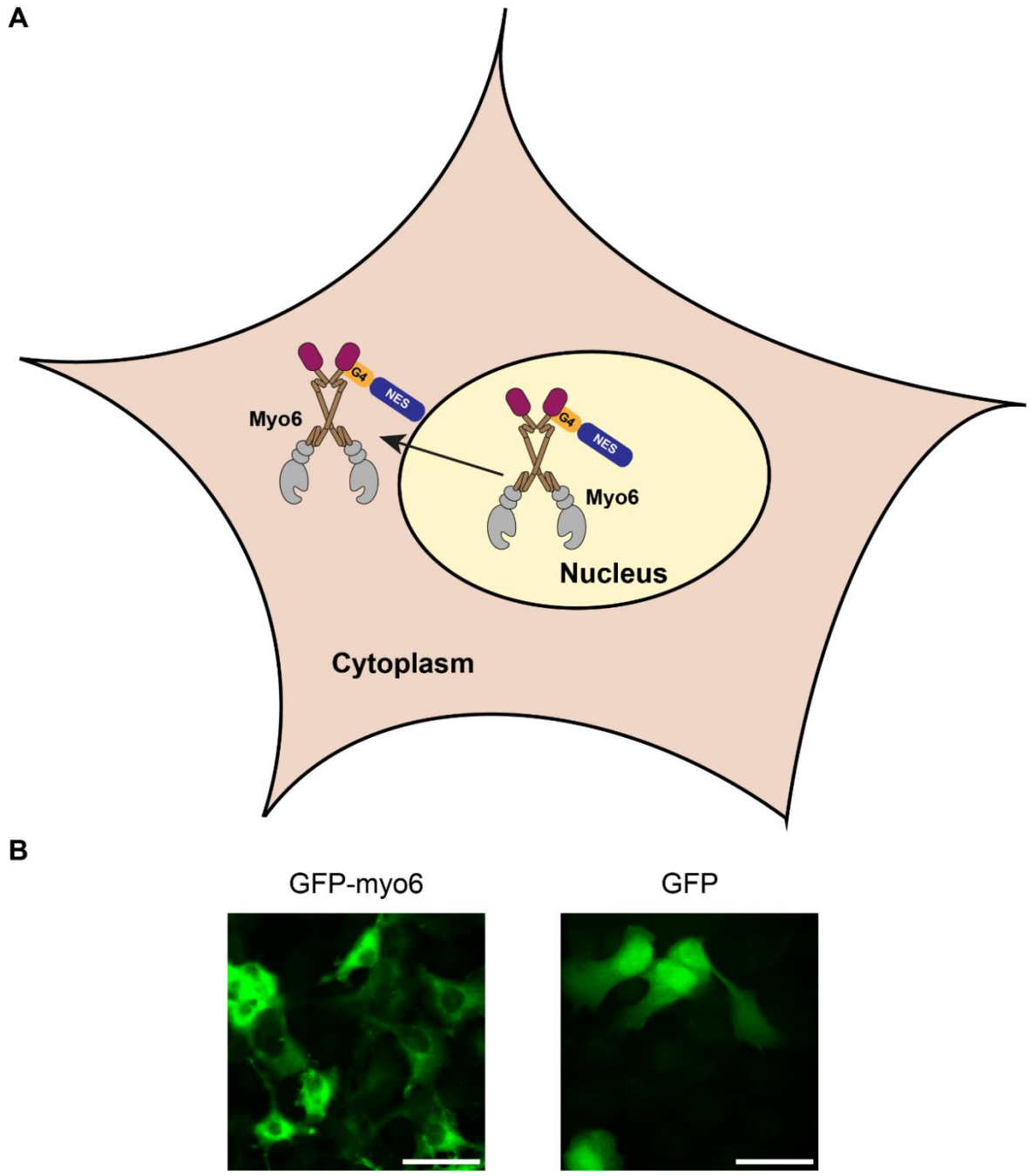

Figure 3.26: Usage of a nuclear export signal (NES) fused to G4, to re-localise myo6 from the nucleus to the cytoplasm.

(A) Schematic of NES-G4 that enters the nucleus, to bind to myo6 and re-localize it to the cytoplasm. **(B)** Left: representative image of GFP-myo6. HEK293 cells stably expressing GFP-myo6 were subjected to microscopy analysis, which showed myo6 to be highly abundant in the cytoplasm and very scarce in the nucleus. Right: representative image of GFP. U2OS cells were transfected with 500 ng GFP and subsequently subjected to microscopy analysis 24 h post transfection, which showed GFP to be more abundant in the nucleus than the cytoplasm. Both proteins were visualised via GFP alone or a GFP-tag and shown in green. Scale bar=40 µm.

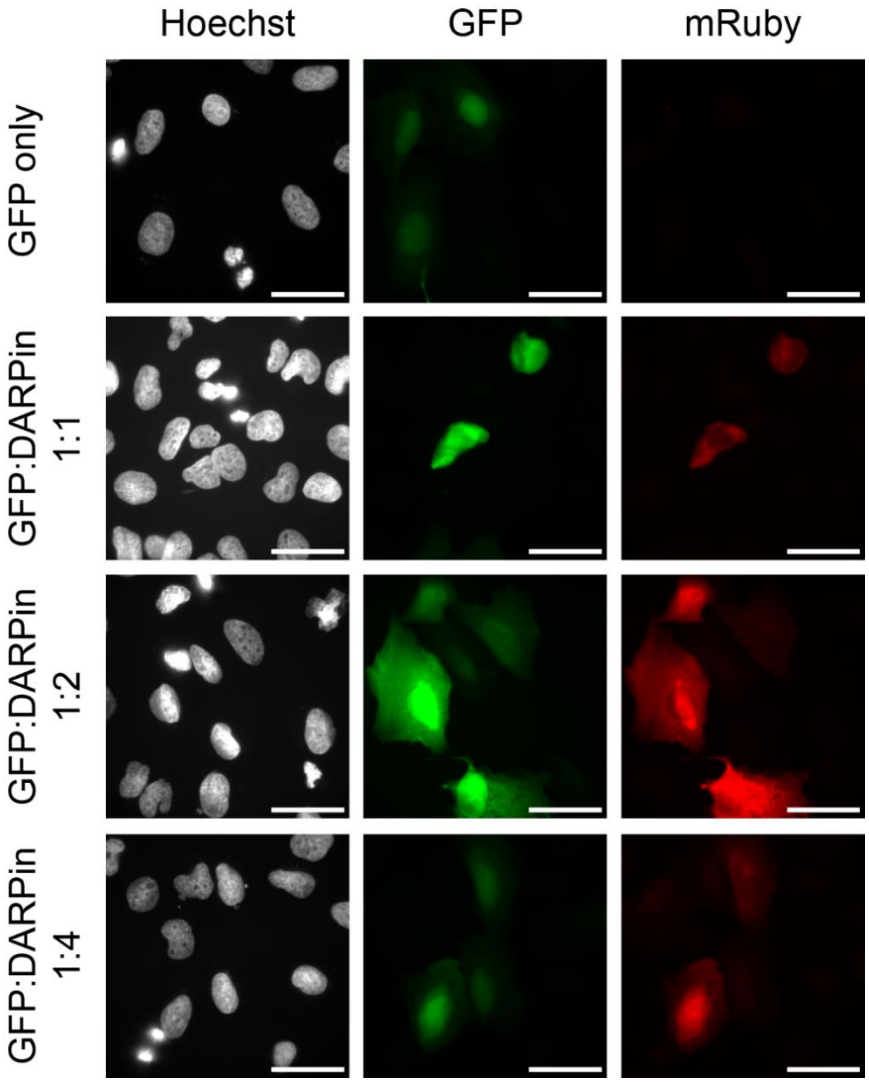

Figure 3.27: Test of different titrations of the NES-GFP-binding DARPin to re-localise GFP from the nucleus to the cytoplasm.

U2OS cells were transfected with 500 ng GFP and a titration of the NES-GFP-binding DARPin against GFP at ratios of 1:1, 1:2 and 1:4 (GFP: DARPin). Cells were subjected to microscopy analysis 24 h post transfection. GFP was visualised and shown in green, expression of the construct was visualised via its mRuby tag and shown in red, and the nuclei were stained with Hoechst, shown in grey. Scale bar=40 µm.

3.5.13 Re-localisation of cytoplasmic myo6 with NLS-G4

To try the opposite approach to NES-G4, I made use of G4 fused to three nuclear localization signals (NLS), hereon referred to as NLS-G4. I hypothesised that the construct would bind to myo6 in the cytoplasm and re-localise it to the nucleus, thus acting as a method to deplete cytoplasmic myo6 (Figure 3.28A). As a control, I used the E3_5 DARPin fused to NLS (NLS-E3_5). As the functionality of this system would be easy to assess, I performed a simple initial experiment, in which I co-transfected

the NLS-E3_5 and NLS-G4 constructs together with GFP-myo6 into HEK293 cells (Figure 3.28B). I observed that the transfection efficiency of NLS-E3_5 was relatively high, compared to NLS-G4, and cells that expressed the NLS-E3_5 construct did not change the predominant cytoplasmic localisation of myo6. Although very few cells expressed NLS-G4, I observed evident localisation of myo6 to the nucleus in the cells expressing the construct. This indicated the NLS system to successfully re-localise and deplete cytoplasmic myo6, as we originally aimed. Having observed this initial promising result, I proceeded to generate stable cell lines that express the NLS-DARPins, to firstly boost the expression level of the constructs as well as to simplify further experiments.

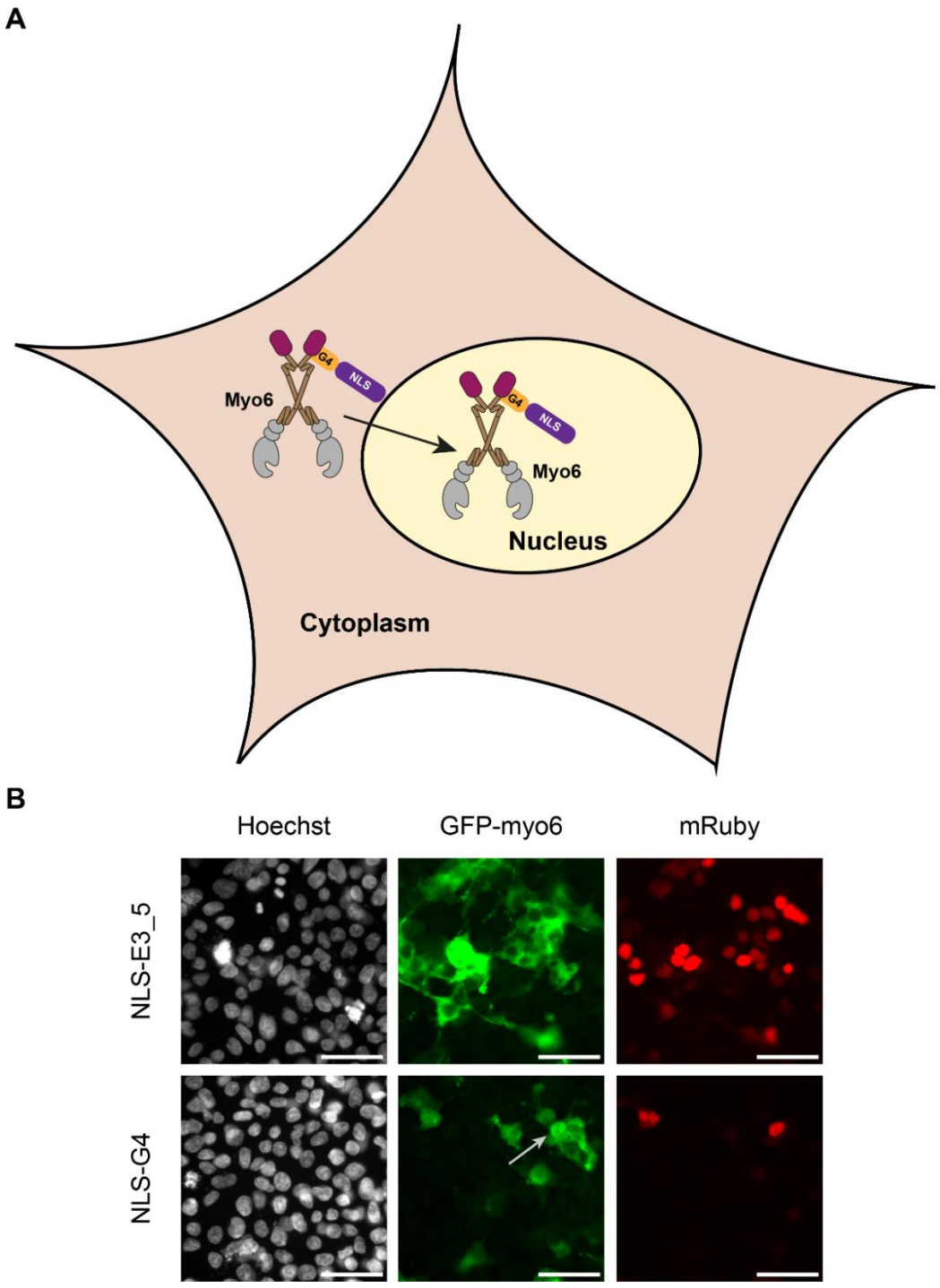

Figure 3.28: Usage of a nuclear localisation signal (NLS) fused to G4, to re-localise myo6 from the cytoplasm to the nucleus.

(A) Schematic of NLS-G4 that binds to myo6 in the cytoplasm and re-localises to the nucleus via the NLS tag. **(B)** HEK293 cells were co-transfected with 3 µg GFP-myo6 and 7 µg NLS-E3_5 or NLS-G4. Cells were harvested 48 h post transfection and subjected to IF microscopy. GFP-myo6 was visualised via the GFP-tag and shown in green, expression of the construct was visualised via its mRuby tag and shown in red, and the nuclei were stained with Hoechst, shown in grey. The grey arrow indicates an example of the successful re-localisation of myo6 to the nucleus. Scale bar=40 µm.

3.5.14 Generation of stable cell lines that inducibly express the NLS-DARPins

To generate stable cell lines that express NLS-E3_5 and NLS-G4, I made use of the same FlpIn system[183] that I had previously used for generating stable cell lines to express the 2xRING and SPOP degradation tools (Figures 3.16A and 3.24B). Having obtained the stable cell lines, I treated them with DOX and assessed the expression level of the constructs by Western blot analysis (Figure 3.29A). I maintained the DOX treatment for up to 72 hours. Already after 24 h, I saw a considerable level of expression of both constructs, which also appeared to be the peak of the expression, as it decreased over time. For future experiments, I will add DOX for only 24 h to induce expression of the constructs.

I could observe the expression level of the constructs via Western blotting but not whether NLS-G4 could efficiently re-localise myo6 to the nucleus. Therefore, I performed an IF experiment to determine myo6's localisation after the 24 hours of DOX induction (Figure 3.29B). I observed very homogenous expression of both constructs in the bulk populations. While there was no significant difference between NLS-E3_5 cells treated with and without DOX, I observed a drastic change in myo6's localisation upon the addition of DOX in the NLS-G4 cells. Not only was NLS-G4 capable of re-localising myo6 to the nucleus, but its high efficiency led to the depletion of the majority of cytoplasmic myo6, judging from the IF images.

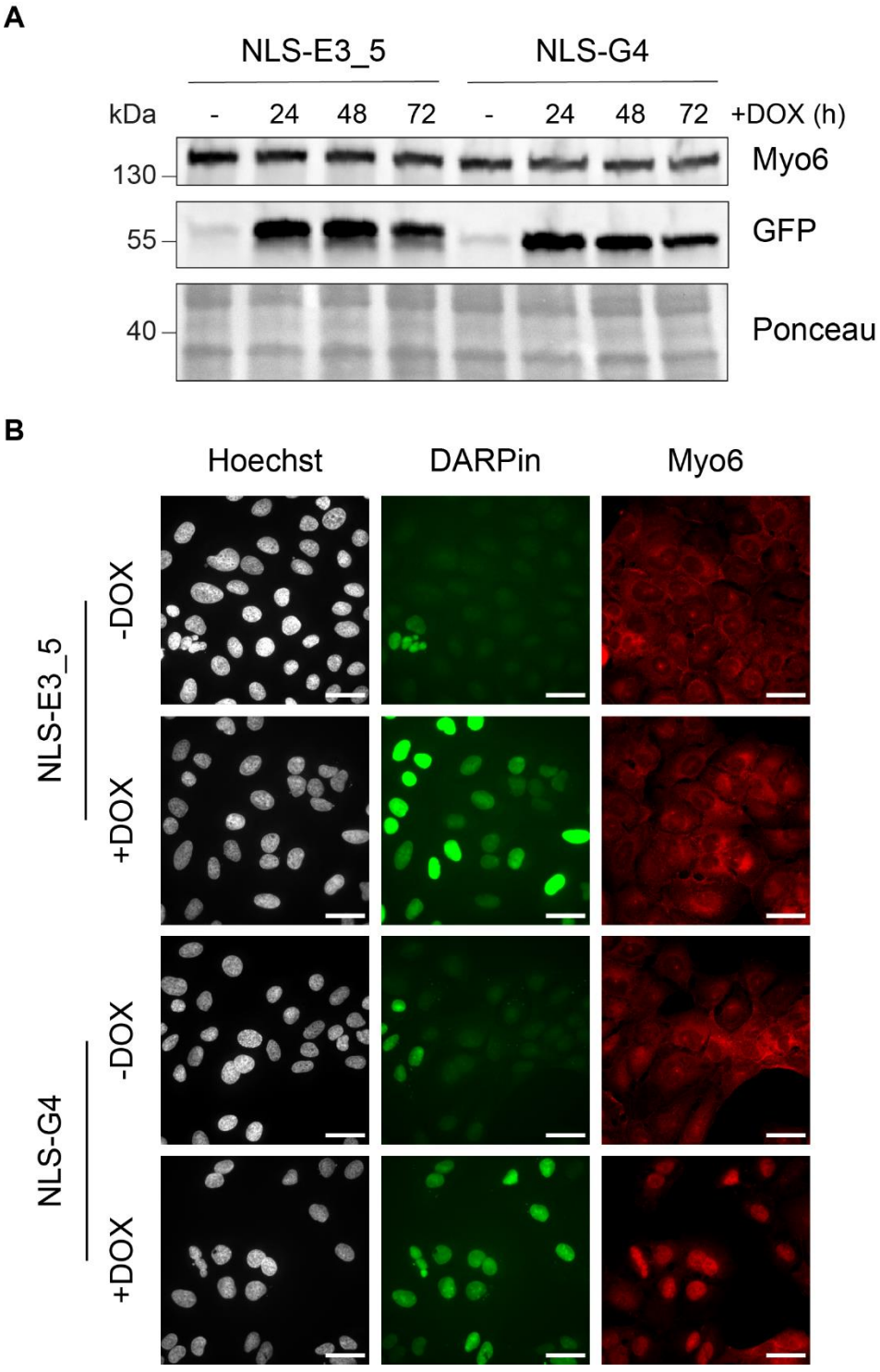

Figure 3.29: Generation of stable cell lines expressing NLS-E3_5 and NLS-G4.

(A) Western blot analysis of U2OS FlpIn cells with stably integrated NLS-E3_5 and NLS-G4 constructs that can be inducibly expressed upon DOX. Cells were treated with 20 ng/ml DOX and samples were collected 24, 48 and 72 h post treatment. **(B)** IF analysis of samples from (A), in which 20 ng/ml DOX was added 20 h prior to the IF experiment. Myo6 was visualised via a fluorescent secondary antibody and shown in red, expression of the constructs was visualised via their GFP tag and shown in green, and the nuclei were stained with Hoechst, shown in grey. Scale bar=40 µm.

3.5.15 Determination of cytoplasmic myo6's contribution to fork protection

Having obtained a tool to deplete cytoplasmic myo6, I could finally test whether the cytoplasmic pool of myo6 contributes to its fork protection function. Therefore, I performed the fork protection fibre assay with NLS-E3_5 and NLS-G4 cells treated with or without DOX (Figure 3.30A). As the positive control, I performed a siRNA-mediated depletion of myo6, in NLS-G4 cells without the DOX treatment. As expected, I observed nascent strand degradation in this sample, indicating fork de-protection to have occurred (Figure 3.30B). NLS-E3_5 cells showed no degradation of the DNA with or without the addition of DOX, which was also expected, as E3_5 is the control DARPin. I observed the same trend in the NLS-G4 cells, scoring no degradation in either sample. This indicated that when myo6 was depleted from the cytoplasm, the forks were still protected, suggesting that it was not cytoplasmic myo6 that was involved in fork protection but rather nuclear myo6. Very intriguingly, I observed a rescue of the siRNA-mediated phenotype upon DOX-induced expression of the NLS-G4 construct. As siRNA-mediated depletion of the target protein occurs in both the nucleus and the cytoplasm but does not fully deplete the protein from the cells, we hypothesised that the addition of DOX in the NLS-G4 cells re-localised the remnants of the cytoplasmic pool into the nucleus. This potentially resulted in a sufficient amount of myo6 in the nucleus that could carry out its fork protection function.

The results with NLS-G4 showed very promising initial indications that nuclear myo6 rather than cytoplasmic myo6 contributed to fork protection, by depletion of cytoplasmic myo6. Therefore, I wanted to strengthen this finding with another approach.

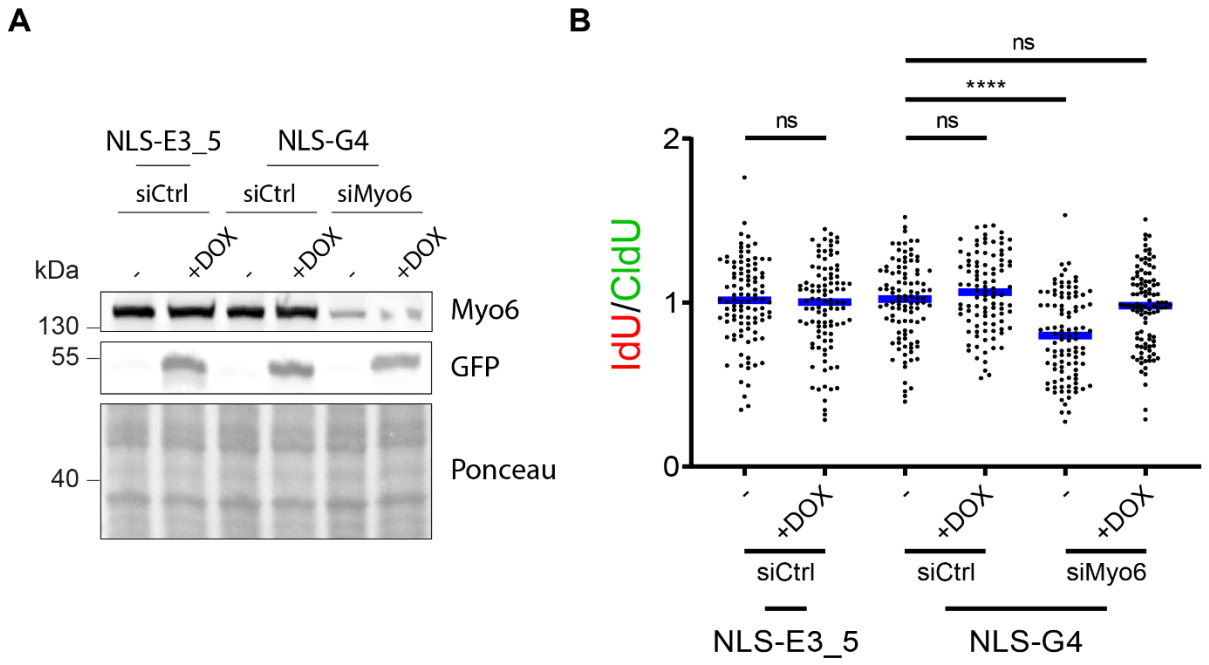

Figure 3.30: Depletion of cytoplasmic myo6 by NLS-G4 does not result in degradation of forks.

(A) Western blot analysis of the knockdown efficiency of myo6 and the expression of the NLS-DARPins in cells stably integrated with NLS-E3_5 or NLS-G4. siRNA-mediated knockdowns were performed 72 h prior to the assay and 20 ng/ml DOX was added 24 h prior to the assay. **(B)** A DNA fibre assay was performed with samples from (A), according to Figure 3.7A. Quantification of the DNA fibre assay was shown as the ratio of IdU/CldU. A minimum of 100 fibres were analysed for each sample. Significance was determined by the Mann-Whitney test where ns=p>0.05 and ****=p<0.0001.

3.5.16 A dominant negative approach to differentiate nuclear and cytoplasmic myo6

In section 3.4.4, I made use of the dominant negative tail of myo6 to show the essentiality of myo6's motor domain in fork protection (Figure 3.11). To address the differentiation of nuclear and cytoplasmic myo6's contribution, I again made use of the dominant negative approach. As WT TAIL was determined to localize to both the nucleus as well as the cytoplasm (result not shown), I wanted to use TAIL-fusions with either a NES or a NLS to change its localisation and hence the compartment of the dominant negative inhibition (Figure 3.31A). I transfected TAIL, NES-TAIL and NLS-TAIL into U2OS cells and carried out IF analysis to first assess their respective localisation patterns. The result confirmed the expected localisations with the NES-TAIL to only localise to the cytoplasm and NLS-TAIL to only localise to the nucleus

(Figure 3.31B). Having determined the TAIL constructs to localise to their expected compartments, I proceeded with subjecting cells with their overexpression to the fork protection assay.

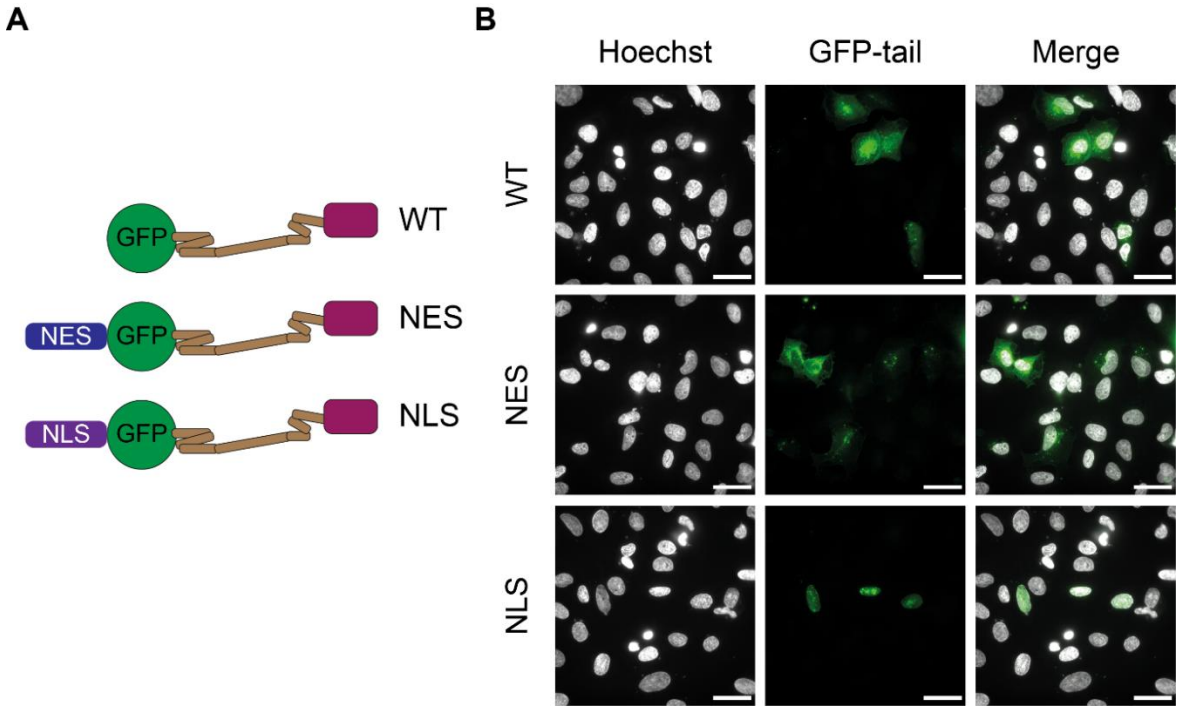

Figure 3.31: Localisation analysis of TAIL, NES-TAIL and NLS-TAIL.
(A) Schematic of TAIL, NES-TAIL and NLS-TAIL (adapted from Magistrati *et al*, 2021)[131]. **(B)** U2OS cells were transfected with 5 µg TAIL, NES-TAIL or NLS-TAIL, 48 h prior to IF analysis. Expression of all constructs was visualised via their GFP-tag and shown in green, and the nuclei were stained with Hoechst, shown in grey. Scale bar=40 µm.

I transfected GFP, TAIL, NES-TAIL and NLS-TAIL constructs into U2OS cells 48 hours before I performed the fork protection assay (Figure 3.32A). GFP acted as the negative control while TAIL acted as the positive control. As shown previously (Figure 3.11), I observed nascent strand degradation in the TAIL sample, confirming its dominant negative effect (Figure 3.32B). I observed the same phenotype in the NLS-TAIL sample while the NES-TAIL sample did not show degradation. This showed that only when myo6 was inhibited in the nucleus, de-protection of the forks occurred.

The dominant negative TAILs and NLS-DARPins proved to be powerful tools in differentiating contributions of nuclear and cytoplasmic myo6. The results obtained with these tools showed a strong indication that it was not cytoplasmic myo6 but nuclear myo6, which was essential to protect forks. Although I have used these tools only to differentiate the contribution of nuclear and cytoplasmic myo6 in fork protection, they

can without a doubt provide valuable information on myo6's other intracellular functions in future research.

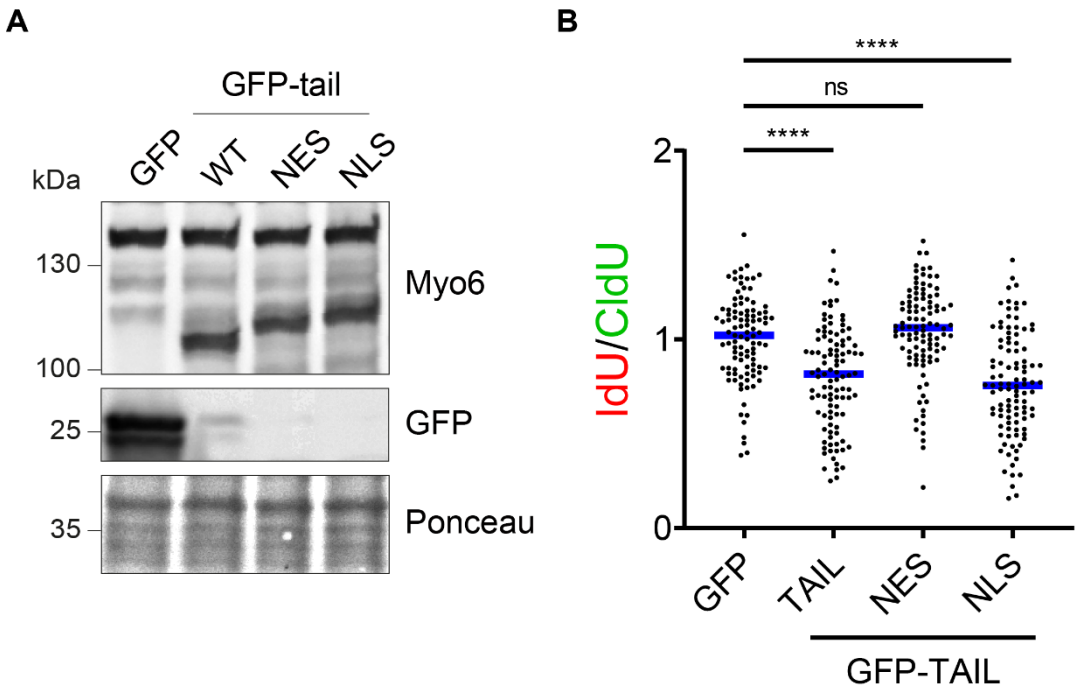

Figure 3.32: Expression of the dominant negative TAIL in the nucleus leads to fork de-protection.

(A) Western blot analysis of the transfection efficiency of TAIL, NES-TAIL and NLS-TAIL. Transfections were performed 48 h prior to the assay. **(B)** A DNA fibre assay was performed with samples from (A), according to Figure 3.7A. Quantification of the DNA fibre assay was shown as the ratio of IdU/CldU. A minimum of 100 fibres were analysed for each sample. Significance was determined by the Mann-Whitney test where ns= $p>0.05$ and ****= $p<0.0001$.

Chapter 4

Discussion

A considerable amount of research into the cytoplasmic functions of the actin-based motor protein, myo6, has been undertaken, and it was found to be involved in important cellular processes such as endocytosis, autophagy, cell migration[140–142]. However, this is not the case for its nuclear functions. While its nuclear function in transcription was discovered nearly two decades ago[149] and understanding of this function has been since then further advanced[150,151], other nuclear functions of myo6 remained unexplored. In this thesis, I have described two novel functions of myo6 in the major genome stability maintenance pathways DNA repair and replication fork protection, particularly highlighting the nuclear pool rather than the cytoplasmic pool of myo6 to contribute to fork protection.

4.1 The mechanism of myo6 in HR

The incentive to investigate myo6's potential role in the HR pathway started with mass spectrometry results, which showed a number of potential interactors of myo6 to be involved in DSB repair as well as the publication of two papers showing the involvement of F-actin in DSB repair [119,120]. As shown in this thesis, repair efficiency by the HR pathway decreases upon the depletion of myo6 (Figure 3.1). Furthermore, phosphorylation of RPA, one of the central steps of the HR pathway, was observed in KO cells to be decreased, indicative of impaired resection (Figure 3.2). These were the initial indications that myo6 is indeed involved in repair of DSBs by HR.

Additional experiments from my colleagues and collaborators shone more light on the role of myo6 in HR. While the decrease of the pRPA level in KO cells is an indication of less resected DNA (Figure 3.2), we wanted to use a more direct approach to determine resection. Therefore, my colleagues carried out immunofluorescence microscopy experiments to follow the formation of RPA foci and BrdU foci, both of which are established methods to study resection[185]. Correlating well with the pRPA results, KO cells showed less RPA and BrdU foci, in comparison to the WT cells, confirming a defect in resection when myo6 is depleted. The impairment in resection was also previously shown for F-actin[120]. As RPA is involved in one of the early events

during HR, we also wanted to determine the effect of myo6 depletion on downstream factors. As expected, [redacted] also observed a decrease in Rad51 foci, the factor that replaces RPA on ssDNA. Having determined myo6 to effect the formation of RPA foci, as well as the downstream step of Rad51 foci formation, we asked the question of whether myo6 potentially functions in a step upstream of RPA, namely the phosphorylation of H2AX, as a general DNA damage response. Microscopic analysis of phosphorylated H2AX (γH2AX) intensity, performed by [redacted], showed no difference between KO and WT cells upon DNA damage, indicating myo6 to play a role in HR, downstream of the initial DNA damage response.

As it was shown that F-actin is not only involved in the resection step of the HR pathway, but also in the mobility of DSBs, we wanted to determine whether this is also the case for myo6. Therefore, we collaborated with the lab of [redacted] to investigate the mobility of Rad52 foci, same as what was done for F-actin to analyse DSB mobility[120]. We observed decreased mobility in myo6 depleted cells, to a similar extent as when the polymerisation of actin is inhibited, showing an additional role of myo6 in the HR pathway.

Although we scored many phenotypes with myo6 in the HR pathway, a clear mechanism remained elusive. As discussed above, a number of DSB repair factors were found in the mass spectrometry screen and it led us to unveiling an involvement of myo6 in HR. Interestingly, the DSB repair factors found in the screen mainly function in the NHEJ pathway, not HR, while simultaneously, we could show the involvement of myo6 in HR with many approaches. While this was initially enigmatic, a paper describing the function of p97/VCP, an AAA-ATPase, in extracting the Ku heterodimer from DNA, helped us in understanding this phenomenon[52,186]. VCP was identified in the mass spectrometry screen and was additionally shown to interact directly with myo6 by [redacted]. Combining these two pieces of information, we proposed the hypothesis that myo6 could cooperate with VCP and participate in the extraction of the KU heterodimer. To challenge our hypothesis, [redacted] compared the quantity of chromatin-bound Ku80 and the number of Ku80 foci between WT and KO cells upon DNA damage. Through cell fractionation experiments, she observed more chromatin-bound Ku80 in KO cells compared to WT cells. In addition, although she observed the resolution of Ku80 foci after DNA damage over time in WT cells using an IF-based approach, this was not the case in VCP-inhibited cells (positive

control) and KO cells. Both results strongly hint towards the proposed mechanism of myo6 participating in the removal of the Ku heterodimer, to promote repair by HR.

While the above-mentioned proposed mechanism of myo6 in DSB repair is a very fitting scenario, it does not exclude the function of myo6 in additional downstream steps of the HR pathway. In addition to the numerous DNA repair and replication factors that were found in the mass spectrometry screen, a number of chromatin remodellers such as NAP1L1, RUVBL1, and RUVBL2 were also identified. RUVBL1 and RUVBL2 are subunits of the INO80 complex[187], which is a large chromatin remodeller that carries out functions such as nucleosome sliding and histone exchange[188,189]. It was shown that INO80 promotes HR-mediated DSB repair by the removal of histone variant H2AZ[190]. Therefore, a role of myo6 participating in chromatin remodelling to facilitate HR is another potential scenario that requires further research.

As a consequence of myo6's depletion that leads to decreased HR, we might expect the scales to be tipped in favour of NHEJ. However, results from the Traffic Light Reporter assay in Figure 3.1 did not show upregulation of NHEJ in myo6-depleted cells. As we could not find suitable positive controls for the NHEJ pathway in this assay, the result of myo6's depletion on the pathway was inconclusive. For a better understanding on the effect of myo6's depletion on NHEJ, other NHEJ reporter assays could be used. One such assay is the bioluminescent repair reporter assay, the accuracy of which in detecting repair efficiencies by HR and NHEJ was shown to be consistent with next generation sequencing results[191].

4.2 Myo6's role in replication

4.2.1 The involvement of myo6 in unperturbed replication and replication restart

Not only did we identify a number of DSB repair factors in the mass spectrometry experiment, but we also identified a plethora of replisome components such as subunits of the MCM helicase, subunits of DNA polymerase α, polymerase ε, polymerase δ etc. Having confirmed the interaction of myo6 with several of the listed replisome components by immunoprecipitation and pull down experiments (results not shown), it would have been unsurprising if depletion of myo6 led to impairments in unperturbed DNA replication. However, initial results from DNA fibre assays showed that A549 WT and KO cells replicate at a similar speed (Figure 3.3). Surprisingly, I observed a different phenotype when I performed the DNA fibre assay after siRNA-mediated depletion of myo6. Depletion of myo6 with siRNAs in U2OS cells (Figure 3.6) as well as A549 cells (result not shown) resulted in overall slower replication compared to control cells. One possible explanation for the different phenotypes is a potential adaptation of the KO cells, as the siRNA-mediated depletion is transient and only performed 72 h before the assays are performed.

Not only was the overall speed of siMyo6 cells slower than the siCtrl cells, but the ratio of the second incorporated analogue (IdU) over the first (CldU) is also below one, indicative of fork stalling or impaired restart after stalling that could arise from spontaneous endogenous stress or damage (Figure 3.6). This is a possible scenario as I have also performed preliminary fork restart fibre assays, in which I observed a defect in fork restart or replication progression after release from HU-induced replication stress in KO cells, compared to WT cells (data not shown). Of note, I observed a similar phenotype when the Arp2/3 inhibitor was used. As these experiments were preliminary, more replicates are needed to come to a conclusion. Nevertheless, these results show an initial indication of another potential function of myo6 and F-actin in fork restart. One other possible explanation for the lower IdU/CldU ratio in siMyo6 cells is the possibility of fork de-protection after spontaneous reversal, resulting in the consequence of the degraded forks requiring more time to restart.

The results from the replication restart fibre assays were reminiscent of the results in Figure 3.4, in which KO cells were impaired in resuming cell cycling after release from a CPT treatment. CPT and HU are without a doubt, different genotoxic agents, with CPT acting as a TOP1 inhibitor that generates DSBs and HU acting as a ribonucleotide

reductase inhibitor that depletes dNTPs, which leads to replication stress[173,176]. However, CPT not only creates DSBs but also induces replication stress, indicating the possibility of the two phenotypes of impaired fork restart and impaired cell cycling resumption discussed above deriving from a similar scenario.

Already introduced extensively in the previous sections of this thesis, DNA damage and replication stress lead to fork reversal[73]. It has however so far not been thoroughly discussed, what happens after the formation of the reversed forks, as those structures are intermediates in the process of damage or stress resolution[80]. In addition to the rescue by another fork or excision repair of a lesion ahead of the reversed fork as two such outcomes of fork reversal, HR-dependent restart was also deemed as a solution for resuming replication. HR-dependent restart was found to be carried out for forks that had undergone breakage as well as forks that had undergone uncoupling and stalling[73,80,85,192]. Furthermore, deliberate cleavage of reversed forks by nucleases was additionally determined as a way to restart forks in a HR-dependent manner[85]. HR-dependent restart involves the crucial recombinase Rad51, together with other HR factors, to carry out strand invasion[192]. As shown and discussed in sections 3.1 and 4.1, we found myo6 to function in the HR pathway and proposed that myo6 might be involved in the removal of the Ku heterodimer from DSBs. The results obtained from the collaboration with [redacted], where we investigated the mobility of Rad52 foci, additionally suggested myo6 to be involved in the downstream step of homology search of the HR pathway. With this in mind, a reasonable explanation for the defect in replication restart observed in KO cells, is the impairment of homology search and subsequent strand invasion that myo6 could potentially contribute to. As mentioned previously, the replication restart fibre assays and cell cycle analysis of CPT-treated cells were preliminary results, indicating a need for further confirmation. These results however, hint at another function of myo6 in fork restart that requires a deeper mechanistic understanding.

4.2.2 The involvement of myo6 in replication slowdown upon DNA damage

Also using the DNA fibre assay, but with the addition of CPT during the second IdU pulse, I observed an interesting phenotype where WT cells slowed down replication upon the addition of the damage but KO cells proceeded with replication at the same speed as the unperturbed condition (Figure 3.3). We initially hypothesised that this could be result of defective checkpoint signalling, as it was shown that activation of the ATR-mediated signalling cascade leads to a number of outcomes, one of which is cell

cycle arrest[193]. However, we observed no difference in ATR activation between U2OS siCtrl and siMyo6 cells either in unperturbed conditions or with a HU treatment of one hour (data shown in Shi *et al*[152]). As already discussed above, CPT and HU treatments are different stressing agents for the cells, and an additional experiment with a CPT treatment to determine any effects of myo6 depletion on ATR activation is needed. But there is definitely the possibility that the siCtrl and siMyo6 cells show no difference in ATR activation also upon the CPT treatment and the absence of replication slowing in KO cells is the consequence of another matter.

Another possible explanation for the absence of replication slow-down in KO cells is that myo6 could be in fact involved in the reversal of forks upon replication stress. As previously mentioned in section 3.2.1, one of the phenotypes that is associated with fork reversal is replication slow-down. It was shown that a wide variety of DNA damaging and replication stress inducing agents, including CPT, trigger fork slowing and reversal[74]. Multiple papers have shown that upon depletion or inhibition of the fork reversal remodellers such as ZRANB3, PARP1, Rad51, Rad51 paralogs etc, the replication slow-down upon the CPT treatment was abolished[74,76,194,195]. This could also be the case for myo6. However, the final concentration of CPT I used in my experiment was 1 μM, while final concentration used in the published papers were exceedingly lower at 25 or 50 nM. It is difficult to judge whether the difference in CPT concentrations would significantly affect the readout of this assay, which is an indication of a protein's involvement in fork reversal. One difference in the outcome of the CPT treatment concentrations lies in the generation of DSBs that was detected in cells treated with 1 μM of CPT but not at a concentration of 25 nM[74]. Therefore, to come to a more robust conclusion, it will be necessary to perform an assay with 25 nM of CPT in myo6-depleted cells. Further discussion on this will be carried out in the next section.

4.3 The role of myo6 in fork protection

Similar to initiating the investigation into myo6's function in the HR pathway, the mass spectrometry results additionally led us to unravel myo6's role in the protection of reversed forks. We had scored WRNIP1 as a factor identified from mass spectrometry and confirmed its interaction with myo6 via pulldown assays (data shown in Shi *et al*[152]). As WRNIP1 was shown to be a protector of reversed forks [83,84], we asked the question of whether this was the same case for myo6. Results in section 3.4 clearly showed that myo6 is indeed involved in reversed fork protection and this function was characterized in detail. Nevertheless, there remain unaddressed points that calls for further discussion, which will follow in the sub-sections below.

4.3.1 Domains of myo6 required for fork protection

Figure 3.12 revealed the motor and MyUb domains to be essential for the fork protection function of myo6. Furthermore, results with point mutations in the two ubiquitin-binding domains of myo6, MIU and MyUb, suggested an additional contribution of ubiquitin.

The process of the covalent attachment of ubiquitin to a substrate protein is named ubiquitylation, which has emerged to be involved in the regulation of a vast number of cellular processes, including cell cycle progression, transcription regulation and proteasomal degradation[196,197]. While its role has also been demonstrated in the DNA damage and replication stress response, its contribution to the specific pathway of fork reversal and protection still remains largely unexplored[198,199]. Findings such as the importance of PCNA ubiquitylation for the pathway is presumably just the tip of the iceberg[76,200].

Interestingly, we observed a direct interaction between WRNIP1 and a MIUMyUb construct of myo6, which was enhanced upon the addition of K63 poly-ubiquitin chains[152]. WRNIP1, like myo6, also has the capability to bind to ubiquitin. This is achieved via its ubiquitin-binding zinc finger (UBZ) domain, which was shown to not only bind to K63-linked chains but also to K48-linked chains and mono-ubiquitin[201]. Moreover, we observed a decrease in the interaction between myo6 and WRNIP1 when cell lysates were treated with the non-selective de-ubiquitylating enzyme USP2cc[152,202]. This is further indication of the potential regulation of the fork reversal and protection pathway by ubiquitylation. With myo6 being an actin-based motor protein, as well as the new data on actin's involvement in the fork reversal pathway[175],

it would be of interest to understand whether there is a connection between ubiquitin and the actin cytoskeleton in this pathway. For instance, questions such as whether actin is ubiquitylated in conditions that trigger fork reversal and whether deliberate addition of different ubiquitin linkages to actin would increase or decrease the efficiency of fork reversal could be addressed. This is by all means not restricted to the actin cytoskeleton, it could also be of benefit to investigate whether the fork remodellers and protectors act in an ubiquitin-dependent manner. The existing Ubiquiton system in our lab that can manipulate the ubiquitin code on target proteins, could be of immense value to answering such questions.

As we proposed Myo6 and WRNIP1 to cooperate in the protection of reversed forks and identified WRNIP1 in the mass spectrometry experiment that was performed with the MyUb domain of myo6, it did not come as a surprise to observe the essentiality of this domain for myo6's fork protection function. In addition, as myo6 is an actin-based motor protein, it was also not unexpected to discover its dependency on its motor domain, through which it associates with actin. However, we cannot exclude the possibility of myo6 acting in an actin-independent manner, similar to recent findings that demonstrate WASp, a protein that regulates Arp2/3-mediated actin polymerization [203], to modulate RPA binding to ssDNA in an Arp2/3-independent manner [204].

4.3.2 The actin-myosin cytoskeleton in fork reversal and protection

Our experiments that showed myo6's involvement in DNA resection and homology search in the HR pathway etc, also showed a similar trend for cells that were subjected to actin polymerization inhibition. Having initially observed myo6 to have a role in reversed fork protection, an obvious question was whether we would see a similar phenotype for F-actin. Figure 3.13 showed that this was actually not the case, as fork de-protection was not observed when a mutant form of actin (R62D) that does not polymerize, was overexpressed exclusively in the nucleus. This was at first unexpected as we determined the F-actin associated motor domain of myo6 to be required for fork protection, indicative of a potential similar role of F-actin. A very recent paper by Palumbieri *et al* provided an explanation for this, as they demonstrated F-actin to be in fact a fork remodeller[175].

Even though F-actin acts as a fork remodeller in one of the upstream steps of the fork reversal/protection pathway, it still may also contribute to the protection of reversed forks, as this would not be detected via our DNA fibre assays due to the absence of

reversal. One such example of a factor to play a role in both the reversal of forks as well as the protection of forks is Rad51. It was originally proposed by Schlacher *et al* that perturbation of Rad51 filament formation causes fork de-protection[177], but a few years later Zellweger *et al* determined Rad51 to be crucial for the reversal of forks[74]. Moreover, it was discovered that cells expressing the Rad51-T131P mutant that cannot form stable filaments still had the capability to promote fork reversal but were incompetent in protection of reversed forks[82]. Although these different observations remained an enigma for a while, further research in the field shone more light on the multi-functions of Rad51. The newly emerged data intriguingly determined the protein level of Rad51 to be important for fork reversal and fork protection, where a low level of Rad51 is sufficient for the reversal process to occur but insufficient for fork protection. By titration of a siRNA against Rad51, Bhat *et al* observed fork degradation at a lower concentration of the siRNA but a rescue of the degradation at a higher concentration of the siRNA, suggesting that more Rad51 is needed to carry out protection of reversed forks than reversal of the forks[205,206].

With the above mentioned findings on Rad51 in mind, it would be beneficial to carry out careful analysis on different extents of actin polymerisation inhibition as well as different extents of inhibition of either branched or unbranched filament polymerisation, to determine whether F-actin would also have a potential additional fork protection role. This without a doubt also applies to myo6, as we have shown that siRNA-mediated knockdown of myo6 in U2OS cells leads to fork de-protection (Figure 3.7) but a complete knockout of myo6 in A549 cells abolished fork slowing upon a CPT treatment, indicative of a possibility of impaired fork reversal (Figure 3.3). Perhaps there is also a difference in the requirement of myo6's protein level between fork protection and fork reversal. It would be firstly of utmost importance to perform electron microscopy on myo6-depleted cells, to determine whether there is an effect of myo6 depletion on the reversal of forks.

4.3.3 Model of myo6 in reversed fork protection

Having fairly extensively characterised the fork protection function of myo6, we wanted as a final step to investigate into its mechanism of action. We hypothesised that myo6, being a motor protein, could transport WRNIP1 to the reversed forks, where it could fulfil its fork protection function, or on the other hand, transport the SLX4/DNA2 nucleases away from the reversed forks to prevent nucleolytic degradation of those forks[152]. To distinguish between the two scenarios, we performed "in situ protein

interaction with nascent DNA replication forks (SIRF)" assays[207] and "isolation of proteins on nascent DNA (iPOND)" experiments[208]. With both methods, we observed an enhanced localisation of both WRNIP1 and myo6 to stalled replication forks in *wildtype* cells, in the same conditions that we used for the fork protection fibre assays. Very interestingly, using the SIRF assay, we observed no such enhancement of WRNIP1 to the stalled forks upon depletion of myo6, which rather supports the model that myo6 brings WRNIP1 to the forks rather than removes the nucleases away from the forks (Figure 4.1)[152].

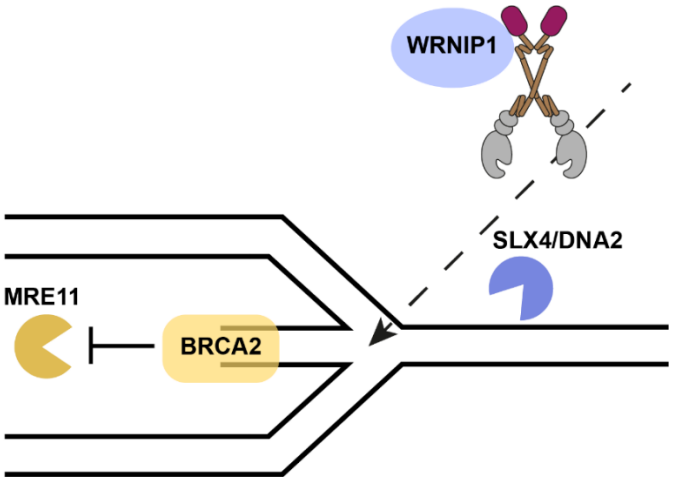

Figure 4.1: Model depicting the mechanism of myo6 in fork protection (adapted from Shi *et al*, 2023)[152]**.**
A model of myo6 in fork protection is proposed, in which it interacts with WRNIP1 to transport it to reversed forks, where it protects the forks from SLX4/DNA2-mediated degradation.

While we proposed a model in which myo6's motor domain is needed for transport to contribute to fork protection, there is an alternative possibility where myo6 acts as an anchor. It was shown that upon forces of more than 2 pN, myo6 undergoes a change in function, from a transporter to an anchor[209]. The latter role of myo6 was proposed to be important for the anchoring of RNA Polymerase II (RNAPII) at transcription sites to promote gene expression, by usage of a myo6 construct with a disrupted anchoring function. However, full distinction between the anchoring and transporting function of myo6's motor with this construct was nevertheless not entirely clearly shown[151]. A scenario, in which myo6 could act as an anchor, to potentially stabilise WRNIP1 at the junction of reversed forks could also be imagined. Therefore, to fully elucidate myo6's mechanism of function in reversed fork protection, more research has to be undertaken to fully distinguish between myo6's transporting and anchoring functions.

Another point that could be of significant interest in the future, is the contribution of the unique directionality of myo6 to fork protection and the orientation of F-actin around reversed forks. As myo6 is the only myosin to date to travel towards the minus end of F-actin, the question arises of whether this directionality is indeed important. There is a unique insert at the end of myo6's motor, which dictates its minus-ended directionality, the removal of which was shown to result in a shift in myo6's directionality towards the plus-end of F-actin[210]. Experiments with a myo6 construct that lacks the unique insert could thus provide insight into myo6's directionality in fork protection. Additional complimentary experiments to investigate into plus-ended nuclear myosins could determine whether there is contribution of multiple myosins to protect reversed forks, which was shown for myosins I and V in DSB repair in *Drosophila melanogaster*[119], or potential competition between the minus and plus-ended motors.

4.4 Nuclear vs cytoplasmic myo6

As myo6 is predominantly localised to the cytoplasm, efforts to visualise and manipulate the nuclear pool have been arduous. Therefore, we made use of the DARPin technology[166] to assist us in differentiating between the contributions of nuclear and cytoplasmic myo6 to fork protection.

4.4.1 Further testing of the SPOP nuclear degradation system

Although there is an existing system for degradation of the nuclear pool of a protein (the SPOP system)[184], we were unsuccessful in determining whether the SPOP-G4 construct was capable of degrading the nuclear pool of myo6 (sections 3.5.8 to 3.5.11). Having tried microscopic approaches, cell fractionation experiments and functional screening assays, we nevertheless did not find a robust approach for testing the efficiency of the nuclear degradation of myo6.

As myo6 is highly abundant in the cytoplasm and barely detectable in the nucleus, one more approach that could be tested is the overexpression of myo6 fused with NLS in cells that have induced expression of SPOP-G4. Through this method, we would be able to visualise a higher abundance of myo6 in the nucleus and potentially determine the functionality of the SPOP-G4 construct.

Other approaches include devoting more effort into the visualization of nuclear myo6. For instance, Fili *et al* performed isolation of nuclei and detected a clear myo6 signal[150]. We could use the same method to determine whether we would see a difference in the nuclear myo6 level in cells expressing SPOP-G4, without the interference of the strong cytoplasmic myo6 signal. Another method would be the usage of super resolution imaging techniques, one of which, Stochastic Optical Reconstruction Microscopy (STORM) Imaging, was used by Hari-Gupta *et al* to investigate the nuclear organization of myo6 under different conditions[151].

4.4.2 Optimisation of the NES-system for re-localising nuclear myo6

We successfully made use of a NLS system with the DARPin technology to re-localise myo6 from the cytoplasm to the nucleus, as a way of depleting the cytoplasmic pool of myo6, to determine whether there was a contribution of cytoplasmic myo6 to fork protection (Figures 3.29 and 3.30). As we did not confirmed the functionality of the SPOP system, other approaches to deplete or re-localise nuclear myo6 were simultaneously considered. Section 3.5.12 showed the trial of using a NES system together with the DARPin technology, to achieve the goal of re-localising nuclear myo6

to the cytoplasm, as a way of depleting the nuclear pool. Unfortunately we were not successful in our proof-of-concept experiment to re-localise GFP from the nucleus to the cytoplasm. One optimisation step would be the usage of three NES tags fused to the DARPin. The NES-DARPin that I used in Figure 3.27 only contained one and I observed that the NES-DARPin was still localised to the nucleus in a percentage of the cells and not exported to the cytoplasm. On the other hand, the NLS-DARPin that was capable of re-localising myo6 from the cytoplasm to the nucleus (Figure 3.30) contained three NLS tags, indicating that we might be more successful in the re-localisation of a nuclear protein with three NES tags instead of one.

4.5 Future perspectives

In this thesis, I have demonstrated two novel functions of myo6, namely its roles in DSB repair and fork protection, contributing to elucidating myo6's largely unknown nuclear functions. Having optimised and characterised a DARPin-tool for the manipulation of myo6, I utilised it for differentiating the contributions of nuclear and cytoplasmic myo6. This provided evidence that it is the nuclear pool of myo6 rather than the cytoplasmic pool, which is responsible for exerting its fork protection function. Utilisation and further optimisation of this powerful DARPin-tool will be highly beneficial for characterisation of myo6's other unknown functions in future research.

Chapter 5

Appendix

5.1 Curriculum Vitae

5.2 Publications

Shi J, Hauschulte K, Mikicic I, *et al*. Nuclear myosin VI maintains replication fork stability. Nat Commun. 2023;14(1):3787. doi:10.1038/s41467-023-39517-y

References

1. Chatterjee N, Walker GC. Mechanisms of DNA damage, repair, and mutagenesis. *Environ Mol Mutagen*. 2017;58(5):235-263. doi:10.1002/em.22087

2. Jackson SP, Bartek J. The DNA-damage response in human biology and disease. *Nature*. 2009;461(7267):1071-1078. doi:10.1038/nature08467

3. Stead ER, Bjedov I. Balancing DNA repair to prevent ageing and cancer. *Exp Cell Res*. 2021;405(2):112679. doi:10.1016/j.yexcr.2021.112679

4. Olafsson S, Anderson CA. Somatic mutations provide important and unique insights into the biology of complex diseases. *Trends Genet*. 2021;37(10):872-881. doi:10.1016/j.tig.2021.06.012

5. Loewe L, Hill WG. The population genetics of mutations: good, bad and indifferent. *Philos Trans R Soc B Biol Sci*. 2010;365(1544):1153-1167. doi:10.1098/rstb.2009.0317

6. Blanpain C, Mohrin M, Sotiropoulou PA, Passegué E. DNA-Damage Response in Tissue-Specific and Cancer Stem Cells. *Cell Stem Cell*. 2011;8(1):16-29. doi:10.1016/j.stem.2010.12.012

7. Caldecott KW. Single-strand break repair and genetic disease. *Nat Rev Genet*. 2008;9(8):619-631. doi:10.1038/nrg2380

8. White RR, Vijg J. Do DNA double-strand breaks drive aging? *Mol Cell*. 2016;63(5):729-738. doi:10.1016/j.molcel.2016.08.004

9. Huang R, Zhou PK. DNA damage repair: historical perspectives, mechanistic pathways and clinical translation for targeted cancer therapy. *Signal Transduct Target Ther*. 2021;6(1):1-35. doi:10.1038/s41392-021-00648-7

10. Krokan HE, Bjørås M. Base Excision Repair. *Cold Spring Harb Perspect Biol*. 2013;5(4):a012583. doi:10.1101/cshperspect.a012583

11. Carter RJ, Parsons JL. Base Excision Repair, a Pathway Regulated by Posttranslational Modifications. *Mol Cell Biol*. 2016;36(10):1426-1437. doi:10.1128/MCB.00030-16

12. Grundy GJ, Parsons JL. Base excision repair and its implications to cancer therapy. *Essays Biochem*. 2020;64(5):831-843. doi:10.1042/EBC20200013

13. Schärer OD. Nucleotide Excision Repair in Eukaryotes. *Cold Spring Harb Perspect Biol*. 2013;5(10):a012609. doi:10.1101/cshperspect.a012609

14. Apostolou Z, Chatzinikolaou G, Stratigi K, Garinis GA. Nucleotide Excision Repair and Transcription-Associated Genome Instability. *BioEssays*. 2019;41(4):1800201. doi:10.1002/bies.201800201

15. Marteijn JA, Lans H, Vermeulen W, Hoeijmakers JHJ. Understanding nucleotide excision repair and its roles in cancer and ageing. *Nat Rev Mol Cell Biol*. 2014;15(7):465-481. doi:10.1038/nrm3822

16. Spivak G. Nucleotide excision repair in humans. *DNA Repair*. 2015;36:13-18. doi:10.1016/j.dnarep.2015.09.003

17. Liu D, Keijzers G, Rasmussen LJ. DNA mismatch repair and its many roles in eukaryotic cells. *Mutat Res Mutat Res*. 2017;773:174-187. doi:10.1016/j.mrrev.2017.07.001

18.Olave MC, Graham RP. Mismatch repair deficiency: The what, how and why it is important. *Genes Chromosomes Cancer*. 2022;61(6):314-321. doi:10.1002/gcc.23015

19.Li GM. Mechanisms and functions of DNA mismatch repair. *Cell Res*. 2008;18(1):85-98. doi:10.1038/cr.2007.115

20.Caldecott KW. DNA single-strand break repair and human genetic disease. *Trends Cell Biol*. 2022;32(9):733-745. doi:10.1016/j.tcb.2022.04.010

21.Caldecott KW. DNA single-strand break repair. *Exp Cell Res*. 2014;329(1):2-8. doi:10.1016/j.yexcr.2014.08.027

22.Vilenchik MM, Knudson AG. Endogenous DNA double-strand breaks: Production, fidelity of repair, and induction of cancer. *Proc Natl Acad Sci U S A*. 2003;100(22):12871-12876. doi:10.1073/pnas.2135498100

23.Jackson SP. Sensing and repairing DNA double-strand breaks. *Carcinogenesis*. 2002;23(5):687-696. doi:10.1093/carcin/23.5.687

24.Trenner A, Sartori AA. Harnessing DNA Double-Strand Break Repair for Cancer Treatment. *Front Oncol*. 2019;9. Accessed June 20, 2023. https://www.frontiersin.org/articles/10.3389/fonc.2019.01388

25.Jeggo PA, Löbrich M. DNA double-strand breaks: their cellular and clinical impact? *Oncogene*. 2007;26(56):7717-7719. doi:10.1038/sj.onc.1210868

26.Lieber MR. The Mechanism of Double-Strand DNA Break Repair by the Nonhomologous DNA End Joining Pathway. *Annu Rev Biochem*. 2010;79:181-211. doi:10.1146/annurev.biochem.052308.093131

27.Scully R, Panday A, Elango R, Willis NA. DNA double-strand break repair-pathway choice in somatic mammalian cells. *Nat Rev Mol Cell Biol*. 2019;20(11):698-714. doi:10.1038/s41580-019-0152-0

28.Bhargava R, Onyango DO, Stark JM. Regulation of Single-Strand Annealing and its Role in Genome Maintenance. *Trends Genet*. 2016;32(9):566-575. doi:10.1016/j.tig.2016.06.007

29.Blasiak J. Single-Strand Annealing in Cancer. *Int J Mol Sci*. 2021;22(4):2167. doi:10.3390/ijms22042167

30.Chang HHY, Pannunzio NR, Adachi N, Lieber MR. Non-homologous DNA end joining and alternative pathways to double-strand break repair. *Nat Rev Mol Cell Biol*. 2017;18(8):495-506. doi:10.1038/nrm.2017.48

31.Sallmyr A, Tomkinson AE. Repair of DNA double-strand breaks by mammalian alternative end-joining pathways. *J Biol Chem*. 2018;293(27):10536-10546. doi:10.1074/jbc.TM117.000375

32.Wang H, Xu X. Microhomology-mediated end joining: new players join the team. *Cell Biosci*. 2017;7(1):6. doi:10.1186/s13578-017-0136-8

33.Liu Q, Lopez K, Murnane J, Humphrey T, Barcellos-Hoff MH. Misrepair in Context: TGFβ Regulation of DNA Repair. *Front Oncol*. 2019;9. Accessed June 21, 2023. https://www.frontiersin.org/articles/10.3389/fonc.2019.00799

34.Stinson BM, Loparo JJ. Repair of DNA Double-Strand Breaks by the Non-homologous End Joining Pathway. *Annu Rev Biochem*. 2021;90:137. doi:10.1146/annurev-biochem-080320-110356

35.Zhao B, Rothenberg E, Ramsden DA, Lieber MR. The molecular basis and disease relevance of non-homologous DNA end joining. *Nat Rev Mol Cell Biol*. 2020;21(12):765-781. doi:10.1038/s41580-020-00297-8

36.Stinson BM, Moreno AT, Walter JC, Loparo JJ. A Mechanism to Minimize Errors during Non-homologous End Joining. *Mol Cell*. 2020;77(5):1080-1091.e8. doi:10.1016/j.molcel.2019.11.018

37.Ensminger M, Löbrich M. One end to rule them all: Non-homologous end-joining and homologous recombination at DNA double-strand breaks. *Br J Radiol*. 2020;93(1115):20191054. doi:10.1259/bjr.20191054

38.Khanna KK, Jackson SP. DNA double-strand breaks: signaling, repair and the cancer connection. *Nat Genet*. 2001;27(3):247-254. doi:10.1038/85798

39.Hariharasudhan G, Jeong SY, Kim MJ, et al. TOPORS-mediated RAD51 SUMOylation facilitates homologous recombination repair. *Nucleic Acids Res*. 2022;50(3):1501-1516. doi:10.1093/nar/gkac009

40.Arnoult N, Correia A, Ma J, et al. Regulation of DNA repair pathway choice in S and G2 phases by the NHEJ inhibitor CYREN. *Nature*. 2017;549(7673):548-552. doi:10.1038/nature24023

41.Wright WD, Shah SS, Heyer WD. Homologous recombination and the repair of DNA double-strand breaks. *J Biol Chem*. 2018;293(27):10524-10535. doi:10.1074/jbc.TM118.000372

42.Ranjha L, Howard SM, Cejka P. Main steps in DNA double-strand break repair: an introduction to homologous recombination and related processes. *Chromosoma*. 2018;127(2):187-214. doi:10.1007/s00412-017-0658-1

43.Maréchal A, Zou L. RPA-coated single-stranded DNA as a platform for post-translational modifications in the DNA damage response. *Cell Res*. 2015;25(1):9-23. doi:10.1038/cr.2014.147

44.Soniat MM, Myler LR, Kuo HC, Paull TT, Finkelstein IJ. RPA Phosphorylation Inhibits DNA Resection. *Mol Cell*. 2019;75(1):145-153.e5. doi:10.1016/j.molcel.2019.05.005

45.Schild D, Wiese C. Overexpression of RAD51 suppresses recombination defects: a possible mechanism to reverse genomic instability. *Nucleic Acids Res*. 2010;38(4):1061-1070. doi:10.1093/nar/gkp1063

46.Toh M, Ngeow J. Homologous Recombination Deficiency: Cancer Predispositions and Treatment Implications. *The Oncologist*. 2021;26(9):e1526-e1537. doi:10.1002/onco.13829

47.Shibata A. Regulation of repair pathway choice at two-ended DNA double-strand breaks. *Mutat Res Mol Mech Mutagen*. 2017;803-805:51-55. doi:10.1016/j.mrfmmm.2017.07.011

48.Tarsounas M, Sung P. The antitumorigenic roles of BRCA1–BARD1 in DNA repair and replication. *Nat Rev Mol Cell Biol*. 2020;21(5):284-299. doi:10.1038/s41580-020-0218-z

49.Ceccaldi R, Rondinelli B, D'Andrea AD. Repair Pathway Choices and Consequences at the Double-Strand Break. *Trends Cell Biol*. 2016;26(1):52-64. doi:10.1016/j.tcb.2015.07.009

50.Lemaître C, Grabarz A, Tsouroula K, et al. Nuclear position dictates DNA repair pathway choice. *Genes Dev*. 2014;28(22):2450-2463. doi:10.1101/gad.248369.114

51.Kalousi A, Hoffbeck AS, Selemenakis PN, et al. The Nuclear Oncogene SET Controls DNA Repair by KAP1 and HP1 Retention to Chromatin. *Cell Rep*. 2015;11(1):149-163. doi:10.1016/j.celrep.2015.03.005

52.van den Boom J, Wolf M, Weimann L, et al. VCP/p97 extracts sterically trapped Ku70/80 rings from DNA in double strand break repair. *Mol Cell*. 2016;64(1):189-198. doi:10.1016/j.molcel.2016.08.037

53.Fell VL, Schild-Poulter C. The Ku heterodimer: Function in DNA repair and beyond. *Mutat Res Mutat Res*. 2015;763:15-29. doi:10.1016/j.mrrev.2014.06.002

54.Grundy GJ, Moulding HA, Caldecott KW, Rulten SL. One ring to bring them all—The role of Ku in mammalian non-homologous end joining. *DNA Repair*. 2014;17:30-38. doi:10.1016/j.dnarep.2014.02.019

55.Ubhi T, Brown GW. Exploiting DNA Replication Stress for Cancer Treatment. *Cancer Res*. 2019;79(8):1730-1739. doi:10.1158/0008-5472.CAN-18-3631

56.Hübscher U. DNA Replication Fork Proteins. In: Vengrova S, Dalgaard JZ, eds. *DNA Replication: Methods and Protocols*. Methods in Molecular Biology. Humana Press; 2009:19-33. doi:10.1007/978-1-60327-815-7_2

57.Saxena S, Zou L. Hallmarks of DNA replication stress. *Mol Cell*. 2022;82(12):2298-2314. doi:10.1016/j.molcel.2022.05.004

58.Magdalou I, Lopez BS, Pasero P, Lambert SAE. The causes of replication stress and their consequences on genome stability and cell fate. *Semin Cell Dev Biol*. 2014;30:154-164. doi:10.1016/j.semcdb.2014.04.035

59.Gaillard H, García-Muse T, Aguilera A. Replication stress and cancer. *Nat Rev Cancer*. 2015;15(5):276-289. doi:10.1038/nrc3916

60.Zeman MK, Cimprich KA. Causes and consequences of replication stress. *Nat Cell Biol*. 2014;16(1):2-9. doi:10.1038/ncb2897

61.Nickoloff JA. Targeting Replication Stress Response Pathways to Enhance Genotoxic Chemo- and Radiotherapy. *Molecules*. 2022;27(15):4736. doi:10.3390/molecules27154736

62.Lukášová E, Řezáčová M, Bačíková A, Šebejová L, Vávrová J, Kozubek S. Distinct cellular responses to replication stress leading to apoptosis or senescence. *FEBS Open Bio*. 2019;9(5):870-890. doi:10.1002/2211-5463.12632

63.Dash RC, Hadden K. Protein–Protein Interactions in Translesion Synthesis. *Molecules*. 2021;26(18):5544. doi:10.3390/molecules26185544

64.Chen J, Bozza W, Zhuang Z. Ubiquitination of PCNA and Its Essential Role in Eukaryotic Translesion Synthesis. *Cell Biochem Biophys*. 2011;60(1):47-60. doi:10.1007/s12013-011-9187-3

65.Vaisman A, Woodgate R. Translesion DNA polymerases in eukaryotes: what makes them tick? *Crit Rev Biochem Mol Biol*. 2017;52(3):274-303. doi:10.1080/10409238.2017.1291576

66.Yang W, Gao Y. Translesion and Repair DNA Polymerases: Diverse Structure and Mechanism. *Annu Rev Biochem*. 2018;87(1):239-261. doi:10.1146/annurev-biochem-062917-012405

67.Shilkin ES, Boldinova EO, Stolyarenko AD, et al. Translesion DNA Synthesis and Carcinogenesis. *Biochem Mosc*. 2020;85(4):425-435. doi:10.1134/S0006297920040033

68.Quinet A, Tirman S, Cybulla E, Meroni A, Vindigni A. To skip or not to skip: choosing repriming to tolerate DNA damage. *Mol Cell*. 2021;81(4):649-658. doi:10.1016/j.molcel.2021.01.012

69.Guilliam TA, Doherty AJ. PrimPol—Prime Time to Reprime. *Genes*. 2017;8(1):20. doi:10.3390/genes8010020

70.Mehta KPM, Thada V, Zhao R, et al. CHK1 phosphorylates PRIMPOL to promote replication stress tolerance. *Sci Adv*. 2022;8(13):eabm0314. doi:10.1126/sciadv.abm0314

71.Mourón S, Rodriguez-Acebes S, Martínez-Jiménez MI, et al. Repriming of DNA synthesis at stalled replication forks by human PrimPol. *Nat Struct Mol Biol*. 2013;20(12):1383-1389. doi:10.1038/nsmb.2719

72.Qiu S, Jiang G, Cao L, Huang J. Replication Fork Reversal and Protection. *Front Cell Dev Biol*. 2021;9. Accessed June 23, 2023. https://www.frontiersin.org/articles/10.3389/fcell.2021.670392

73.Neelsen KJ, Lopes M. Replication fork reversal in eukaryotes: from dead end to dynamic response. *Nat Rev Mol Cell Biol*. 2015;16(4):207-220. doi:10.1038/nrm3935

74.Zellweger R, Dalcher D, Mutreja K, et al. Rad51-mediated replication fork reversal is a global response to genotoxic treatments in human cells. *J Cell Biol*. 2015;208(5):563-579. doi:10.1083/jcb.201406099

75.Mutreja K, Krietsch J, Hess J, et al. ATR-Mediated Global Fork Slowing and Reversal Assist Fork Traverse and Prevent Chromosomal Breakage at DNA Interstrand Cross-Links. *Cell Rep*. 2018;24(10):2629-2642.e5. doi:10.1016/j.celrep.2018.08.019

76.Vujanovic M, Krietsch J, Raso MC, et al. Replication Fork Slowing and Reversal upon DNA Damage Require PCNA Polyubiquitination and ZRANB3 DNA Translocase Activity. *Mol Cell*. 2017;67(5):882-890.e5. doi:10.1016/j.molcel.2017.08.010

77.Bai G, Kermi C, Stoy H, et al. HLTF Promotes Fork Reversal, Limiting Replication Stress Resistance and Preventing Multiple Mechanisms of Unrestrained DNA Synthesis. *Mol Cell*. 2020;78(6):1237-1251.e7. doi:10.1016/j.molcel.2020.04.031

78.Bétous R, Mason AC, Rambo RP, et al. SMARCAL1 catalyzes fork regression and Holliday junction migration to maintain genome stability during DNA replication. *Genes Dev*. 2012;26(2):151-162. doi:10.1101/gad.178459.111

79.Liu W, Saito Y, Jackson J, et al. RAD51 bypasses the CMG helicase to promote replication fork reversal. *Science*. 2023;380(6643):382-387. doi:10.1126/science.add7328

80.Bhat KP, Cortez D. RPA and RAD51: fork reversal, fork protection, and genome stability. *Nat Struct Mol Biol*. 2018;25(6):446-453. doi:10.1038/s41594-018-0075-z

81.Dhoonmoon A, Nicolae CM, Moldovan GL. The KU-PARP14 axis differentially regulates DNA resection at stalled replication forks by MRE11 and EXO1. *Nat Commun*. 2022;13(1):5063. doi:10.1038/s41467-022-32756-5

82.Mijic S, Zellweger R, Chappidi N, et al. Replication fork reversal triggers fork degradation in BRCA2-defective cells. *Nat Commun*. 2017;8(1):859. doi:10.1038/s41467-017-01164-5

83.Porebski B, Wild S, Kummer S, Scaglione S, Gaillard PHL, Gari K. WRNIP1 Protects Reversed DNA Replication Forks from SLX4-Dependent Nucleolytic Cleavage. *iScience*. 2019;21:31-41. doi:10.1016/j.isci.2019.10.010

84.Leuzzi G, Marabitti V, Pichierri P, Franchitto A. WRNIP1 protects stalled forks from degradation and promotes fork restart after replication stress. *EMBO J*. 2016;35(13):1437-1451. doi:10.15252/embj.201593265

85.Sarbajna S, West SC. Holliday junction processing enzymes as guardians of genome stability. *Trends Biochem Sci*. 2014;39(9):409-419. doi:10.1016/j.tibs.2014.07.003

86.Quinet A, Tirman S, Jackson J, et al. PRIMPOL-Mediated Adaptive Response Suppresses Replication Fork Reversal in BRCA-Deficient Cells. *Mol Cell*. 2020;77(3):461-474.e9. doi:10.1016/j.molcel.2019.10.008

87.Quinet A, Lerner LK, Martins DJ, Menck CFM. Filling gaps in translesion DNA synthesis in human cells. *Mutat Res Toxicol Environ Mutagen*. 2018;836:127-142. doi:10.1016/j.mrgentox.2018.02.004

88.Lemaçon D, Jackson J, Quinet A, et al. MRE11 and EXO1 nucleases degrade reversed forks and elicit MUS81-dependent fork rescue in BRCA2-deficient cells. *Nat Commun*. 2017;8(1):860. doi:10.1038/s41467-017-01180-5

89.Taglialatela A, Alvarez S, Leuzzi G, et al. Restoration of Replication Fork Stability in BRCA1- and BRCA2-Deficient Cells by Inactivation of SNF2-Family Fork Remodelers. *Mol Cell*. 2017;68(2):414-430.e8. doi:10.1016/j.molcel.2017.09.036

90.Lim KS, Li H, Roberts EA, et al. USP1 Is Required for Replication Fork Protection in BRCA1-Deficient Tumors. *Mol Cell*. 2018;72(6):925-941.e4. doi:10.1016/j.molcel.2018.10.045

91.Panzarino NJ, Krais JJ, Cong K, et al. Replication Gaps Underlie BRCA Deficiency and Therapy Response. *Cancer Res*. 2021;81(5):1388-1397. doi:10.1158/0008-5472.CAN-20-1602

92.Hohmann T, Dehghani F. The Cytoskeleton—A Complex Interacting Meshwork. *Cells*. 2019;8(4):362. doi:10.3390/cells8040362

93.Fletcher DA, Mullins RD. Cell mechanics and the cytoskeleton. *Nature*. 2010;463(7280):485-492. doi:10.1038/nature08908

94.Pegoraro AF, Janmey P, Weitz DA. Mechanical Properties of the Cytoskeleton and Cells. *Cold Spring Harb Perspect Biol*. 2017;9(11):a022038. doi:10.1101/cshperspect.a022038

95.Damania D, Subramanian H, Tiwari AK, et al. Role of Cytoskeleton in Controlling the Disorder Strength of Cellular Nanoscale Architecture. *Biophys J*. 2010;99(3):989-996. doi:10.1016/j.bpj.2010.05.023

96.Dutour-Provenzano G, Etienne-Manneville S. Intermediate filaments. *Curr Biol*. 2021;31(10):R522-R529. doi:10.1016/j.cub.2021.04.011

97.Sanghvi-Shah R, Weber GF. Intermediate Filaments at the Junction of Mechanotransduction, Migration, and Development. *Front Cell Dev Biol*. 2017;5. Accessed June 26, 2023. https://www.frontiersin.org/articles/10.3389/fcell.2017.00081

98.Lowery J, Kuczmarski ER, Herrmann H, Goldman RD. Intermediate Filaments Play a Pivotal Role in Regulating Cell Architecture and Function*. *J Biol Chem*. 2015;290(28):17145-17153. doi:10.1074/jbc.R115.640359

99.Janke C, Magiera MM. The tubulin code and its role in controlling microtubule properties and functions. *Nat Rev Mol Cell Biol*. 2020;21(6):307-326. doi:10.1038/s41580-020-0214-3

100.Goodson HV, Jonasson EM. Microtubules and Microtubule-Associated Proteins. *Cold Spring Harb Perspect Biol*. 2018;10(6):a022608. doi:10.1101/cshperspect.a022608

101.Akhmanova A, Hoogenraad CC. Microtubule Minus-End-Targeting Proteins. *Curr Biol*. 2015;25(4):R162-R171. doi:10.1016/j.cub.2014.12.027

102.Ferro LS, Can S, Turner MA, ElShenawy MM, Yildiz A. Kinesin and dynein use distinct mechanisms to bypass obstacles. Surrey T, Malhotra V, Cross RA, eds. *eLife*. 2019;8:e48629. doi:10.7554/eLife.48629

103.Ross JL, Shuman H, Holzbaur ELF, Goldman YE. Kinesin and Dynein-Dynactin at Intersecting Microtubules: Motor Density Affects Dynein Function. *Biophys J*. 2008;94(8):3115-3125. doi:10.1529/biophysj.107.120014

104.Attard TJ, Welburn JPI, Marsh JA. Understanding molecular mechanisms and predicting phenotypic effects of pathogenic tubulin mutations. *PLOS Comput Biol*. 2022;18(10):e1010611. doi:10.1371/journal.pcbi.1010611

105.Binarová P, Tuszynski J. Tubulin: Structure, Functions and Roles in Disease. *Cells*. 2019;8(10):1294. doi:10.3390/cells8101294

106.Svitkina T. The Actin Cytoskeleton and Actin-Based Motility. *Cold Spring Harb Perspect Biol*. 2018;10(1):a018267. doi:10.1101/cshperspect.a018267

107.Chou SZ, Pollard TD. Mechanism of actin polymerization revealed by cryo-EM structures of actin filaments with three different bound nucleotides. *Proc Natl Acad Sci*. 2019;116(10):4265-4274. doi:10.1073/pnas.1807028115

108.Cooper GM. Structure and Organization of Actin Filaments. In: *The Cell: A Molecular Approach. 2nd Edition*. Sinauer Associates; 2000. Accessed June 26, 2023. https://www.ncbi.nlm.nih.gov/books/NBK9908/

109.Pinto-Costa R, Sousa MM. Profilin as a dual regulator of actin and microtubule dynamics. *Cytoskeleton*. 2020;77(3-4):76-83. doi:10.1002/cm.21586

110.Bamburg JR, Minamide LS, Wiggan O, Tahtamouni LH, Kuhn TB. Cofilin and Actin Dynamics: Multiple Modes of Regulation and Their Impacts in Neuronal Development and Degeneration. *Cells*. 2021;10(10):2726. doi:10.3390/cells10102726

111.Rottner K, Faix J, Bogdan S, Linder S, Kerkhoff E. Actin assembly mechanisms at a glance. *J Cell Sci*. 2017;130(20):3427-3435. doi:10.1242/jcs.206433

112.Chesarone MA, Goode BL. Actin Nucleation and Elongation Factors: Mechanisms and Interplay. *Curr Opin Cell Biol*. 2009;21(1):28-37. doi:10.1016/j.ceb.2008.12.001

113.Goley ED, Welch MD. The ARP2/3 complex: an actin nucleator comes of age. *Nat Rev Mol Cell Biol*. 2006;7(10):713-726. doi:10.1038/nrm2026

114.Plessner M, Grosse R. Dynamizing nuclear actin filaments. *Curr Opin Cell Biol*. 2019;56:1-6. doi:10.1016/j.ceb.2018.08.005

115.Serebryannyy L, de Lanerolle P. Nuclear actin: The new normal. *Mutat Res Mol Mech Mutagen*. 2020;821:111714. doi:10.1016/j.mrfmmm.2020.111714

116.Hurst V, Shimada K, Gasser SM. Nuclear Actin and Actin-Binding Proteins in DNA Repair. *Trends Cell Biol*. 2019;29(6):462-476. doi:10.1016/j.tcb.2019.02.010

117.Plessner M, Melak M, Chinchilla P, Baarlink C, Grosse R. Nuclear F-actin Formation and Reorganization upon Cell Spreading*♦. *J Biol Chem*. 2015;290(18):11209-11216. doi:10.1074/jbc.M114.627166

118.Roukos V. Actin proteins assemble to protect the genome. *Nature*. 2018;559(7712):35-37. doi:10.1038/d41586-018-05339-y

119.Caridi CP, D'Agostino C, Ryu T, et al. Nuclear F-actin and myosins drive relocalization of heterochromatic breaks. *Nature*. 2018;559(7712):54-60. doi:10.1038/s41586-018-0242-8

120.Schrank BR, Aparicio T, Li Y, et al. Nuclear ARP2/3 drives DNA break clustering for homology-directed repair. *Nature*. 2018;559(7712):61-66. doi:10.1038/s41586-018-0237-5

121.Lamm N, Read MN, Nobis M, et al. Nuclear F-actin counteracts nuclear deformation and promotes fork repair during replication stress. *Nat Cell Biol*. 2020;22(12):1460-1470. doi:10.1038/s41556-020-00605-6

122.Sweeney HL, Houdusse A, Robert-Paganin J. Myosin Structures. In: Coluccio LM, ed. *Myosins: A Superfamily of Molecular Motors*. Advances in Experimental Medicine and Biology. Springer International Publishing; 2020:7-19. doi:10.1007/978-3-030-38062-5_2

123.Hartman MA, Spudich JA. The myosin superfamily at a glance. *J Cell Sci*. 2012;125(7):1627-1632. doi:10.1242/jcs.094300

124.Ryan JM, Nebenführ A. Update on Myosin Motors: Molecular Mechanisms and Physiological Functions. *Plant Physiol*. 2018;176(1):119-127. doi:10.1104/pp.17.01429

125.Sellers JR. Myosins: a diverse superfamily. *Biochim Biophys Acta BBA - Mol Cell Res*. 2000;1496(1):3-22. doi:10.1016/S0167-4889(00)00005-7

126.Vicente-Manzanares M, Ma X, Adelstein RS, Horwitz AR. Non-muscle myosin II takes centre stage in cell adhesion and migration. *Nat Rev Mol Cell Biol*. 2009;10(11):778-790. doi:10.1038/nrm2786

127.Cook AW, Gough RE, Toseland CP. Nuclear myosins – roles for molecular transporters and anchors. *J Cell Sci*. 2020;133(11):jcs242420. doi:10.1242/jcs.242420

128.Maly IV, Hofmann WA. Myosins in the Nucleus. In: Coluccio LM, ed. *Myosins: A Superfamily of Molecular Motors*. Advances in Experimental Medicine and Biology. Springer International Publishing; 2020:199-231. doi:10.1007/978-3-030-38062-5_10

129.Philimonenko VV, Zhao J, Iben S, et al. Nuclear actin and myosin I are required for RNA polymerase I transcription. *Nat Cell Biol*. 2004;6(12):1165-1172. doi:10.1038/ncb1190

130.Wilkie AR, Sharma M, Pesola JM, Ericsson M, Fernandez R, Coen DM. A Role for Myosin Va in Human Cytomegalovirus Nuclear Egress. *J Virol*. 2018;92(6):e01849-17. doi:10.1128/JVI.01849-17

131.Magistrati E, Polo S. Myomics: myosin VI structural and functional plasticity. *Curr Opin Struct Biol*. 2021;67:33-40. doi:10.1016/j.sbi.2020.09.005

132.Wells AL, Lin AW, Chen LQ, et al. Myosin VI is an actin-based motor that moves backwards. *Nature*. 1999;401(6752):505-508. doi:10.1038/46835

133.Ménétrey J, Bahloul A, Wells AL, et al. The structure of the myosin VI motor reveals the mechanism of directionality reversal. *Nature*. 2005;435(7043):779-785. doi:10.1038/nature03592

134.Mukherjea M, Llinas P, Kim H, et al. Myosin VI Dimerization Triggers an Unfolding of a Three-Helix Bundle in Order to Extend Its Reach. *Mol Cell*. 2009;35(3):305-315. doi:10.1016/j.molcel.2009.07.010

135.Ökten Z, Churchman LS, Rock RS, Spudich JA. Myosin VI walks hand-over-hand along actin. *Nat Struct Mol Biol*. 2004;11(9):884-887. doi:10.1038/nsmb815

136.Geeves MA. Review: The ATPase mechanism of myosin and actomyosin. *Biopolymers*. 2016;105(8):483-491. doi:10.1002/bip.22853

137.He F, Wollscheid HP, Nowicka U, et al. Myosin VI Contains a Compact Structural Motif that Binds to Ubiquitin Chains. *Cell Rep*. 2016;14(11):2683-2694. doi:10.1016/j.celrep.2016.01.079

138.Wollscheid HP, Biancospino M, He F, et al. Diverse functions of myosin VI elucidated by an isoform-specific α-helix domain. *Nat Struct Mol Biol*. 2016;23(4):300-308. doi:10.1038/nsmb.3187

139.Tumbarello DA, Kendrick-Jones J, Buss F. Myosin VI and its cargo adaptors – linking endocytosis and autophagy. *J Cell Sci*. 2013;126(12):2561-2570. doi:10.1242/jcs.095554

140.Buss F, Arden SD, Lindsay M, Luzio JP, Kendrick-Jones J. Myosin VI isoform localized to clathrin-coated vesicles with a role in clathrin-mediated endocytosis. *EMBO J*. 2001;20(14):3676-3684. doi:10.1093/emboj/20.14.3676

141.Tumbarello DA, Waxse BJ, Arden SD, Bright NA, Kendrick-Jones J, Buss F. Autophagy receptors link myosin VI to autophagosomes to mediate Tom1-dependent autophagosome maturation and fusion with the lysosome. *Nat Cell Biol*. 2012;14(10):1024-1035. doi:10.1038/ncb2589

142.Geisbrecht ER, Montell DJ. Myosin VI is required for E-cadherin-mediated border cell migration. *Nat Cell Biol*. 2002;4(8):616-620. doi:10.1038/ncb830

143.Self T, Sobe T, Copeland NG, Jenkins NA, Avraham KB, Steel KP. Role of Myosin VI in the Differentiation of Cochlear Hair Cells. *Dev Biol*. 1999;214(2):331-341. doi:10.1006/dbio.1999.9424

144.Avraham KB, Hasson T, Steel KP, et al. The mouse Snell's waltzer deafness gene encodes an unconventional myosin required for structural integrity of inner ear hair cells. *Nat Genet*. 1995;11(4):369-375. doi:10.1038/ng1295-369

145.Yoshida H, Cheng W, Hung J, et al. Lessons from border cell migration in the Drosophila ovary: A role for myosin VI in dissemination of human ovarian cancer. *Proc Natl Acad Sci U S A*. 2004;101(21):8144-8149. doi:10.1073/pnas.0400400101

146.Dunn TA, Chen S, Faith DA, et al. A Novel Role of Myosin VI in Human Prostate Cancer. *Am J Pathol*. 2006;169(5):1843-1854. doi:10.2353/ajpath.2006.060316

147.Jung EJ, Liu G, Zhou W, Chen X. Myosin VI Is a Mediator of the p53-Dependent Cell Survival Pathway. *Mol Cell Biol*. 2006;26(6):2175-2186. doi:10.1128/MCB.26.6.2175-2186.2006

148.Cho SJ, Chen X. Myosin VI Is Differentially Regulated by DNA Damage in p53- and Cell Type-dependent Manners. *J Biol Chem*. 2010;285(35):27159-27166. doi:10.1074/jbc.M110.142117

149.Vreugde S, Ferrai C, Miluzio A, et al. Nuclear Myosin VI Enhances RNA Polymerase II-Dependent Transcription. *Mol Cell*. 2006;23(5):749-755. doi:10.1016/j.molcel.2006.07.005

150.Fili N, Hari-Gupta Y, dos Santos Á, et al. NDP52 activates nuclear myosin VI to enhance RNA polymerase II transcription. *Nat Commun*. 2017;8(1):1871. doi:10.1038/s41467-017-02050-w

151.Hari-Gupta Y, Fili N, dos Santos Á, et al. Myosin VI regulates the spatial organisation of mammalian transcription initiation. *Nat Commun*. 2022;13(1):1346. doi:10.1038/s41467-022-28962-w

152.Shi J, Hauschulte K, Mikicic I, et al. Nuclear myosin VI maintains replication fork stability. *Nat Commun*. 2023;14(1):3787. doi:10.1038/s41467-023-39517-y

153.Helma J, Cardoso MC, Muyldermans S, Leonhardt H. Nanobodies and recombinant binders in cell biology. *J Cell Biol*. 2015;209(5):633-644. doi:10.1083/jcb.201409074

154.Boersma YL, Plückthun A. DARPins and other repeat protein scaffolds: advances in engineering and applications. *Curr Opin Biotechnol*. 2011;22(6):849-857. doi:10.1016/j.copbio.2011.06.004

155.Jovčevska I, Muyldermans S. The Therapeutic Potential of Nanobodies. *BioDrugs*. 2020;34(1):11-26. doi:10.1007/s40259-019-00392-z

156.Stumpp MT, Binz HK, Amstutz P. DARPins: A new generation of protein therapeutics. *Drug Discov Today*. 2008;13(15):695-701. doi:10.1016/j.drudis.2008.04.013

157.Hamers-Casterman C, Atarhouch T, Muyldermans S, et al. Naturally occurring antibodies devoid of light chains. *Nature*. 1993;363(6428):446-448. doi:10.1038/363446a0

158.Jin B kyung, Odongo S, Radwanska M, Magez S. Nanobodies: A Review of Generation, Diagnostics and Therapeutics. *Int J Mol Sci*. 2023;24(6):5994. doi:10.3390/ijms24065994

159.Barakat S, Berksöz M, Zahedimaram P, Piepoli S, Erman B. Nanobodies as molecular imaging probes. *Free Radic Biol Med*. 2022;182:260-275. doi:10.1016/j.freeradbiomed.2022.02.031

160.Muyldermans S. Applications of Nanobodies. *Annu Rev Anim Biosci*. 2021;9(1):401-421. doi:10.1146/annurev-animal-021419-083831

161.Kobe B, Kajava AV. The leucine-rich repeat as a protein recognition motif. *Curr Opin Struct Biol*. 2001;11(6):725-732. doi:10.1016/S0959-440X(01)00266-4

162.D'Andrea LD, Regan L. TPR proteins: the versatile helix. *Trends Biochem Sci*. 2003;28(12):655-662. doi:10.1016/j.tibs.2003.10.007

163.Li J, Mahajan A, Tsai MD. Ankyrin Repeat: A Unique Motif Mediating Protein−Protein Interactions. *Biochemistry*. 2006;45(51):15168-15178. doi:10.1021/bi062188q

164.Harmansa S, Affolter M. Protein binders and their applications in developmental biology. *Development*. 2018;145(2):dev148874. doi:10.1242/dev.148874

165.Dreier B, Plückthun A. Ribosome Display: A Technology for Selecting and Evolving Proteins from Large Libraries. In: Park DJ, ed. *PCR Protocols*. Methods in Molecular Biology. Humana Press; 2011:283-306. doi:10.1007/978-1-60761-944-4_21

166.Plückthun A. Designed Ankyrin Repeat Proteins (DARPins): Binding Proteins for Research, Diagnostics, and Therapy. *Annu Rev Pharmacol Toxicol*. 2015;55(1):489-511. doi:10.1146/annurev-pharmtox-010611-134654

167.Yao Q, Weaver SJ, Mock JY, Jensen GJ. Fusion of DARPin to Aldolase Enables Visualization of Small Protein by Cryo-EM. *Structure*. 2019;27(7):1148-1155.e3. doi:10.1016/j.str.2019.04.003

168.Walser M, Mayor J, Rothenberger S. Designed Ankyrin Repeat Proteins: A New Class of Viral Entry Inhibitors. *Viruses*. 2022;14(10):2242. doi:10.3390/v14102242

169.Rothenberger S, Hurdiss DL, Walser M, et al. The trispecific DARPin ensovibep inhibits diverse SARS-CoV-2 variants. *Nat Biotechnol*. 2022;40(12):1845-1854. doi:10.1038/s41587-022-01382-3

170.Certo MT, Ryu BY, Annis JE, et al. Tracking genome engineering outcome at individual DNA breakpoints. *Nat Methods*. 2011;8(8):671-676. doi:10.1038/nmeth.1648

171.Sartori AA, Lukas C, Coates J, et al. Human CtIP promotes DNA end resection. *Nature*. 2007;450(7169):509-514. doi:10.1038/nature06337

172.Spagnolo L, Rivera-Calzada A, Pearl LH, Llorca O. Three-Dimensional Structure of the Human DNA-PKcs/Ku70/Ku80 Complex Assembled on DNA and Its Implications for DNA DSB Repair. *Mol Cell*. 2006;22(4):511-519. doi:10.1016/j.molcel.2006.04.013

173.Hsiang YH, Hertzberg R, Hecht S, Liu LF. Camptothecin induces protein-linked DNA breaks via mammalian DNA topoisomerase I. *J Biol Chem*. 1985;260(27):14873-14878.

174.Pommier Y. Topoisomerase I inhibitors: camptothecins and beyond. *Nat Rev Cancer*. 2006;6(10):789-802. doi:10.1038/nrc1977

175.Palumbieri MD, Merigliano C, Acosta DG, et al. Replication fork plasticity upon replication stress requires rapid nuclear actin polymerization. Published online March 25, 2023:2023.03.24.534097. doi:10.1101/2023.03.24.534097

176.Bianchi V, Pontis E, Reichard P. Changes of deoxyribonucleoside triphosphate pools induced by hydroxyurea and their relation to DNA synthesis. *J Biol Chem*. 1986;261(34):16037-16042. doi:10.1016/S0021-9258(18)66672-4

177.Schlacher K, Christ N, Siaud N, Egashira A, Wu H, Jasin M. Double-Strand Break Repair-Independent Role for BRCA2 in Blocking Stalled Replication Fork Degradation by MRE11. *Cell*. 2011;145(4):529-542. doi:10.1016/j.cell.2011.03.041

178.Przetocka S, Porro A, Bolck HA, et al. CtIP-Mediated Fork Protection Synergizes with BRCA1 to Suppress Genomic Instability upon DNA Replication Stress. *Mol Cell*. 2018;72(3):568-582.e6. doi:10.1016/j.molcel.2018.09.014

179.Mukherjee C, Tripathi V, Manolika EM, et al. RIF1 promotes replication fork protection and efficient restart to maintain genome stability. *Nat Commun*. 2019;10(1):3287. doi:10.1038/s41467-019-11246-1

180.Rageul J, Park JJ, Zeng PP, et al. SDE2 integrates into the TIMELESS-TIPIN complex to protect stalled replication forks. *Nat Commun*. 2020;11(1):5495. doi:10.1038/s41467-020-19162-5

181.Posern G, Sotiropoulos A, Treisman R. Mutant Actins Demonstrate a Role for Unpolymerized Actin in Control of Transcription by Serum Response Factor. *Mol Biol Cell*. 2002;13(12):4167-4178. doi:10.1091/mbc.02-05-0068

182.Ibrahim AFM, Shen L, Tatham MH, et al. Antibody RING-Mediated Destruction of Endogenous Proteins. *Mol Cell*. 2020;79(1):155-166.e9. doi:10.1016/j.molcel.2020.04.032

183.Andrews BJ, Proteau GA, Beatty LG, Sadowski PD. The FLP recombinase of the 2μ circle DNA of yeast: Interaction with its target sequences. *Cell*. 1985;40(4):795-803. doi:10.1016/0092-8674(85)90339-3

184.Ju Shin Y, Kyun Park S, Jung Jung Y, et al. Nanobody-targeted E3-ubiquitin ligase complex degrades nuclear proteins. *Sci Rep*. 2015;5(1):14269. doi:10.1038/srep14269

185.Mukherjee B, Tomimatsu N, Burma S. Immunofluorescence-based methods to monitor DNA end resection. *Methods Mol Biol Clifton NJ*. 2015;1292:67-75. doi:10.1007/978-1-4939-2522-3_5

186.Meyer H, Bug M, Bremer S. Emerging functions of the VCP/p97 AAA-ATPase in the ubiquitin system. *Nat Cell Biol*. 2012;14(2):117-123. doi:10.1038/ncb2407

187.Aramayo RJ, Willhoft O, Ayala R, Bythell-Douglas R, Wigley DB, Zhang X. Cryo-EM structures of the human INO80 chromatin-remodeling complex. *Nat Struct Mol Biol*. 2018;25(1):37-44. doi:10.1038/s41594-017-0003-7

188.Shen X, Mizuguchi G, Hamiche A, Wu C. A chromatin remodelling complex involved in transcription and DNA processing. *Nature*. 2000;406(6795):541-544. doi:10.1038/35020123

189.Brahma S, Udugama MI, Kim J, et al. INO80 exchanges H2A.Z for H2A by translocating on DNA proximal to histone dimers. *Nat Commun*. 2017;8(1):15616. doi:10.1038/ncomms15616

190.Alatwi HE, Downs JA. Removal of H2A.Z by INO80 promotes homologous recombination. *EMBO Rep*. 2015;16(8):986-994. doi:10.15252/embr.201540330

191.Chien JCY, Tabet E, Pinkham K, et al. A multiplexed bioluminescent reporter for sensitive and non-invasive tracking of DNA double strand break repair dynamics in vitro and in vivo. *Nucleic Acids Res*. 2020;48(17):e100. doi:10.1093/nar/gkaa669

192.Naiman K, Campillo-Funollet E, Watson AT, Budden A, Miyabe I, Carr AM. Replication dynamics of recombination-dependent replication forks. *Nat Commun*. 2021;12(1):923. doi:10.1038/s41467-021-21198-0

193.Maréchal A, Zou L. DNA Damage Sensing by the ATM and ATR Kinases. *Cold Spring Harb Perspect Biol*. 2013;5(9):a012716. doi:10.1101/cshperspect.a012716

194.Ray Chaudhuri A, Hashimoto Y, Herrador R, et al. Topoisomerase I poisoning results in PARP-mediated replication fork reversal. *Nat Struct Mol Biol*. 2012;19(4):417-423. doi:10.1038/nsmb.2258

195.Berti M, Teloni F, Mijic S, et al. Sequential role of RAD51 paralog complexes in replication fork remodeling and restart. *Nat Commun*. 2020;11(1):3531. doi:10.1038/s41467-020-17324-z

196.Damgaard RB. The ubiquitin system: from cell signalling to disease biology and new therapeutic opportunities. *Cell Death Differ*. 2021;28(2):423-426. doi:10.1038/s41418-020-00703-w

197.McClellan AJ, Laugesen SH, Ellgaard L. Cellular functions and molecular mechanisms of non-lysine ubiquitination. *Open Biol*. 2019;9(9):190147. doi:10.1098/rsob.190147

198.Ghosh S, Saha T. Central Role of Ubiquitination in Genome Maintenance: DNA Replication and Damage Repair. *ISRN Mol Biol*. 2012;2012:146748. doi:10.5402/2012/146748

199.García-Rodríguez N, Wong RP, Ulrich HD. Functions of Ubiquitin and SUMO in DNA Replication and Replication Stress. *Front Genet*. 2016;7:87. doi:10.3389/fgene.2016.00087

200.Thakar T, Leung W, Nicolae CM, et al. Ubiquitinated-PCNA protects replication forks from DNA2-mediated degradation by regulating Okazaki fragment maturation and chromatin assembly. *Nat Commun*. 2020;11(1):2147. doi:10.1038/s41467-020-16096-w

201.Crosetto N, Bienko M, Hibbert RG, et al. Human Wrnip1 Is Localized in Replication Factories in a Ubiquitin-binding Zinc Finger-dependent Manner*. *J Biol Chem*. 2008;283(50):35173-35185. doi:10.1074/jbc.M803219200

202.Baker RT, Catanzariti AM, Karunasekara Y, et al. Using deubiquitylating enzymes as research tools. *Methods Enzymol*. 2005;398:540-554. doi:10.1016/S0076-6879(05)98044-0

203.Padrick SB, Doolittle LK, Brautigam CA, King DS, Rosen MK. Arp2/3 complex is bound and activated by two WASP proteins. *Proc Natl Acad Sci*. 2011;108(33):E472-E479. doi:10.1073/pnas.1100236108

204.Han SS, Wen KK, García-Rubio ML, et al. WASp modulates RPA function on single-stranded DNA in response to replication stress and DNA damage. *Nat Commun*. 2022;13(1):3743. doi:10.1038/s41467-022-31415-z

205.Bhat KP, Krishnamoorthy A, Dungrawala H, Garcin EB, Modesti M, Cortez D. RADX modulates RAD51 activity to control replication fork protection. *Cell Rep*. 2018;24(3):538-545. doi:10.1016/j.celrep.2018.06.061

206.Tye S, Ronson GE, Morris JR. A fork in the road: Where homologous recombination and stalled replication fork protection part ways. *Semin Cell Dev Biol*. 2021;113:14-26. doi:10.1016/j.semcdb.2020.07.004

207.Roy S, Schlacher K. SIRF: A Single-cell Assay for in situ Protein Interaction with Nascent DNA Replication Forks. *Bio-Protoc*. 2019;9(18):e3377. doi:10.21769/BioProtoc.3377

208.Dungrawala H, Cortez D. Purification of proteins on newly synthesized DNA using iPOND. *Methods Mol Biol Clifton NJ*. 2015;1228:123-131. doi:10.1007/978-1-4939-1680-1_10

209.Altman D, Sweeney HL, Spudich JA. The Mechanism of Myosin VI Translocation and Its Load-Induced Anchoring. *Cell*. 2004;116(5):737-749. doi:10.1016/S0092-8674(04)00211-9

210.Park H, Li A, Chen LQ, Houdusse A, Selvin PR, Sweeney HL. The unique insert at the end of the myosin VI motor is the sole determinant of directionality. *Proc Natl Acad Sci*. 2007;104(3):778-783. doi:10.1073/pnas.0610066104